Thesis

Dynamics and Thermodynamics of Dissipative Quantum Systems

摩擦のある量子系でのダイナミクスと熱力学

Takeo Kato

加藤 岳生

Institute for Solid State Physics, University of Tokyo
Kashiwanoha 5-1-5, Kashiwa-shi, Chiba 277-8581

Thesis

Dynamics and Thermodynamics of Dissipative Quantum Systems

Takeo Kato

Institute for Solid State Physics, University of Tokyo
Roppongi, Minato-ku, Tokyo 106

January, 1999

Acknowledgments

The author would like to express his sincere gratitude to Prof. M. Imada for kind advices, continual encouragement and stimulating discussions. He also acknowledges useful advise by Dr. N. Furukawa and S. Onoda, and he also thanks B. Ammon for a reading of the manuscript to correct grammatical errors. He wishes to thank all the other members of the research group of Prof. M. Imada. He is very grateful to Mrs. Kyoko Fujii, Miyuki Toda and Noriko Sasaki for their continual help and encouragement.

Finally, he would like to thank my old friends, H. Kojima, K. Kitanishi, Y. Kudo, K. Takayama and Y. Sekiguchi for their warm-hearted encouragement and support. Without their support, this work would have been finished.

Contents

Chapter 1

General Introduction

1.1 Introduction

Theoretical studies on open systems have long history and are traced back to early work for the Brownian motion in the 19th century. Since then, many different areas have been studied in terms of the open systems [1]. Particularly in condensed matter physics, the dissipation plays a very important role and sometimes crucially determine both classical and quantum properties of systems. Dissipative dynamics has been studied recently on the following subjects: an order parameter in superconductors, phase dynamics in charge density waves and in Josephson junctions, muon motion in solids, vortex dynamics in superconductors and in Josephson arrays, quantum optics, and various other systems. These dissipative systems have attracted interest ranging from the viewpoint of statistical mechanics to technological applications.

Usually, classical analyses based on a classical Langevin equation or a master equation are sufficient to explain various behaviors of dissipative systems. This is due to the very large mass (or action) of the system, or because of strong dissipation destroying the coherence of the system. The quantum phenomena in dissipative systems, however, can be observed when dissipation and system mass are controlled properly. The observation of the quantum phenomena in dissipative systems proves validity of quantum mechanics on the macroscopic level. Additionally, quantum effects in complex dissipative systems may give possibilities to observe new phenomena.

In this thesis, dynamics of quantum dissipative systems is studied on several different

systems. In Chapter 2, quantum effects on long Josephson junctions are discussed. This part is published in [2, 3]. In these systems, various phenomena such as interplay of classical behavior including exchange of vortices and quantum effects in Josephson lines are expected. In Chapter 3, a dissipative tight-binding model is studied. This part is already published in [5]. This model with ohmic damping is directly related to voltage-current properties in small Josephson junctions with ohmic shunts. The results obtained there are expected to be applicable also for other systems, since the model captures general characteristics of dissipative systems.

In the following subsections, studies on dissipative quantum systems are reviewed, and the motivation and their relation to each part of this thesis are noted. Detailed reviews related to each subject are also given in the introduction of each chapter. In this thesis, we take $\hbar = k_B = 1$ except for the cases explicitly specified.

1.2 Dissipative Quantum Systems

In this section, phenomenological descriptions of quantum dissipative system are reviewed. Here, theoretical aspects of dissipative systems are stressed based on phenomenological models. In the later sections (Sec. 1.3 and Sec. 1.4), applications to real systems are considered. First, the Caldeira-Leggett phenomenological model is introduced (Sec. 1.2.1). Then, quantum Brownian motion (Sec. 1.2.2), quantum tunneling (Sec. 1.2.3), two-state systems (Sec. 1.2.4 and sec 1.2.5), and multi-state systems (Sec. 1.2.6) are reviewed.

Some results obtained in this section are used in the following chapters, which constitute the main parts of this thesis. Particularly, the tunneling rate formula in Sec. 1.2.3 is used in Chapter 2, and knowledge about quantum Brownian motion, two-state systems, and multi-state systems are referred to in Chapter 3.

1.2.1 Caldeira-Leggett phenomenological model

In the classical limit, dynamics of dissipative systems can be properly described in many cases by the Langevin equation

$$M\ddot{q}(t) + M\gamma\dot{q}(t) + \frac{\partial V}{\partial q} = \xi(t) \tag{1.1}$$

for a system variable q. Here, M is the mass, $V(q)$ is the potential energy, and $\xi(t)$ is a random force.

To study quantum effects in dissipative systems, a proper quantization scheme which can reproduce (1.1) in the classical limit is needed. The most natural way is to introduce a reservoir coupled to the system variable q. This system-plus-reservoir model has been constituted first by Zwanzig [6], Mori [7], and many authors. Although we have no clear understanding about the microscopic origin of dissipation for many complex systems, it is always possible to set up phenomenological system-plus-reservoir models from the information of the classical equation (1.1). Such a model can be constituted by preparing many oscillators as the reservoir. This model has been introduced by Feynman and Vernon [8], and Ullersma [9], about 15 years later it has been revived by Caldeira and Leggett [10, 11], and applied to tunneling problems.

The simplified system-plus-reservoir model is described by the Hamiltonian

$$H = \frac{p^2}{2M} + V(q) + \sum_j \left\{ \frac{p_j^2}{2m_j} + \frac{1}{2}m_j\omega_j^2 \left(x_j - \frac{c_j}{m_j\omega_j^2} q \right)^2 \right\}. \tag{1.2}$$

Here, $\{x_j\}$ is a set of heat-bath variables. The harmonic oscillators represent the reservoir and cause dissipation of the system. The properties of the reservoir are determined only by the spectral density defined as

$$J(\omega) = \frac{\pi}{2} \sum_j \frac{c_j^2}{m_j\omega_j} \delta(\omega - \omega_j). \tag{1.3}$$

In the classical limit, the Hamiltonian gives a generalized Langevin equation [1]

$$M\ddot{q}(t) + M\int_{-\infty}^{t} \mathrm{d}t'\gamma(t-t')\dot{q}(t') + \frac{\partial V}{\partial q} = \xi(t), \tag{1.4}$$

$$\gamma(t) = \frac{2}{\pi M}\int_0^\infty \mathrm{d}\omega \frac{J(\omega)}{\omega}\cos\omega t. \tag{1.5}$$

Hence, the spectral function $J(\omega)$ can be determined from the classical behavior of the dissipative systems. For example, the classical equation with Markovian damping (1.1) is reproduced when the spectral function is taken as

$$J(\omega) = M\gamma\omega. \tag{1.6}$$

This is often called 'ohmic' damping. Generally we may take other arbitrary forms for $J(\omega)$. Usually $J(\omega)$ is taken in the simple form

$$J(\omega) = M\gamma_s \left(\frac{\omega}{\tilde{\omega}}\right)^s. \tag{1.7}$$

where $\gamma_s\omega^{-s}$ is the damping strength, and ω is the reference frequency. The exponent s for small ω controls dissipation properties. The case $s > 1$ is called super-ohmic, and $s < 1$ is sub-ohmic. In reality, $J(\omega)$ must fall off in the limit $\omega \to \infty$, otherwise certain physical quantities would diverge. Hence a cut-off determined by microscopic time scale must be introduced as

$$J(\omega) = M\gamma_s \left(\frac{\omega}{\bar{\omega}}\right)^s f(\omega;\omega_c), \tag{1.8}$$

where $f(\omega;\omega_c)$ is a cutoff function which vanishes for $\omega \gg \omega_c$.

Let us consider the partition function Z given in the imaginary-time functional-integral representation. The integrals over the heat-bath variables are Gaussian and they can be evaluated exactly [1, 12]. After integrating out the degrees of freedom for the environment, the partition function is expressed as

$$Z = Z_R \oint \mathcal{D}q(\tau) \exp(-S[q(\tau)]). \tag{1.9}$$

Here Z_R is the partition function of the heat bath, and in the following calculation Z_R is removed in order to focus only on the damping effects on the particle. The paths $q(\tau)$ satisfy the periodic boundary condition $q(\beta) = q(0)$, where $\beta = 1/T$ is the inverse temperature. The effective action $S[q(\tau)]$ is given by

$$S[q(\tau)] = \int_0^\beta \mathrm{d}\tau \left(\frac{1}{2}M\dot{q}^2 + V(q)\right) - \frac{1}{2}\int_0^\beta \mathrm{d}\tau\mathrm{d}\tau' K(\tau-\tau')(q(\tau)-q(\tau'))^2. \tag{1.10}$$

Damping effects are described by the last term, which takes a nonlocal form for τ. The kernel $K(\tau)$ is calculated as

$$\begin{aligned} K(\tau) &= \frac{1}{\pi}\int_0^\infty \mathrm{d}\omega J(\omega) D_\omega(\tau), & (1.11)\\ D_\omega(\tau) &= \frac{1}{\beta}\sum_{n=-\infty}^{\infty} \frac{2\omega}{\nu_n^2+\omega^2} e^{i\nu_n\tau} & (1.12)\\ &= \frac{\cosh[\omega(\beta/2-|\tau|)]}{\sinh(\beta\omega/2)}, & (1.13) \end{aligned}$$

where $\nu_n = 2\pi n/\beta$ are the Matsubara frequencies.

This phenomenological model is so simplified that we should be careful when applying it to real systems. In some systems, effective actions calculated from microscopic descriptions take different forms than Eq. (1.10). Such an example is discussed in Sec.1.4.

Based on this phenomenological model, various dissipative systems are reviewed in the following subsections.

1.2.2 Quantum Brownian motion

Historically, the Langevin equation was used to analyze the irregular motion of a heavy particle moving in a thermally equilibrated molecular medium. The essence of this phenomenon is qualitatively understood by considering the Hamiltonian (1.2) with $V(q) = 0$. This model gives the generalized Langevin equation (1.1). To study properties of the damping on a qualitative level, it is convenient to introduce new coordinates y_j and new masses μ_j for the bath oscillators [13],

$$\begin{aligned} y_j &= \frac{m_j\omega_j^2}{C_j}x_j, & (1.14)\\ \mu_j &= \frac{C_j^2}{m_j\omega_j^4}. & (1.15) \end{aligned}$$

With these variables, the Hamiltonian (1.1) and the spectral function (1.3) become

$$\begin{aligned} H &= \frac{p^2}{2M} + \frac{1}{2}\sum_j \mu_j\left\{\dot{y}_j^2 + \omega_j^2(y_j-q)^2\right\}, & (1.16)\\ J(\omega) &= \frac{\pi}{2}\sum_j \mu_j\omega_j^3\delta(\omega-\omega_j). & (1.17) \end{aligned}$$

Since this Hamiltonian is translation-invariant, the total momentum

$$P_{\mathrm{tot}} = P + \sum_j p_j = M_{\mathrm{tot}}V \tag{1.18}$$

is conserved. Here V is the center-of-mass velocity, and M_{tot} is the total mass calculated by

$$M_{\mathrm{tot}} = M + \frac{2}{\pi}\int_0^\infty \mathrm{d}\omega \frac{J(\omega)}{\omega^3}. \tag{1.19}$$

This quantity is convergent when the exponent s in Eq. (1.7) is larger than 2. In this case, the damping effects appear only in the mass renormalization and the particle essentially behaves as a quantum particle with a mass M_{tot}. On the other hand, when $s \le 2$, the integral in (1.19) is infrared-divergent. This indicates that the low-energy excitations of the reservoir do not simply have the effect of mass renormalization but rather cause damping at long times.

Fortunately, the Hamiltonian (1.2) with $V(q) = 0$ can be treated exactly. The mean square displacement defined by

$$d(t) = \langle (q(t)-q(0))^2\rangle \tag{1.20}$$

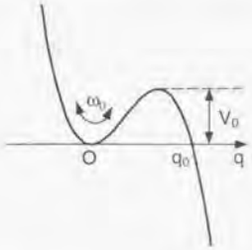

Figure 1.1: The potential describing decay from metastable states.

can be evaluated at long times t as [14]

$$d(t) = \begin{cases} \dfrac{2\sin(\pi s/2)}{M\beta\gamma_s\tilde{\omega}\Gamma(s+1)}(\tilde{\omega}t)^s, & (s<2), \\ \dfrac{2}{M_{\rm tot}\beta}t^2, & (s>2). \end{cases} \tag{1.21}$$

Here, $\beta = 1/T$ is the inverse temperature, and $\Gamma(z)$ is the gamma function. For sub-ohmic damping ($s < 1$) the mean square displacement grows subdiffusively, while for super-ohmic damping ($1 < s < 2$) the particle shows superdiffusive spreading. For $s > 2$ the spreading shows free particle behavior.

1.2.3 Dissipative quantum tunneling

The theory of reaction rate coefficients has a long history in physics, chemistry, and biology since the days of Arrhenius [15]. The transition rates in thermally activated regimes were derived by Kramers in 1940 [16], and thereafter, several theoretical concepts and ideas in reaction rate theory extending from classical rate theory to quantum version have been considered [17]. Recently it has become possible to treat quantum tunneling of dissipative systems [10, 11] by utilizing the path integral method. This method also allows to study the crossover behavior from classical to quantum regimes [18, 19, 20, 21].

In this subsection, the tunneling rate in dissipative systems is discussed based on the phenomenological model (1.2). Here, we only focus on quantum tunneling at zero temperature, though it is also possible to discuss decay rates at finite temperatures. The form of the potential $V(q)$ is taken as in Fig. 1.1. The simplest analytic form of the potential is

given as

$$V(q) = \frac{27}{4}V_0\left\{\left(\frac{q}{q_0}\right)^2 - \left(\frac{q}{q_0}\right)^3\right\}, \tag{1.22}$$

where q_0 is the coordinate of the exit point, which satisfies $V(q_0) = 0$, and V_0 is the potential barrier height.

Naturally, the concept of metastable states only makes sense when the barrier is large enough such that the decay time from the metastable state is very large compared to all the other characteristic time scales of the system dynamics. This condition is realized when

$$\omega_0 \ll V_0, \tag{1.23}$$

where ω_0 is the frequency of small oscillations around the metastable minimum defined by

$$\omega_0 = \left(\frac{V''(0)}{M}\right)^{1/2}. \tag{1.24}$$

In this situation, the WKB approximation based on the imaginary-time path integral is applicable. This method was developed first by Langer [22] in connection with nucleation theory and applied to quantum decay of false vacuum later by Callen and Colemann [23, 24].

In the semiclassical regime, the stationary solutions of the action (1.10) dominate in the functional integral (1.9). The stationary paths $q_s(\tau)$ are determined by an equation of motion with a nonlocal term

$$-M\ddot{q}_s(\tau) + \frac{\partial V}{\partial q}(q_s) - \int_0^\beta d\tau' k(\tau-\tau')q_s(\tau') = 0. \tag{1.25}$$

Note that the sign of the potential term is reversed, because the motion occurs in the imaginary-time direction. Here, the solution is periodic in the τ-direction ($q_s(\tau+\beta) = q_s(\tau)$), and the kernel $k(\tau)$ is defined from $K(\tau)$ in (1.11) as

$$k(\tau) = \sum_j \frac{c_j^2}{m_j\omega_j^2}\delta'(\tau) - K(\tau), \tag{1.26}$$

$$\delta'(\tau) = \sum_{n=-\infty}^{+\infty} \delta(\tau - n\beta). \tag{1.27}$$

There are two important solutions which predominantly contribute to the value of the partition function. One is the trivial solution $q_s(\tau) = 0$ which expresses the thermal equilibrium nature of the system in a metastable state, and the other is the nontrivial solution $q_s(\tau) = q_B(\tau)$ which describes tunneling effects. This nontrivial solution is called

a 'bounce' solution. Then the partition function is approximately obtained by these two contributions as

$$Z \simeq Z^{(0)} + Z^{(B)}. \tag{1.28}$$

It is easily proved that $Z^{(0)}$ is real, while $Z^{(B)}$ is purely imaginary [24]. Hence, the free energy $F = -\beta^{-1}\ln Z$ has an imaginary part. This result comes from the fact that the system is metastable. At zero temperature, the free energy F coincides to the system energy E, and the probability $P(t)$ that the system stays in the metastable state at the time t is calculated as

$$P(t) \sim |e^{-iEt}|^2 = e^{2\mathrm{Im}Et}. \tag{1.29}$$

Therefore, the quantum decay rate Γ is associated with the free energy as

$$\Gamma = -2\mathrm{Im}F. \tag{1.30}$$

at least for zero temperature [23, 24]. The extension of this formula to finite temperatures has been proposed by Affleck [18], and in accordance with this formulation, systematic studies of the decay rates from the quantum tunneling regime to the thermally activated regime have been performed [19, 20, 21]. At this time, a general justification of the equation (1.30) does not exist. It has been found that this method produces identical results to those obtained by means of the more complicated procedure [1] for one-dimensional dissipative system within the Caldeira-Leggett model. However, it is an open question whether the formula (1.30) is valid for more complex systems such as multi-dimensional systems.

Let us continue the calculation of the tunneling rate at zero temperature. In the WKB condition (1.23), $|Z^{(0)}| \gg |Z^{(B)}|$ is satisfied, and the rate formula is approximated as

$$\Gamma = \frac{2}{\beta}\mathrm{Im}\left(\frac{Z^{(B)}}{Z^{(0)}}\right). \tag{1.31}$$

After evaluating the contribution of paths in the vicinity of the stationary solution, the tunneling rate is obtained

$$\Gamma = A\exp(-S_B), \tag{1.32}$$

where S_B is the action of the bounce solution $q_B(\tau)$. The prefactor is determined by fluctuations $\xi(\tau)$ about the stationary solution $(q(\tau) = 0, q_B(\tau))$ and given by

$$A = \left(\frac{S_0}{2\pi}\right)^{1/2}\left(\frac{D_0}{|D_B'|}\right)^{1/2}. \tag{1.33}$$

where D_0 and D_B' are determinants of the fluctuation operators $\mathbf{K}_0$ and $\mathbf{K}_B$, defined by

$$\mathbf{K}_0\xi(\tau) \equiv -\ddot{\xi}(\tau) + \omega_0^2\xi(\tau) + \frac{1}{M}\int_0^\beta d\tau' k(\tau-\tau')\xi(\tau') \tag{1.34}$$

$$\mathbf{K}_B\xi(\tau) \equiv -\ddot{\xi}(\tau) + \frac{1}{M}V''(q_B(\tau))\xi(\tau) + \frac{1}{M}\int_0^\beta d\tau' k(\tau-\tau')\xi(\tau'), \tag{1.35}$$

and the prime in D_B means that the zero eigenvalue is omitted.

The bounce action S_B and the prefactor A can be calculated in an analytic form only in a few limiting cases. For the potential (1.22), the zero temperature bounce in the absence of dissipation has the form

$$q_B(\tau) = q_0\,\mathrm{sech}^2(\omega_0\tau/2). \tag{1.36}$$

For weak ohmic damping, the exponent and prefactor are calculated as [11, 25]

$$S_B = \frac{36V_0}{5\omega_0}\left(1 + \frac{45\zeta(3)}{\pi^3}\alpha + \mathcal{O}(\alpha^2)\right), \tag{1.37}$$

$$A = \sqrt{60}\omega_0\left(\frac{S_B^{(\alpha=0)}}{2\pi\hbar}\right)^{1/2}\left(1 + 2.86\alpha + \mathcal{O}(\alpha^2)\right), \tag{1.38}$$

where $\alpha = \gamma/2\omega_0$, $\zeta(3)$ is the Riemann number, and $S_B^{\alpha=0} = 36V_0/5\hbar\omega_0$. For asymptotically large ohmic damping, the zero temperature bounce takes the Lorentzian form

$$q_B(\tau) = \frac{4q_0/3}{1 + (\omega_0\tau/2\alpha)^2}, \tag{1.39}$$

yielding the exponent and prefactor [21]

$$S_B = 6\pi\alpha\frac{V_0}{\omega_0}\left(1 + \frac{1}{4\alpha^2} + \mathcal{O}(\alpha^{-4})\right), \tag{1.40}$$

$$A = 16\pi\sqrt{6}\alpha^{7/2}\frac{\omega_0}{2\pi}\sqrt{\frac{V_0}{\omega_0}}\left(1 + 2\alpha^{-2}\ln\alpha + 1.107\alpha^{-2} + \cdots\right). \tag{1.41}$$

In both cases dissipation suppresses the tunneling rate in the Caldeira-Leggett theory. These result are used in Chapter 2 to estimate the tunneling rate in realistic experimental situations.

In this thesis, the tunneling rate of many-body systems is evaluated in a simplified phenomenological model. It is still an open question how the tunneling rate of general multi-dimensional systems should be formulated. Several works based on approximate treatments have been performed [17, 26, 27, 28, 29], though there exists no clear and efficient way to treat quantum tunneling in complex systems.

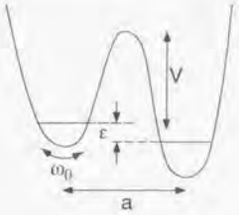

Figure 1.2: The potential with two wells. This system can be truncated into a two-state system with the tunneling matrix Δ_0 and bias ε for the condition $V \gg \omega_0$, where V is the barrier height, and ω_0 the frequency of the potential minima.

1.2.4 Dissipative two-state systems (thermodynamics)

One of the most interesting aspects of quantum theory is the phenomenon of constructive and destructive interference. The simplest systems which shows up the quantum coherence is the two-state systems, which have been studied in various areas of physics and chemistry. Such systems are frequently interacting with a heat bath, allowing the system to enter a state of thermal equilibrium, and breaking the system coherence. In this subsection, the Caldeira-Leggett theory is reviewed for dissipative two-state systems [30].

The two-state systems can be realized for potentials shown in Fig 1.2. The potential is characterized by the potential height V and the frequency ω_0 of small oscillation around the potential minima. If the condition $V \gg \omega_0$ is satisfied, the system is characterized only by two parameters: the (bare) tunneling matrix Δ_0 and the bias energy ε. These parameters may be determined by standard WKB technique, and satisfy $\Delta_0, \varepsilon \ll \omega_0$. At low temperatures ($T \ll \omega_0$), the system can be truncated to a two-dimensional Hilbert space. As a result, the Hamiltonian is described by

$$H_0 = -\frac{\Delta_0}{2}\sigma_x + \frac{\varepsilon}{2}\sigma_z, \tag{1.42}$$

where the σ's are Pauli matrices, and the basis is chosen such that the localized state in the right(left) well has an eigenvalue $+1(-1)$ for σ_z. The dissipation is introduced in accordance with the Caldeira-Leggett theory as

$$H = H_0 + \sum_j \left(\frac{p_j^2}{2m_j} + \frac{1}{2}m_j\omega_j^2 x_j^2 - \frac{1}{2}a\sigma_z c_j x_j \right), \tag{1.43}$$

where a is the distance between the wells. This model is called the spin-boson model, and the exact solution is not known in most of the parameter space. Nontrivial problems remain even for this simplified model.

The slow modes in the heat bath cause long-ranged memory effects in (1.10), while the fast modes give short-ranged effects. Actually, the fast modes can quickly respond to the slow motion of the system variable q, and can be treated by an adiabatic approximation. The spectral function is divided into two parts:

$$J_{\rm lf}(\omega) = J(\omega) f(\omega; \omega_c), \tag{1.44}$$

$$J_{\rm hf}(\omega) = J(\omega) - J_{\rm lf}(\omega), \tag{1.45}$$

where ω_c ($\sim \omega_0 \gg \Delta_0$) is a cut-off frequency, and $f(\omega; \omega_c)$ is a cut-off function, which has vanishing amplitude at $\omega \gg \omega_c$. Then, the bare matrix element Δ_0 is dressed by a Frank-Condon factor due to the high-frequency part of oscillators as

$$\Delta = \Delta_0 \exp\left(-\frac{a^2}{2\pi} \int_0^\infty {\rm d}\omega \frac{J_{\rm hf}(\omega)}{\omega^2} \coth(\beta\omega/2) \right). \tag{1.46}$$

Throughout this thesis, $J_{\rm lf}(\omega)$ is replaced by $J(\omega)$, and Δ is interpreted as a free parameter. For a discussion of the truncation scheme in two-state systems, readers are referred to Refs. [30, 31, 32, 33].

For the ohmic case ($J(\omega) = M\gamma\omega$), this adiabatic approximation also gives the characteristic frequency $\Delta_{\rm eff}$. It is determined self-consistently such that the integration in (1.46) gives $\Delta_{\rm eff}$ for $\omega_c = \Delta_{\rm eff}$. As a result, $\Delta_{\rm eff}$ is estimated as

$$\Delta_{\rm eff} = \Delta \left(\frac{\Delta}{\omega_c} \right)^{K/(1-K)}. \tag{1.47}$$

Here, K is a dimensionless coupling constant defined by

$$M\gamma = \frac{2\pi K}{a^2}. \tag{1.48}$$

For the ohmic damping case, the cut-off frequency ω_c may be removed in all expressions by replacing Δ by $\Delta_{\rm eff}$ [30].

The thermodynamics of dissipative two-state systems can be discussed by evaluating the partition function given in (1.9) and (1.10). For two-state systems, the contribution from the right well is exactly calculated as

$$Z_{\rm right} = \sum_{m=0}^{\infty} \left(\frac{\Delta}{2} \right)^{2m} \int_0^\beta {\rm d}\tau_{2m} \int_0^{\tau_{2m}} {\rm d}\tau_{2m-1} \cdots \int_0^{\tau_2} {\rm d}\tau_1$$

$$\times \exp\left(-\varepsilon\beta + \varepsilon\sum_{l=1}^{m}(\tau_{2l}-\tau_{2l-1}) + \sum_{k<l}^{2m}(-1)^{k+l}\phi(\tau_l-\tau_k)\right), \tag{1.49}$$

$$\phi(\tau) = \frac{a^2}{\pi}\int_0^\infty \mathrm{d}\omega \frac{J(\omega)}{\omega^2}\left(D_\omega(0) - D_\omega(\tau)\right), \tag{1.50}$$

where $D_\omega(\tau)$ is defined in (1.12). Particularly, for the ohmic damping case, the kernel is calculated as

$$\phi(\tau) = 2K\ln\left(\frac{\beta\omega_c}{\pi}\sin\left(\frac{\pi\tau}{\beta}\right)\right), \tag{1.51}$$

and this form is used for a comparison with the Kondo model in the final part of this subsection.

Based on (1.49)-(1.50) the specific heat of the system may be calculated [34]. For the dissipationless case ($J(\omega) = 0$), the specific heat of the two-state system C shows the well-known Schottky behavior

$$C = \left(\frac{\beta\Delta_b}{2}\right)^2 \mathrm{sech}^2(\beta\Delta_b/2), \tag{1.52}$$

where $\Delta_b = \sqrt{\Delta^2+\varepsilon^2}$. For the ohmic damping case, the high-temperature expansion is calculated for $\varepsilon = 0$ and $K < 1$ as

$$C = \frac{(1-K)(1-2K)}{\cos(\pi K)}\left(\frac{(2\pi)^K}{2\Gamma(1-K)}\right)^2\theta^{2K-2} + \mathrm{O}(\theta^{4K-1}), \tag{1.53}$$

and the low-temperature expansion is calculated as

$$C = K\lambda^2\sum_{n=1}^{\infty}(2n-1)\pi^{2n}|B_{2n}|(2\lambda\theta)^{2n-1}, \tag{1.54}$$

where $\theta = T/\Delta_{\mathrm{eff}}$, $\lambda = \Delta_{\mathrm{eff}}/\sqrt{\Delta_{\mathrm{eff}}^2+\varepsilon^2}$, and B_m is the Bernoulli number. It should be noted that ohmic damping causes the T-linear specific heat at low temperatures, in contrast to the exponential singularity of the Shottkey behavior. This implies that the low-energy property of the system is affected drastically by the ohmic damping. This change may also be seen in superohmic and subohmic damping. For a discussion of non-ohmic damping, readers are referred to Ref. [34]

For high-temperature and/or strong damping, the system exhibits overdamped behavior and shows exponential relaxation. In this case, the system is controlled only by the tunneling rate, which can be calculated by analytic continuation of the free energy as discussed

in Sec. 1.2.3. In other words, this regime is well described by the Fermi's golden rule. From the expression of the free energy

$$F_{\mathrm{right}} \equiv -\frac{1}{\beta}\ln(Z_{\mathrm{right}}) \tag{1.55}$$

$$= \frac{\varepsilon}{2} - \frac{\Delta^2}{4}\int_0^\beta \mathrm{d}\tau e^{\varepsilon\tau-\phi(\tau)} + \mathrm{O}(\Delta^4), \tag{1.56}$$

it is observed that the integrand of the free energy is largest at $\tau = \tau_s$, where τ_s is the saddle point with the direction of steepest descent perpendicular to the real axis of the complex-τ plane. Following Langer [22], the integration contour is changed at τ_s, and the integration is continued along the imaginary axis from τ_s to $\tau_s + \mathrm{i}\infty$. This modified integration for the free energy gives an imaginary part given by

$$\mathrm{Im}F_{\mathrm{right}} = -\mathrm{Im}\frac{\Delta^2}{8}\int_{\tau_s-\mathrm{i}\infty}^{\tau_s+\mathrm{i}\infty}\mathrm{d}\tau e^{\varepsilon\tau-\phi(\tau)}. \tag{1.57}$$

Then, the tunneling rate from the right to left well is calculated by (1.30) as

$$k^+ = \frac{\Delta^2}{2}\int_0^\infty \mathrm{d}t\cos(\varepsilon t - R(t))e^{-S(t)}, \tag{1.58}$$

$$\phi(\tau = \mathrm{i}t) \equiv S(t) + \mathrm{i}R(t), \tag{1.59}$$

$$S(t) = \frac{a^2}{\pi}\int_0^\infty \mathrm{d}\omega\frac{J(\omega)}{\omega^2}\coth\left(\frac{\beta\omega}{2}\right)(1-\cos(\omega t)), \tag{1.60}$$

$$R(t) = \frac{a^2}{\pi}\int_0^\infty \mathrm{d}\omega\frac{J(\omega)}{\omega^2}\sin(\omega t). \tag{1.61}$$

The tunneling rate k^- from the left well satisfies $k^-(\varepsilon) = k^+(-\varepsilon)$. For $s < 2$, the integrand in (1.58) is convergent since

$$\lim_{t\to\infty} S(t) = 0. \tag{1.62}$$

Hence, this treatment is applicable for the incoherent regimes of $s < 2$.

Finally, let us consider the relation between the spin-boson model with an ohmic spectral function and the Kondo problem, which deals with a single impurity of spin 1/2 coupled to conduction electrons. The essence of the Kondo problem comes from high-density electron-hole excitation in the vicinity of the Fermi surface [35, 36]. In the adiabatic scheme, this leads to a logarithmic infrared divergence of the static magnetic susceptibility. This problem is also related to the X-ray absorption edge anomaly [37, 38] and the diffusion of a heavy particle in metals [39, 40, 41].

The second quantized Kondo Hamiltonian reads

$$H_{\rm K} = v_{\rm F}\sum_{k,\sigma} k c^\dagger_{k,\sigma} c_{k,\sigma} + J\mathbf{S}\cdot\mathbf{s}(\mathbf{0}), \tag{1.63}$$

$$s_i(0) = \frac{1}{2}\sum_{\sigma,\sigma'} c^\dagger_\sigma(0)\tau^i_{\sigma,\sigma'} c_{\sigma'}(0), \tag{1.64}$$

$$c^\dagger_\sigma(0) = \frac{1}{\sqrt{L}}\sum_k c^\dagger_{k,\sigma}, \tag{1.65}$$

where $\tau^i (i = x, y, z)$ are the Pauli matrices, L is a normalization constant, and $\mathbf{S}$ is a local impurity spin. Here, the dispersion of the conduction electrons is linearized. In order to associate the Kondo problem with the two-state problem, it is necessary to generalize the Kondo model to anisotropic couplings as

$$H_{\rm K} = v_{\rm F}\sum_{k,\sigma} k c^\dagger_{k,\sigma} c_{k,\sigma} + \frac{J_1}{4}\tau^z\sum_\sigma \sigma c^\dagger_\sigma c_\sigma + \frac{J_2}{2}\left(\tau^+ c^\dagger_\downarrow c_\uparrow + \tau^- c^\dagger_\uparrow c_\downarrow\right), \tag{1.66}$$

with $\tau^\pm = (\tau^x \pm i\tau^y)/2$. Here, the original Kondo Hamiltonian (1.65) is reproduced when $J_1 = J_2 = J$. The equivalence between the Kondo model and the spin-boson model has been proved first by the Bosonization technique [42]. However, here we follow the steps of Yuval and Anderson [43], who have calculated the partition function of the impurity in the form of a perturbation series in powers of ρJ_2, where $\rho = (2\pi v_{\rm F})^{-1}$ is the density of states. The series takes the form

$$\begin{aligned} Z_{\rm K} &= \sum_{m=0}^{\infty}\left(\frac{\rho J_2\omega_c\cos^2\delta_K}{2}\right)^{2m}\int_0^\beta {\rm d}\tau_{2m}\int_0^{\tau_{2m}}{\rm d}\tau_{2m-1}\cdots\int_0^{\tau_2}{\rm d}\tau_1 \\ &\times \exp\left\{2\left(1-\frac{2}{\pi}\delta_K\right)^2\sum_{j>k}^{2m}(-1)^{j+k}\ln\left[\frac{\beta\omega_c}{\pi}\sin\left(\frac{\pi(\tau_j-\tau_k)}{\beta}\right)\right]\right\}. \end{aligned} \tag{1.67}$$

Here, δ_K is the scattering phase shift at the singular non-spin-flip potential $J_1\delta(x)/4$, and the series is formally equivalent to the expression (1.49) with (1.51) for $\varepsilon = 0$ with

$$\Delta = \rho J_2\omega_c\cos^2\delta_K, \tag{1.68}$$

$$K = \left(1-\frac{2}{\pi}\delta_K\right)^2. \tag{1.69}$$

Thus, the spin-boson model is equivalent to the Kondo problem in the low-energy limit.

In a similar way, the Caldeira-Leggett theory for dissipative multi-state systems can be related to heavy particle motion in metal. Here, the Fermi surface effect strongly affects the particle motion in the same way as it affects the impurity spin. A detailed discussion is given in Sec. 1.4.1.

1.2.5 Dissipative two-state systems (dynamics)

The dynamics of two-state systems is fully described by the time evolution of the density matrix $W(t)$ of the total system. For convenience of the calculation, the initial density matrix is often taken in a factorized form $W(t_0) = \rho(t_0)W_{\rm R}(t_0)$ at some large negative time t_0, where ρ and $W_{\rm R}$ are the density matrices of the system and the environment, respectively. Then the system is allowed to evolve under the action of the Hamiltonian (1.43). Here, let us consider the situation where the system is held in the right well (eigenvalue $\sigma_z = +1$) for $t_0 < t < 0$, such that the environment could have come into thermal equilibrium. This can be achieved, e.g., by applying a strong bias for all $t(< 0)$. At $t = 0$, the constraint is removed, and for $t > 0$ the dynamics is governed by the spin boson Hamiltonian. In this subsection, we only consider the non-bias case $\varepsilon = 0$ for simplicity.

The occupation probability $P_{\rm L(R)}(t)$ of the left (right) well is associated with the expectation value of $P(t) \equiv \langle\sigma_z\rangle$ as

$$P(t) = P_{\rm R}(t) - P_{\rm L}(t) = 2P_{\rm R}(t) - 1. \tag{1.70}$$

Within the real-time functional integral approach, we obtain

$$P_{\rm R}(t) = \int \mathcal{D}q(t')\int \mathcal{D}q'(t'')\mathcal{A}[q]\mathcal{A}^*[q']\mathcal{F}[q,q'], \tag{1.71}$$

where the summation is over all paths with constraints $q(t') = q'(t') = a/2$ for $t_0 < t' < 0$. The quantity $\mathcal{A}[q]$ is the probability amplitude of the system decoupled from its environment to follow the path $q(t')$, and $\mathcal{F}[q,q']$ is the real-time influence functional first calculated by Feynman and Vernou [8] as

$$\mathcal{F}[q,q'] = \exp\{-\Phi[q,q']\}, \tag{1.72}$$

$$\Phi[q,q'] = \int_0^t {\rm d}t'\int_0^{t'}{\rm d}t''\{q(t')-q'(t')\}\{L(t'-t'')q(t'') - L^*(t'-t'')q'(t'')\}, \tag{1.73}$$

$$L(t) = \frac{1}{\pi}\int_0^\infty {\rm d}\omega J(\omega)[\cosh(\omega\beta/2)\cos\omega t - i\sin\omega t]. \tag{1.74}$$

For the two-state systems, the paths $q(t')$ and $q'(t')$ jump between the two discrete values $a/2$ and $-a/2$ which correspond to the states in the right (R) and left (L) well, respectively. Defining the coordinates

$$\xi(t') \equiv [q(t') - q'(t')]/a, \tag{1.75}$$

$$\chi(t') \equiv [q(t') + q'(t')]/a, \tag{1.76}$$

and performing partial integrations, we have the influence functional in the form [30]

$$\mathcal{F} = \exp\left(\int_{t_0}^{t} dt' \int_{t_0}^{t'} dt''[\dot{\xi}(t')S(t'-t'')\dot{\xi}(t'') + i\dot{\xi}(t')R(t'-t'')\dot{\chi}(t'')]\right), \tag{1.77}$$

where

$$S(t) = \frac{a^2}{\pi}\int_0^\infty d\omega \frac{J(\omega)}{\omega^2}(1-\cos\omega t)\coth\left(\frac{\beta\omega}{2}\right), \tag{1.78}$$

$$R(t) = \frac{a^2}{\pi}\int_0^\infty d\omega \frac{J(\omega)}{\omega^2}\sin\omega t. \tag{1.79}$$

A general path with $2n$ transitions at times t_j $(j = 1, 2, \cdots, 2n)$ in the interval $0 < t' < t$ is parameterized by

$$\dot{\chi}^{(n)}(t') = \sum_{j=1}^{n} \chi_j[\delta(t'-t_{2j}) - \delta(t'-t_{2j-1})], \tag{1.80}$$

$$\dot{\xi}^{(n)}(t') = \sum_{j=1}^{n} \xi_j[\delta(t'-t_{2j}) - \delta(t'-t_{2j-1})]. \tag{1.81}$$

If we define the quantities

$$S_{jk} = S(t_j - t_k); \quad R_{jk} = R(t_j - t_k), \tag{1.82}$$

$$\Lambda_{jk} = S_{2j,2k-1} + S_{2j-1,2k} - S_{2j,2k} - S_{2j-1,2k-1}, \tag{1.83}$$

$$X_{jk} = R_{2j,2j+1} + R_{2j-1,2k} - R_{2j,2k} - R_{2j-1,2k+1}, \tag{1.84}$$

the influence functional (1.77) for this path takes the form

$$P(t) = \sum_{n=0}^{\infty}\left(-\frac{\Delta_c^2}{4}\right)\int_0^t dt_{2n}\int_0^{t_{2n}} dt_{2n-1}\cdots\int_0^{t_2} dt_1 \sum_{\{\xi_j\}}\sum_{\{\chi_j\}} G_n H_n, \tag{1.85}$$

$$G_n = \exp\left(-\sum_{j=1}^{n} S_{2j,2j-1} - \sum_{j=2}^{n}\sum_{k=1}^{j-1}\xi_j\xi_k\Lambda_{jk}\right), \tag{1.86}$$

$$H_n = \exp\left(i\sum_{j=1}^{n}\xi_j\sum_{k=0}^{j-1}\chi_k X_{jk}\right). \tag{1.87}$$

The expressions obtained above are exact for arbitrary forms of the spectral function $J(\omega)$. For simplicity, we restricts ourselves to the ohmic damping case in the following discussion. The dimensionless damping strength is given by $K = m\gamma a^2/2\pi$, where γ is the damping parameter in (1.1). The formal expressions for $P(t)$ derived above can be

evaluated in certain limits of K and temperature by analytic methods. For example, if $K = 0$, the expansion of $P(t)$ is summed up to

$$P(t) = cos(\Delta t), \tag{1.88}$$

at any temperature. This means that for the isolated system the expectation value of σ_z oscillates with the frequency Δ retaining the coherence completely.

For the special value $K = 1/2$ of the ohmic damping strength, the formal expression for $P(t)$ can also be summed exactly [44]. In this case, we obtain

$$P(t) = \exp\left(-\frac{\pi\Delta^2}{2\omega_c}t\right), \tag{1.89}$$

for any temperature T. This exponential decay indicates that for $K \geq 1/2$ the system is incoherent behavior at all temperature.

For sufficiently strong damping and/or in the high temperature region, incoherent hopping motion occurs, and Fermi's golden rule is applicable. As a result, $P(t)$ shows exponential behavior, and its relaxation rate is determined by the bounce method based on the imaginary-time path integral as discussed in the previous subsection.

On the other hand, in the weak coupling limit $K \ll 1$, we obtain

$$P(t) = \cos(\Omega t)e^{-\gamma t/2} + (1 - e^{-\gamma t})/2 \tag{1.90}$$

$$\Omega^2 = \Delta^2 + 2K\left(\mathrm{Re}\,\phi(i\beta\Delta/2\pi) - \ln(\beta\Delta/2\pi)\right), \tag{1.91}$$

$$\gamma = \pi K\Delta\coth(\beta\Delta/2), \tag{1.92}$$

where $\phi(z)$ is the digamma function. In this case, $P(t)$ shows damped oscillating behavior at low temperatures, indicating that the system coherence is retained in this region.

I shall now describe an approximation called the noninteracting-blip approximation (NIBA) based on two assumption: (1) put $X_{jk} = 0$ for $j \neq k+1$, and let only $X_{k+1,k} = R(t_{2k+2} - t_{2k+1})$ be nonzero, and (2) put $\Lambda_{jk} = 0$. For the ohmic case, this approximation reproduces correct results in the following three regions: the $K = 1/2$ case, the weak coupling limit $K \ll 1$, and the strong damping and/or high-temperature region (incoherent region). Therefore, the NIBA approximation gives proper interpolation among these regions. For a more detailed discussion of the consistency, readers are referred to Ref. [30]. Although it is known from recent numerical simulations [45, 46] that the NIBA

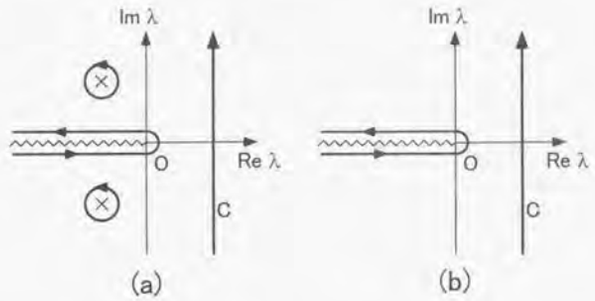

Figure 1.3: Singularities of $P(\lambda)$ and the Bromwich contour: (a) $K < 1/2$; (b) $1/2 < K < 1$.

approximation gives incorrect asymptotic behavior of $P(t)$ for $t \to \infty$, it reproduces at least the qualitative nature of $P(t)$ for intermediate values of t.

In the NIBA approximation, $P(t)$ is calculated as

$$P(\lambda) = \int_0^\infty \mathrm{d}t\, e^{-\lambda t} P(t) = \frac{1}{\lambda + f(\lambda)}, \tag{1.93}$$

$$f(\lambda) = \Delta^2 \int_0^\infty \mathrm{d}t\, e^{-\lambda t} \left(\frac{2\pi T t}{2\sinh(2\pi T t)} \right)^{2K} \frac{\cos[2K \arctan(\omega_c t)]}{(1+\omega_c^2 t^2)^K}. \tag{1.94}$$

Let us discuss zero-temperature properties first. For $0 < K < 1/2$, $P(\lambda)$ has three singularities as shown in Fig. 1.3 (a): a branch cut at $\lambda = 0$ and a complex conjugated pair of simple poles at

$$\lambda = \Delta_{\mathrm{eff}} \exp[\pm \mathrm{i}\pi/2(1-K)]. \tag{1.95}$$

Then, $P(t)$ is obtained by the inverse Laplace transformation

$$P(t) = \int_{\mathrm{C}} \mathrm{d}\lambda\, P(\lambda) e^{\lambda t}, \tag{1.96}$$

where C is the Bromwich contour shown in Fig. 1.3. The result of $P(t)$ consists of two parts: the integral arising from the poles (the coherent part) and branch cut (the incoherent part). For $1/2 < K < 1$, the poles given by (1.95) are not on the principal λ sheet (see Fig. 1.3 (b)), and $P(t)$ is given only by the branch-cut contribution (incoherent part). Further, for $K > 1$, the leading term gives $P(\lambda) = 1/\lambda$, which leads to $P(t) = 1$ for all t. This is the localization phenomenon first discussed in Refs. [47, 48].

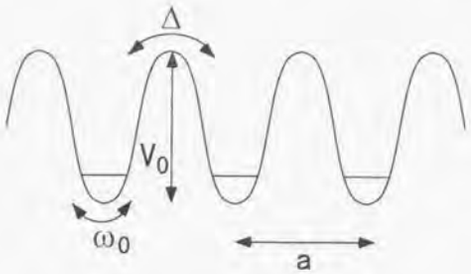

Figure 1.4: The periodic potential considered in the text.

It is possible to follow the behavior of the poles of $P(\lambda)$ as the temperature increases [30]. For $0 < K < 1/2$ there exists the temperature T^*, beyond which the poles disappear. Hence, at $T > T^*$, $P(t)$ is given only by the incoherent part. In other words, T^* gives the coherence temperature of the system. The temperature T^* is evaluated as

$$\frac{T^*}{\Delta_{\mathrm{eff}}} = \begin{cases} 1/\pi K + \mathcal{O}(\ln K), & (K \to 0), \\ 1/\pi + \mathcal{O}(K - 1/2), & (K \to 1/2), \\ 0, & (K > 1/2). \end{cases} \tag{1.97}$$

From these results, the phase diagram in two-state systems with ohmic damping can be drawn (see Fig. 3.2). Later, in Chapter 3, we start with this diagram, and use it to explain a strategy to study a tight-binding model with ohmic damping.

1.2.6 Dissipative multi-state systems

In this subsection, we consider a periodic potential as shown in Fig. 1.4. The typical corresponding Hamiltonian is given by

$$H = H_0 + H_{\mathrm{d}}, \tag{1.98}$$

$$H_0 = \frac{p^2}{2M} - V_0 \cos(2\pi \frac{q}{a}), \tag{1.99}$$

$$H_{\mathrm{d}} = \sum_j \left\{ \frac{p_j^2}{2m_j} + \frac{m_j \omega_j^2}{2} \left(x_j - \frac{c_j}{m_j \omega_j^2} q \right)^2 \right\}, \tag{1.100}$$

where V_0 is the potential strength and a is the period of the potential. This model was first studied to clarify polaronic effects. More recent attention has focused on the influence of an ohmic damping mechanism. The most relevant systems where ohmic damping occurs are small Josephson junction systems, and heavy particle motion in metals, as discussed in the following sections. The tight-binding model can be studied analytically in two regions: the weak corrugation limit $V_0 \ll \omega_0$ and the tight-binding limit $V_0 \gg \omega_0$, where ω_0 is the frequency of small oscillation at potential minima. It has been found that these two regions can be connected by a duality mapping through the parameter mapping:

$$K \leftrightarrow 1/K, \tag{1.101}$$

$$V_0 \leftrightarrow \Delta, \tag{1.102}$$

where Δ is the hopping amplitude between the wells in the tight-binding limit [49, 50]. It has also been claimed by using the method of renormalization groups that a particle is localized for $K > 1$ at all V_0 at zero temperature [50]. The dynamics of a particle has been studied in detail in the weak corrugation limit later [50, 51, 52], and the results have been connected to the tight-binding limit by the duality mapping.

In this subsection, only the tight-binding limit is focused on. The results in this limit can always be connected to the weak corrugation limit by the duality mapping. Further, in this subsection, only the real-time path integral formalism is discussed. The study based on the imaginary-time path integral is the main subject of Chapter 3.

In the limit $V_0 \gg \omega_0$, the model may be mapped to a discrete Hilbert space. When the lattice number is taken as $n = q/a$, the system Hamiltonian H_0 is truncated in a second quantized form as

$$H_0 = -\Delta \sum_l (c_l^\dagger c_{l+1} + c_{l+1}^\dagger c_l) - \varepsilon \sum_l l c_l^\dagger c_l. \tag{1.103}$$

Here, the bias ε is introduced to study transport properties. Based on this model, let us consider dynamics of a single dissipative particle. We assume that the bath is initially in thermal equilibrium and the coupling to the particle is suddenly switched on at $t = 0$. When the particle is prepared to start out at $t = 0$ from the site $n = 0$, the probability $P_n(t)$ for finding the particle at the site n at a later time $t > 0$ is formulated in a similar way to the one adopted in two-state systems. The only difference is that the parameterization

(1.80)-(1.81) is replaced by

$$\chi^{(n)}(t') = \sum_{l=1}^{2m} \chi_l \delta(t' - t_l), \tag{1.104}$$

$$\xi^{(n)}(t') = \sum_{l=1}^{2m} \xi_l \delta(t' - t_l), \tag{1.105}$$

where $\xi_l = \pm 1$ and $\chi_l = \pm 1$. Then, $P_n(t)$ is formulated as [53, 1]

$$\begin{aligned} P_n(t) &= \sum_{m=|n|}^{\infty} (-1)^{m-n} \Delta^{2m} \int_0^t \mathrm{d}t_{2m} \int_0^{t_{2m}} \mathrm{d}t_{2m-1} \cdots \int_0^{t_2} \mathrm{d}t_1 \\ &\times \sum_{\{\xi_l\}'} B_{2m} G_{2m} \sum_{\{\chi_l\}'} H_{2m}, \end{aligned} \tag{1.106}$$

$$B_{2m} = \exp\left(-\mathrm{i}\varepsilon \sum_{l=1}^{2m} \xi_l t_l\right), \tag{1.107}$$

$$G_{2m} = \exp\left[\sum_{k<l}^{2m} \xi_l \xi_k S(t_l - t_k)\right], \tag{1.108}$$

$$H_{2m} = \exp\left[\mathrm{i} \sum_{l=1}^{2m-1} \chi_l \eta_{l,2m}\right] \tag{1.109}$$

$$\eta_{l,2m} = \sum_{k=l+1}^{2m} \xi_k R(t_k - t_l), \tag{1.110}$$

where $S(t)$ and $R(t)$ are defined by (1.78)-(1.79), and the prime in $\{\xi_l\}'$ and $\{\chi_l\}'$ denotes summation in accordance with the constraints

$$\sum_{l=1}^{2m} \chi_l = 2n, \qquad \sum_{l=1}^{2m} \xi_l = 0. \tag{1.111}$$

The transport properties are studied through the mobility μ defined by

$$\mu = \lim_{t\to\infty} \frac{\langle q(t)\rangle}{Ft}, \tag{1.112}$$

$$\langle q(t)\rangle = \sum_{n=-\infty}^{\infty} anP_n(t), \tag{1.113}$$

where $F = \varepsilon/a$ is an external force on a particle.

The mobility μ was calculated in the literature [51, 53, 54, 55, 56, 57]. However, analytical treatment is possible for few regions only. For simplicity, we restrict ourselves to the ohmic case here.

In the limit of high temperatures and/or strong dissipation, the particle tunnels incoherently. The dynamics is described by a nearest neighbor hopping model in this case, and the

occupation probabilities follow simple master equations [54]. The quantum effects appear only through the tunneling rate. Then, the mobility $\mu(\varepsilon)$ is calculated as [56]

$$\mu(\varepsilon) = \frac{4a^2\Delta^2}{\varepsilon}\int_0^\infty \mathrm{d}t \sin\varepsilon t \sin R(t) e^{-S(t)}. \tag{1.114}$$

The mobility at $T = 0$ is given by

$$\mu(T=0) = \mu_0 2\pi K \sin(\pi K)\left(\frac{\Delta_{\rm eff}}{\varepsilon}\right)^{2-2K}, \tag{1.115}$$

and the linear mobility $\mu_l = \lim_{\varepsilon\to 0}\mu$ is given by

$$\mu_l(T) = \mu_0 2\pi^2 \frac{\Gamma(1+K)}{\Gamma(1-K)}\left(\frac{\Delta_{\rm eff}}{2\pi T}\right)^{2-2K}. \tag{1.116}$$

Here, the linear mobility of a free Brownian particle

$$\mu_0 = \frac{1}{M\gamma} = \frac{a^2}{2\pi K} \tag{1.117}$$

is introduced.

For the special case $K = 1/2$, the expressions (1.106)-(1.110) can be evaluated for arbitrary T, ε, and t. The mobility μ is calculated as

$$\mu(\omega) = \frac{2\mu_0\gamma}{\varepsilon}\mathrm{Im}\varphi(1/2 + \gamma/\pi T + \mathrm{i}\varepsilon/2\pi T), \tag{1.118}$$

where $\varphi(z)$ is the digamma function, and $\gamma = \pi\Delta^2/2\omega_c$.

1.3 Macroscopic Dissipative Systems

In the previous section, theoretical aspects of open systems based on the Caldeira-Leggett phenomenological model have been reviewed. This phenomenological model may be applied to several systems including macroscopic, mesoscopic, and microscopic dissipative systems. In this section, we consider macroscopic systems, where the phenomenological treatment is most effective. Among several macroscopic systems, we mainly focus on Josephson junction systems, because they are most controllable, and treated in Chapter 2.

In Sec. 1.3.1, a general discussion of macroscopic quantum effects is given. Then, in Sec. 1.3.2 and Sec. 1.3.3, Josephson junction systems are reviewed in detail. This review is also an introduction to Chapter 2 and Chapter 3.

1.3.1 Macroscopic quantum phenomena

It is now well known that every particle can show interference patterns, for example in the Young's interference experiments. Interference effects are explained by a linear combination of two distinct states, e. g., two paths through two different holes in the case of Young's experiments. It is, however, unbelievable that the interference effects can occur for macroscopic objects at our ordinary life level. We believe that the interference of macroscopic objects can *never* be observed. In other words, we cannot believe that there exists an entangled state described by a linear combination of 'two distinct macroscopic states'. This problem often called 'Schödinger's cat problem' has been discussed since quantum mechanics was developed in the 1920's. One of the interesting questions arising in the study of this problem is 'to what extend can we enlarge physical systems which show interference phenomena'. This question is often answered pessimistically, because the interference effects are strongly suppressed by decoherence caused by environments coupled to macroscopic objects. Nevertheless, there may exist a possibility that recent experimental developments will enable us to observe linear combinations of macroscopic distinct states in a controlled way at low temperatures [58, 59].

The simplest way to observe quantum effects for macroscopic system experimentally is macroscopic quantum tunneling (MQT). Theoretical approaches to MQT have been considered in several systems: phase difference in Josephson junctions [10, 11], phase in charge density waves (CDW) [60], magnetization of mesoscopic ferromagnetic system [61], and nucleation of bubbles in liquids [62, 63]. Actually, MQT has been observed for some systems. The MQT phenomena, however, do not prove the existence of a linear combination of macroscopic distinct states. To prove this, it is sufficient to observe oscillating behavior in two-state systems, called macroscopic quantum coherence (MQC) [64]. The MQC experiments are very hard to be performed, and the MQC have not been observed yet. Particularly, dissipation is usually so strong to destroy the system coherence as discussed in the previous section.

In the following subsections, theoretical and experimental reviews are given for Josephson junction systems. In these systems, experiments to observe MQT and MQC are expected to be most controllable.

1.3.2 Small Josephson junctions

In this subsection, we consider a small Josephson junction where the phase difference ϕ is spatially uniform in the absence of a magnetic field. The classical dynamics of small single junctions has been investigated phenomenologically in early times [65, 66]. We start with the Josephson relation

$$\frac{d\phi}{dt} = \frac{\Phi_0}{2\pi}V, \tag{1.119}$$

where $\Phi_0 = h/2e$ is a quantum of magnetic flux and V is the voltage across the junction. By using this relation, the dynamics is determined in the equivalent circuit shown in Fig. 1.5. Here, C is the capacitance of the junction and I_0 is the critical current of the junction, and the junction is assumed to be shunted by a parallel ohmic resister R. The junction is biased by external current I. The equation of motion is obtained by considering the balance of current as

$$C\frac{d^2}{dt^2}\left(\frac{\Phi_0}{2\pi}\phi\right) + \frac{1}{R}\frac{d}{dt}\left(\frac{\Phi_0}{2\pi}\phi\right) + I_0 \sin\phi = I, \tag{1.120}$$

where $I_0 \cos\phi$ denotes a Josephson current. If we identify $\frac{\Phi_0}{2\pi}\phi$ with a space coordinate, the capacitance C with a mass, $1/R$ with a damping constant, (1.120) is equivalent to the equation of motion of a mechanical particle in a potential $U(\phi)$. For a current biased junction, this potential is a tilted-washboard potential

$$U(\phi) = -I\phi - I_0 \cos\phi.$$

This system is directly related to the content of Chapter 3 in the tight-binding limit. The mobility calculated in Chapter 3 can be measured directly from the I-V characteristics of the junctions.

By introducing convenient normalizations, (1.120) can be reduced to a simple form

$$\phi_{tt} + \alpha\phi_t + \sin\phi = f. \tag{1.121}$$

Here the time t is measured in units of $1/\omega_p$, where the plasma frequency ω_p is given by $\omega_p = (2\pi I_0/\Phi_0 C)^{1/2}$, which corresponds to the frequency of small oscillations at the bottom of the cosine-potential in case of no bias $I = 0$. The normalized bias current f is defined by $f = I/I_0$, and α is a damping parameter given by $\alpha = (\omega_p RC)^{-1}$.

For this (damped) classical equation of motion, the Caldeira-Leggett theory can be applied [66]. Actually, macroscopic quantum phenomena in Josephson junctions have been

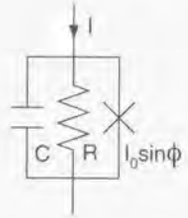

Figure 1.5: The equivalent circuits for a small Josephson junction.

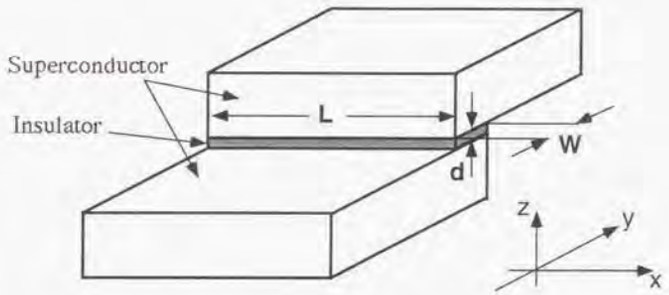

Figure 1.6: Schematic drawing of a long Josephson junction.

studied experimentally, and the results have been compared with theoretical predictions. For current-biased junctions, macroscopic quantum tunneling (MQT) [67, 68] and level quantization [69, 70] have been observed, and for SQUIDs, incoherent quantum tunneling in two-state systems [71, 72], quantum tunneling from metastable states [73], resonant tunneling [74], and generation of a population inversion [75] have been observed.

1.3.3 Long Josephson junctions

In this subsection, let us consider the case where the junction length L is large in the x-direction, and the width W is small in the y-direction as shown in Fig. 1.6. An equivalent circuit diagram is shown in Fig. 1.7. It consists of a series of a small Josephson junctions linked together with inductances L, the physical origin of which is a super current within a

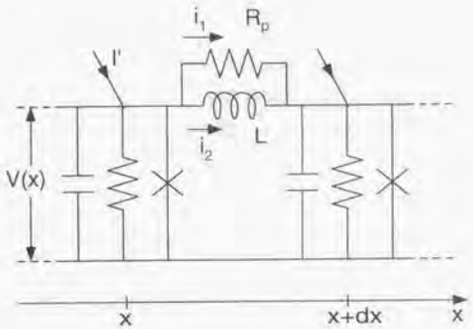

Figure 1.7: The equivalent circuits for a long Josephson junction.

layer of thickness $2\lambda_L$, where λ_L is the London penetration depth [76]. A possible resistance R_p due to a flow of normal electrons in the penetration layer is also considered.

In the equivalent circuit, the current parallel to the x-direction changes spatially. We denote the current with $i(x)$. It is separated into two parts,

$$i(x) = i_1(x) + i_2(x), \tag{1.122}$$

where $i_1(x)$ is the super current through the inductance L, while $i_2(x)$ is the normal current through the resistance, R_p. We may write equations of the long Josephson junction (LJJ),

$$\frac{di}{dx} = -\frac{V}{R'} - I'_0 \cos\phi - C'\frac{dV}{dt} + I', \tag{1.123}$$

$$\frac{dV}{dx} = -L'\frac{di_1}{dt} = -R'_p i_2. \tag{1.124}$$

Here R' and R'_p are the resistances per unit length for the normal current in the y- and x-direction, respectively, while L', C', I'_0, and I' denote the amplitudes of inductance, capacitance, critical current, and external current per unit length of x, i.e.,

$$L' = \frac{\mu_0 2\lambda_L}{W}, \tag{1.125}$$

$$C' = \frac{W\varepsilon_r\varepsilon_0}{d}, \tag{1.126}$$

$$I'_0 = j_0 W, \tag{1.127}$$

$$I' = jW. \tag{1.128}$$

Here μ_0 and ε_0 are, respectively, the magnetic permeability and the dielectric constant in the vacuum, ε_r is the relative dielectric constant, and d is thickness of the insulating oxide barrier, and j_0 and j are the values of the critical current density and the external current density. Using Eqs. (1.124)-(1.128) with the time scaled as in (1.121), the equation of motion is obtained as

$$\phi_{tt} - \frac{\Phi_0}{2\pi\mu_0 2\lambda_L j}\phi_{xx} + \sin\phi + \alpha\phi_t - \beta\phi_{xxt} - f = 0. \tag{1.129}$$

Here the term $\beta\phi_{xxt}$ is a loss term due to the normal electrons in the penetration layer, $\beta = \omega_p L'/R'_p$. Finally normalizing x to the so-called Josephson penetration depth, $\lambda_J = (\Phi_0/2\pi\mu_0 2\lambda_L j_c)^{1/2}$, which gives the size of solitons, one obtains

$$\phi_{tt} - \phi_{xx} + \sin\phi + \alpha\phi_t - \beta\phi_{xxt} - f = 0. \tag{1.130}$$

This is the equation describing the LJJ. The condition where the junction can be treated as one dimensional is given by

$$L \gg \lambda_J \gg W. \tag{1.131}$$

The advantages of the study of LJJs is that various perturbations can be made along the Josephson line. In this situation, various types of macroscopic quantum phenomena may be expected. Macroscopic quantum effects in LJJs are studied theoretically in Chapter 2 from this view point.

1.4 Microscopic Dissipative Systems

1.4.1 Heavy particle motion in metals

In this subsection, dissipative motion of heavy particles, such as muons, are discussed. The interest of this problem expands from the verification of quantum mechanics to applications improving the quality of semiconductors [77]. Particularly, low-energy electronic excitations near the Fermi surface have a strong effect on the motion of heavy particles in metals, and have been studied in detail in Refs. [36, 39, 40, 41, 78, 79]. This problem is reformulated in a simple form based on the path integral [80, 81], which is used in the following discussion.

Since macroscopic classical equations of motion cannot be obtained in this problem, a microscopic description of the particle is necessary. Hence, to study heavy particle motion

in metals, we start with the underlying Hamiltonian

$$H = H_0 + H_R + H_I, \tag{1.132}$$

$$H_0 = \frac{\mathbf{p}^2}{2M} + V(\mathbf{q}), \tag{1.133}$$

$$H_R = \sum_{\mathbf{k},\sigma} \omega_{\mathbf{k}} c^\dagger_{\mathbf{k}\sigma} c_{\mathbf{k}\sigma}, \tag{1.134}$$

$$H_I = \sum_{\mathbf{k},\mathbf{k}',\sigma,\sigma'} \langle \mathbf{k},\sigma|U|\mathbf{k}',\sigma'\rangle - e^{i(\mathbf{k}-\mathbf{k}')\cdot\mathbf{q}} c^\dagger_{\mathbf{k}\sigma} c_{\mathbf{k}'\sigma'}, \tag{1.135}$$

where $c^\dagger_{\mathbf{k}\sigma}$ is the creation operator for a conduction electron with a wave vector $\mathbf{k}$, spin polarization σ, and energy $\omega_{\mathbf{k}}$. Here, for simplicity, the matrix element of the perturbation is assumed to be local, i. e., $\langle \mathbf{k},\sigma|U|\mathbf{k}',\sigma'\rangle = \delta_{\sigma,\sigma'} U_0$. When the self energy is calculated up to the second order of H_I, the action is calculated as

$$\begin{aligned} S_{\rm eff} &= \int_0^\beta d\tau \left(\frac{1}{2}M\dot{\mathbf{q}}^2 + V(\mathbf{q})\right) \\ &+ \frac{3}{2k_F^2}\int_0^\beta d\tau \int_0^\tau d\tau' K(\tau-\tau')\left(1 - \frac{\sin^2(k_F\Delta q)}{(k_F\Delta q)^2}\right), \end{aligned} \tag{1.136}$$

where k_F is the Fermi momentum of the conduction electrons, and $\Delta q = |\mathbf{q}(\tau) - \mathbf{q}(\tau')|$. The kernel $K(\tau)$ is obtained as

$$K(\tau) = \frac{1}{\pi}\int_0^\infty d\omega J(\omega) D_\omega(\tau), \tag{1.137}$$

$$J(\omega) = \eta\omega, \tag{1.138}$$

$$\eta = \frac{4\pi}{3} U_0^2 N_0^2 k_F^2, \tag{1.139}$$

where N_0 is the density of states at the Fermi level. Further, this result may be improved up to the higher order of H_I, and the coefficient η is corrected to [82]

$$\eta = \frac{4}{3\pi} k_F^2 \sin^2\delta_0, \tag{1.140}$$

$$\tan\delta_0 = -\pi U_0 N_0. \tag{1.141}$$

Here, let us consider the case where the path satisfying $k_F\Delta q \sim \Delta q/a \ll 1$ is dominant in the path integral. This case is realized at least in the incoherent hopping region at high temperatures and/or strong damping. In this case, the action (1.136) is simplified as

$$S = \int_0^\beta d\tau \left(\frac{1}{2}M\mathbf{q}^2 + V(\mathbf{q})\right) \tag{1.142}$$

$$+ \frac{1}{2}\int_0^\beta d\tau \int_0^\tau d\tau' K(\tau-\tau')(\mathbf{q}(\tau) - \mathbf{q}(\tau'))^2. \tag{1.143}$$

By comparing this action with (1.10), the Caldeira-Leggett theory is justified to be valid in the present problem. Hence, the result of the Caldeira-Leggett theory is applicable to the problem of heavy particle motion in metals at least in the incoherent hopping region. Actually, the hopping rate of muons in copper has been measured and it has been observed to be proportional to T^{2K-2} at low temperatures (T=10mK∼100mK), where K is the exponent estimated as $K \sim 0.1$ [83, 84]. This behavior is predicted in (1.116) in the Caldeira-Leggett theory with ohmic damping.

Besides the incoherent hopping region, coherent motion of heavy particles in metals has been discussed in Refs. [85, 86, 87, 88, 89]. This problem, however, has not been solved explicitly, and only qualitative discussions such as renormalization group and perturbative treatment have been performed. For this problem, the Caldeira-Leggett theory is not applicable because the path satisfying $k_F\Delta q \gg 1$ is dominant in (1.136) in the coherent region. Thus, unfortunately, the results obtained for the Caldeira-Leggett model for the tight-binding model discussed in Chapter 3 are not applicable in the coherent regime.

1.4.2 Acoustic polarons, interstitials, and defects

In semiconductors and metals, the distortion of the lattice occurs by moving electrons. In this subsection, for simplicity of discussion, we consider the case that the electron-phonon interaction is attributed to the deformation potential with longitudinal acoustic phonons.

In the large-polaron system which is the case for almost semiconductors and metals, the Hamiltonian in the absence of lattice vibrations is given by $H_0 = p^2/2M$, where M is the effective mass [90]. On the other hand, in the opposite small-polaron limit, the particle moves in a discrete lattice. The dynamics of the particle is described by a tight-binding Hamiltonian. This model has first been discussed to study the polarons in molecular crystals [91, 92, 93]. Later, this model has been used to study quantum diffusion of light interstitials and defects [77, 94, 95, 96]. In this subsection, the relation between this small-polaron model and the Caldeira-Leggett model is explained.

The interaction by the deformation potential is given by

$$H_{e-p} = \sum_{\mathbf{k}} v_{\mathbf{k}} \cdot u_{\mathbf{k}} e^{i\mathbf{k}\cdot\mathbf{q}}. \tag{1.144}$$

Here, $v_{\mathbf{k}}$ is the strength of the interaction, and $u_{\mathbf{k}}$ is the normal mode amplitude represented

by annihilation and creation operators as

$$u_{\mathbf{k}} = (2M\omega_{\mathbf{k}})^{-1/2}(b_{\mathbf{k}} + b_{\mathbf{k}}^{\dagger}). \tag{1.145}$$

When we define $g_{\mathbf{k}} = v_{\mathbf{k}}/(2M)^{1/2}$, the total Hamiltonian is written as

$$\begin{aligned} H &= H_0 + H_{\mathrm{p}} + H_{e-\mathrm{p}}, & (1.146)\\ H_0 &= \frac{\mathbf{p}^2}{2M} + V(\mathbf{q}), & (1.147)\\ H_{\mathrm{p}} &= \sum_{\mathbf{k}} \omega_{\mathbf{k}} b_{\mathbf{k}}^{\dagger} b_{\mathbf{k}}, & (1.148)\\ H_{e-\mathrm{p}} &= \sum_{\mathbf{k}} \left(\frac{g_{\mathbf{k}}}{\sqrt{\omega_{\mathbf{k}}}} e^{i\mathbf{k}\cdot\mathbf{q}} b_{\mathbf{k}} + \frac{g_{\mathbf{k}}^*}{\sqrt{\omega_{\mathbf{k}}}} e^{-i\mathbf{k}\cdot\mathbf{q}} b_{\mathbf{k}}^{\dagger} + \sum_{\mathbf{k}} \frac{|g_{\mathbf{k}}|^2}{\omega_{\mathbf{k}}^2} \right), & (1.149) \end{aligned}$$

where the last term in $H_{e-\mathrm{p}}$ is a counter term to adjust the zero energy. In an isotropic medium, the dispersion of acoustic phonons is given as $\omega_{\mathbf{k}} = c|\mathbf{k}|$ at small frequencies, where c is the velocity of sound. Then, the coupling coefficient becomes a function of ω, and takes a simple power-law form for small ω as

$$g(\omega) = g_0 \left(\frac{\omega}{\tilde{\omega}}\right)^{\lambda} \quad \text{for} \quad \omega \ll \omega_c, \tag{1.150}$$

where $\tilde{\omega}$ is the appropriate reference frequency, and ω_c is the cut-off frequency of the order of the Debye frequency. The power λ is determined by the geometry of crystals [77, 94, 96]. For the case where there exists only one stable site of interstitials or defects in the unit cell, we take $\lambda = 1$, and otherwise $\lambda = 0$.

The phonon variables can be traced out in the following way. The partition function is written in the influence functional forms as

$$\begin{aligned} Z &= Z_{\mathrm{phonon}} \oint \mathcal{D}\mathbf{q}(\tau) \exp\left(-\int_0^{\beta} \mathrm{d}\tau H_0[q(\tau)]\right) F[\mathbf{q}(\tau)], & (1.151)\\ F[\mathbf{q}(\tau)] &= \langle T_\tau \exp\left[-\int_0^{\beta} \mathrm{d}\tau \tilde{H}_{e-\mathrm{p}}(\tau)\right]\rangle_\beta. & (1.152) \end{aligned}$$

Here, T_τ is the imaginary-time ordering operator, and $\langle\cdots\rangle_\beta$ denotes the thermal average with respect to non-interacting phonons H_{p}. The coupling term $\tilde{H}_{e-\mathrm{p}}(\tau)$ in the interacting picture is calculated as

$$\tilde{H}_{e-\mathrm{p}}(\tau) = \sum_{\mathbf{k}} \left(\frac{g_{\mathbf{k}}}{\sqrt{\omega_{\mathbf{k}}}} e^{i\mathbf{k}\cdot\mathbf{q}(\tau) - \omega_{\mathbf{k}}\tau} b_{\mathbf{k}} + \frac{g_{\mathbf{k}}^*}{\sqrt{\omega_{\mathbf{k}}}} e^{-i\mathbf{k}\cdot\mathbf{q}(\tau) + \omega_{\mathbf{k}}\tau} b_{\mathbf{k}}^{\dagger} \right). \tag{1.153}$$

To calculate $F[\mathbf{q}(\tau)]$, we expand (1.152) into a series in $\tilde{H}_{e-\mathrm{p}}$ and use Wick's theorem. The series can be exactly summed up as

$$F[\mathbf{q}(\tau)] = \exp\left(\int_0^{\beta} \mathrm{d}\tau \int_0^{\tau} \mathrm{d}\tau' \langle \tilde{H}_{e-\mathrm{p}}(\tau)\tilde{H}_{e-\mathrm{p}}(\tau')\rangle_\beta\right). \tag{1.154}$$

By substituting (1.153), the influence functional is evaluated as

$$\begin{aligned} F[\mathbf{q}(\tau)] &= \exp(-S_{\mathrm{inf}}[\mathbf{q}(\tau)]), & (1.155)\\ S_{\mathrm{inf}}[\mathbf{q}(\tau)] &= \sum_{\mathbf{k}} \frac{g_{\mathbf{k}}^2}{\omega_{\mathbf{k}}} \int_0^{\beta} \mathrm{d}\tau \int_0^{\tau} \mathrm{d}\tau' D_{\omega_{\mathbf{k}}}(\tau - \tau') \left\{1 - e^{i\mathbf{k}\cdot(\mathbf{q}(\tau) - \mathbf{q}(\tau'))}\right\}, & (1.156)\\ D_\omega(\tau) &= \frac{\cosh[\omega(\beta/2 - \tau)]}{\sinh(\beta\omega/2)} & (1.157) \end{aligned}$$

where the first term in the curly bracket is due to the counter term in (1.149).

In the small-polaron system, we can assume that the relevant contribution in (1.156) comes from $\mathbf{k}$ values which satisfy $|\mathbf{k}|a \ll 1$, where a is the period of the lattice potential. The Caldeira-Leggett action is then obtained by expanding (1.156) around $k = 0$ as

$$\begin{aligned} S'_{\mathrm{inf}}[\mathbf{q}(\tau)] &= \frac{1}{2} \int_0^{\beta} \mathrm{d}\tau \int_0^{\tau} \mathrm{d}\tau' K(\tau - \tau')(\mathbf{q}(\tau) - \mathbf{q}(\tau'))^2, & (1.158)\\ K(\tau) &= \frac{1}{\pi} \int_0^{\infty} \mathrm{d}\omega J(\omega) D_\omega(\tau), & (1.159) \end{aligned}$$

Here, we should note that the Caldeira-Leggett action is justified when the difference of the coordinate is small ($|\mathbf{q}(\tau) - \mathbf{q}(\tau')| \sim a$). This condition is well satisfied, when we assume that the paths which move to the neighboring site and return to the original site are dominant. In other words, this condition is satisfied when physical quantities such as the conductivity are well approximated by the terms of the order of Δ^2 in series of Δ, where Δ is the hopping amplitude. On the other hand, for the case where the paths with large coordinate difference $|\mathbf{q}(\tau) - \mathbf{q}(\tau')| \gg a$ are dominant, i. e., for the case where the higher order terms of Δ are not small, there may exists qualitative differences between the Caldeira-Leggett model (1.159) and the polaron model (1.156).

The spectral function $J(\omega)$ in (1.159) is expressed by using the spectral density of phonons $\rho(\omega)$ as

$$J(\omega) = \frac{\pi}{D}\rho(\omega)\left(\frac{\omega}{c}\right)^2 \frac{g(\omega)^2}{\omega}. \tag{1.160}$$

Here, D is the dimension of space. From the theoretical view point, the exponent of ω in $J(\omega)$ at $\omega = 0$ controls the dissipation properties. The spectral density of the phonons

takes the form $\rho(\omega) = \rho_0 \omega^{D-1}$ for small ω, where ρ_0 is a constant. Hence, $J(\omega)$ behaves as $J(\omega) \sim \omega^{D+2\lambda}$ for small ω.

The ohmic damping ($J(\omega) \propto \omega$) is obtained when $\lambda = 0$ and $D = 1$. Note that in this case, the spectral density of phonons diverges at $\omega = 0$ as ω^{-1}. Though this case is unrealistic, it can be related to the ohmic dissipative tight-binding model which is discussed in Sec. 3.3. Here, we must be careful to the condition to justify the Caldeira-Leggett model in the small-polaron problem. As noted already, if the higher order terms of Δ are dominant in physical quantities, the Caldeira-Leggett theory cannot be applied to this problem. Actually, in the low-temperatures and weak-damping region, the higher order terms of Δ are dominant within the Caldeira-Leggett theory. Hence, in this region, we cannot connect the results obtained in Sec. 3.3 to the polaron problem.

Chapter 2

Quantum Effects in Long Josephson Junctions

In this chapter, macroscopic quantum effects in long Josephson junctions are considered. This chapter consists of two parts. In the first part, quantum effects of a single dissipative soliton in long Josephson junctions are studied, while in the latter part quantum effects of two half vortices in long Josephson junctions including so-called π junctions are studied. The content of this chapter is already published [2, 3].

In both cases, the Caldeira-Leggett theory can be applied, since the system is macroscopic, and has a limit described by a classical equation of motion. The tunneling rate in these systems is formulated within the WKB method as discussed in Sec. 1.2.3.

2.1 Long Josephson Junctions with Inhomogeneities

2.1.1 Introduction

It is commonly recognized that the sine-Gordon equation plays an outstanding role in many physical problems. One of the most important applications is a long Josephson junction (LJJ). It is believed that dynamics of the phase difference ϕ in LJJs is well described by a classical equation [76]

$$\phi_{tt} - \phi_{xx} + \sin\phi + \alpha\phi_t - \beta\phi_{xxt} + f = 0, \tag{2.1}$$

Here x and t are measured in units of the Josephson penetration length λ_J and of the inverse Josephson plasma frequency ω_p^{-1}, respectively. The dissipation coefficient α is related to quasiparticle tunneling through the oxide barrier, and β is related to the normal current of quasiparticle parallel to the junction. The external current f is assumed to be spatially uniform.

It is known that solitons in the form of fluxons propagate along the junction following the classical equation (2.1). Experimentally, fluxons in LJJs were first observed indirectly by zero-field steps on the current voltage (I-V) characteristics of the junction [97]. The zero-field steps are well explained by fluxon propagation governed by Eq. (2.1) with repeated reflections at the open ends of the junction[98]. Since then, development of experimental techniques has made it possible to directly observe profiles of separate fluxons and a space-time pattern of their interaction [99, 100].

These experiments are basically explained by 'classical' theories, and there is no clear experimental indication so far which needs 'quantum' theories to explain its results. One might argue that it is natural to expect an essentially classical motion for a single fluxon of the size of micrometers. However, in this section we show that quantum effects can indeed show up in this extended object. Recently, Hermon *et al.* discussed the quantum dynamics of a single fluxon in a long circular Josephson junction [101]. In a subsequent paper [102], they discussed a possible fluxon interference experiment. However in those papers, decoherence effects due to couplings to the environment, i. e., dissipation has completely been neglected. From the study in dissipative two-level systems [30], it is expected that the quantum effects are strongly suppressed by the dissipation so that in real experiments, the observation of the quantum effects proposed by Hermon *et al.* may be much more difficult than in the ideal case without dissipation.

In this section, we propose other experiments to observe quantum effects of a single fluxon. The effect which we deal with here is quantum tunneling of a fluxon. The quantum tunneling phenomenon is one of the most typical ones which cannot be explained by classical theories. Because a fluxon is a macroscopic object with a length scale of micrometers, the quantum tunneling of a fluxon can be recognized as the macroscopic quantum tunneling (MQT). Further, I believe that the methods to treat quantum tunneling of a fluxon is applicable to the study of a vortex in one or two dimensional Josephson arrays.

To consider the quantum tunneling of a fluxon, we introduce structural inhomogeneities

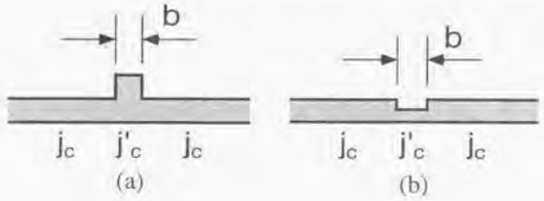

Figure 2.1: Schematic drawings of (a) a microresister ($j_c > j_c'$) and (b) a microshort ($j_c < j_c'$). The normalized strength of pinning is given by $\varepsilon = b(j_c - j_c')/j_c\lambda_J$ in both cases. Here b is the length of the area where the critical current is modified.

which capture a fluxon at a certain point in a Josephson junction line. Such inhomogeneities have been studied by McLaughlin and Scott in a pioneering paper [103]. In that paper, they have considered the interaction between a fluxon and a microresister (i. e., a narrow region where critical current density j_c is reduced to j_c') or a microshort (i. e., a narrow region with an enhanced critical current density). Schematic drawings of these inhomogeneities are shown in Fig. 2.1. McLaughlin and Scott have proposed a model of LJJs with a local inhomogeneity in the form of the equation of motion

$$\phi_{tt} - \phi_{xx} + \sin\phi + \alpha\phi_t - \beta\phi_{xxt} + f - \varepsilon\delta(x)\sin\phi = 0. \tag{2.2}$$

The last term on the left hand side represents a local change of the critical current density at $x = 0$. The normalized strength of the inhomogeneity ε is defined by $\varepsilon = b(j_c - j_c')/j_c\lambda_J$. The cases $\varepsilon > 0$ and $\varepsilon < 0$ correspond to a microresister and a microshort, respectively. When $\varepsilon > 0$ (i. e., a microresister), the fluxon is attracted to the microresister and captured there if the fluxon does not have enough kinetic energy. In other words, the microresister plays a role of a pinning potential for the fluxon. We only deal with the case $\varepsilon > 0$, i. e., microresisters. Throughout this section, we assume $b \ll \lambda_J$ (i. e. $\varepsilon \ll 1$) so that the soliton size is larger than b to justify the description by $\delta(x)$ in (2.2) for the microresister.

2.1.2 Formulation

In this subsection, we first derive the classical equation of motion for a fluxon. For this purpose, we analyze the equation (2.2) with the assumption that the parameters α, β, f,

and ε are all small. In this case, Eq. (2.2) can be considered as a perturbed sine-Gordon equation. The soliton solution of the unperturbed sine-Gordon equation takes the form of a kink

$$\phi_0(x,t;u) = 4\arctan\left[\exp\left(\frac{x-q(t)}{(1-u^2)^{1/2}}\right)\right], \tag{2.3}$$

which corresponds to a fluxon in LJJs. Here $q(t) = ut$ is the center coordinate of the kink, and u is the kink velocity ($|u| < 1$). The velocity is normalized by the light velocity, $\bar{c} = \lambda_J\omega_p$. In this section, we only discuss the nonrelativistic limit $|u| \ll 1$.

Based on the kink solution (2.3), the classical perturbation theory can be applied to Eq. (2.2). McLaughlin and Scott have shown that the perturbations only affect dynamics of the center coordinate $q(t)$ and do not change the form of the kink within the lowest approximation [103]. The equation of motion for $q(t)$ is obtained as

$$m\ddot{q} + m\Big(\alpha + \frac{\beta}{3}\Big)\dot{q} + \frac{\partial V(q)}{\partial q} = 0, \tag{2.4}$$

in the nonrelativistic limit. Here m is the classical soliton mass and identically equals to 8. Note that the damping strength working on the dynamics of a fluxon is related to α and β which are the coefficients of the dissipative terms in the field equation (2.2) for $\phi(x,t)$. The effective potential $V(q)$ for a fluxon is given by

$$V(q) = -2\pi f q - \frac{2\varepsilon}{\cosh^2 q}. \tag{2.5}$$

The first term is a driving force due to the external current, and the second term is a pinning potential caused by the microresister located at the origin.

As shown in Eq. (2.4), the classical equation of motion for a fluxon includes a damping term due to the fact that the phase difference ϕ is a macroscopic variable. To deal with dissipation effects on MQT of a fluxon phenomenologically, the Caldeira-Leggett model is introduced as

$$H = \frac{p^2}{2m} + V(q) + \sum_j \frac{1}{2}\left[\frac{p_j^2}{m_j} + m_j\omega_j^2\Big(x_j - \frac{c_j}{m_j\omega_j^2}q\Big)^2\right]. \tag{2.6}$$

Here $p = m\dot{q}$ is a momentum variable conjugate to q, whereas q_j and $p_j = m\dot{q}_j$ are a space coordinate and a momentum of harmonic oscillators, respectively. The reservoir parameters m_j, ω_j, and c_j are characterized by the spectral function

$$J(\omega) = \frac{\pi}{2}\sum_j \frac{c_j^2}{m_j\omega_j}\delta(\omega - \omega_j). \tag{2.7}$$

We choose the spectral function as

$$J(\omega) = m\Big(\alpha + \frac{\beta}{3}\Big)\omega. \tag{2.8}$$

Then, the classical equation (2.4) is derived from the Hamiltonian (2.6) by eliminating the reservoir degrees of freedom.

From this model, we obtain the partition function Z after integrating out the reservoir degrees of freedom as

$$Z = Z_R \oint \mathcal{D}q(\tau)\exp\Big(-\frac{1}{g^2}S_{\rm eff}[q(\tau)]\Big). \tag{2.9}$$

Here Z_R is the partition function of the unperturbed reservoir, and g^2 is the normalized Planck constant defined in the next subsection. The effective action $S_{\rm eff}$ is calculated as

$$S_{\rm eff}[q(\tau)] = \int_0^{1/T} d\tau\Big(\frac{1}{2}m\dot{q}^2 + V(q)\Big) + \frac{1}{2}\int_0^{1/T} d\tau \int_0^{\tau} d\tau' K(\tau-\tau')\Big(q(\tau) - q(\tau')\Big)^2, \tag{2.10}$$

where T is a temperature normalized by ω_p. The kernel $K(\tau)$ is defined by

$$K(\tau) = \frac{1}{\pi}\int_0^\infty m\Big(\alpha + \frac{\beta}{3}\Big)\omega D_\omega(\tau)\,d\omega, \tag{2.11}$$

$$D_\omega(\tau) = \frac{\cosh[\,\omega(1/2T - |\tau|\,)\,]}{\sinh(\omega/2T)}. \tag{2.12}$$

In the later subsections, we make an estimate of the tunneling rate based on the effective action (2.10). Although the derivation of the effective action is quite intuitive, it has been proven that the action (2.10) can be derived from the classical equation of motion (2.2) by using the semiclassical approximation in the Caldeira-Leggett theory [2].

2.1.3 Experimental parameters

In this subsection, we summarize controllable experimental parameters relevant to the quantum tunneling of a fluxon. A layout of a LJJ is shown in Fig. 2.2, and experimentally realizable parameters within the available techniques are given in Table 2.1. The values given in the table are indeed typical ones in actual experiments [104]. The width of the Josephson junction W is now a controllable variable and scaled by micrometers. In this subsection, $\hbar$ is revived to clarify discussion.

First, we associate the experimental parameters with the parameters in the normalized sine-Gordon equation (2.1). In the derivation of (2.1), the normalized length, time, and

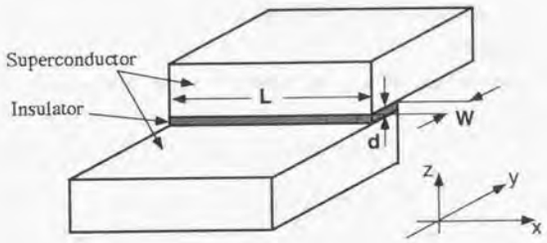

Figure 2.2: A layout of a LJJ. The junction length L is taken large enough compared with the junction width W.

Table 2.1: Experimental parameters used for an estimate.

Parameters	Estimated value
d : Thickness of the junction	2 [nm]
ε_r : Relative dielectric constant	8
j_c : Critical current density	3×10^6 [A/m^2]
W : Width of the junction	W [μm] (variable)
λ_L : London penetration length	60 [nm]

energy are introduced. In the original unit, the equation of motion without inhomogeneities is written as

$$\omega_p^{-2}\phi_{tt} - \lambda_J^2\phi_{xx} + \sin\phi + \alpha\omega_p^{-1}\phi_t - \beta\omega_p^{-1}\lambda_J^2\phi_{xxt} + j/j_c = 0. \tag{2.13}$$

Here, j is the external current density applied to the junction.

The length scale in the LJJ is given by the Josephson penetration length λ_J, which may be varied in the range from 20 [μm] to 200 [μm] by controlling the critical current density j_c [99]. In the present estimate, λ_J is obtained as

$$\lambda_J = \left(\frac{\Phi_0}{4\pi\mu_0\lambda_L j_c}\right)^{1/2} \sim 27\ [\mu\text{m}]. \tag{2.14}$$

Here $\Phi_0 = h/2e$ is the unit flux and $\mu_0(= 4\pi \times 10^{-7}\ [\text{Hm}^{-1}])$ is the permeability of the vacuum.

The time is scaled by ω_p^{-1} where ω_p is the plasma frequency of the Josephson junction, which is estimated from the values given in Table 2.1 as

$$\omega_p = \left(\frac{2\pi j_c d}{\Phi_0\varepsilon_r\varepsilon_0}\right)^{1/2} \sim 5.1 \times 10^{11}\ [1/\text{s}], \tag{2.15}$$

where $\varepsilon_0(= 8.85 \times 10^{-12}\ [\text{Fm}^{-1}])$ is the dielectric constant of the vacuum. Note that ω_p is independent of W. From this estimate, the plasmon excitation gap is estimated as

$$\hbar\omega_p \sim 3.9\ [\text{K}]. \tag{2.16}$$

Well below this temperature, the plasmon excitations can be neglected.

The energy is measured by a unit energy E_0.

$$E_0 = \frac{\Phi_0}{2\pi} j_c W \lambda_J \sim 1.93 \times 10^3 W\ [\text{K}]. \tag{2.17}$$

From this, the energy of a single fluxon is obtained.

$$8E_0 \sim 1.55 \times 10^4 W\ [\text{K}] \tag{2.18}$$

where the factor 8 comes from the dimensionless mass of a fluxon. The energy of a single fluxon is so large that nucleation of soliton-antisoliton pairs can be neglected at sufficiently low temperatures.

The normalized Planck constant g^2 is given as

$$g^2 = \frac{\hbar\omega_p}{E_0} = \frac{16\pi}{137}\left(\frac{2\lambda_J d}{W^2\varepsilon_t}\right)^{1/2}. \tag{2.19}$$

Note that g^2 is independent of the critical current j_c. In the present estimate, the value of g^2 becomes

$$g^2 \sim \frac{2.0\times 10^{-3}}{W}. \tag{2.20}$$

When $W \sim 1[\mu\mathrm{m}]$, we get a small value, $g^2 \sim 0.002$.

The mass of a fluxon is estimated as

$$m_f = \frac{8E_0}{\bar{c}^2} \sim 1.25\times 10^{-3} W\, m_e, \tag{2.21}$$

where m_e is the electron mass and $\bar{c}$ is defined by $\bar{c} = \lambda_J\omega_p$. Since we find that the fluxon mass is remarkably small ($\sim 10^{-3} m_e$ if we take W as 1 $[\mu\mathrm{m}]$), we can expect substantial quantum effects of fluxons, in spite of the large fluxon size and the small normalized Planck constant. Moreover, it should be noted that m_f is proportional to the junction width W. Hence, the fluxon mass can be controlled by changing the value of W.

Finally, we estimate the dissipation coefficients α and β. The coefficient α is related to the quasiparticle resistance per area r_{qp} as $\alpha = 1/r_{qp}C'\omega_p$. Here, $C' = \varepsilon_r\varepsilon_0/d$ is the capacitance per unit area. This relation has been obtained experimentally by Pedersen and Welner [105]. The quasiparticle resistance r_{qp} obtained below the gap voltage is strongly enhanced at low temperatures. Hence, the dissipation coefficient α becomes very small at sufficiently low temperatures of mK order.

To make a comparison, we introduce a dissipation coefficient α_n defined by $\alpha_n = 1/r_n C'\omega_p$. Here, r_n is the normal resistance obtained above the gap voltage. Since r_n is much smaller than r_{qp}, the dissipation coefficient α_n gives the upper limit for α, i. e., $\alpha \ll \alpha_n$. Then, r_n can be associated with j_c as [106]

$$j_c r_n = \frac{\pi\Delta_0}{2e}, \tag{2.22}$$

at sufficiently low temperatures ($k_B T \ll \Delta_0$). Here Δ_0 is the gap of the superconducter at zero temperature. From (2.15) and (2.22) we obtain

$$\alpha_n = \frac{\hbar\omega_p}{\pi\Delta_0}, \tag{2.23}$$

which gives a good estimate for α_n. Using $\Delta_0 = 14[\mathrm{K}]$ and (2.15), we have $\alpha_n = 0.088$. Thus, we evaluate $\alpha \ll 0.088$.

The dissipation coefficient β also originates from quasiparticle current. It has been observed that the ratio between α and β is independent of the temperature [104, 107]. Hence, it is expected that β is also strongly suppressed at sufficiently low temperatures. We estimate the upper bound for β as $\beta \ll 0.01$, which is an experimentally determined value by Davidson *et al.* [104, 107] at relatively high temperatures ($\sim 4\,[\mathrm{K}]$). This evaluation for β is rough, because the experimental situation in Ref. [104] is rather different from the ones employed in this section. The dissipation amplitude $\alpha + \beta/3$ is, however, not changed drastically even if β is enlarged several times, because α is expected to be dominant in the dissipation amplitude.

On the basis of the values given in this subsection, we estimate the tunneling rate in the later subsections.

2.1.4 Quantum tunneling from a metastable state

In this section, we consider the quantum tunneling from a metastable state made by a single microresister in a LJJ. First, we formulate the decay rate using the Langer's WKB method. The potential form $V(q)$ is given as

$$V(q) = -2\pi f q - \frac{2\varepsilon}{\cosh^2 q}. \tag{2.24}$$

The first term is the driving force due to the external current, and the second term is the pinning potential caused by a single microresister. If f is small, the potential $V(q)$ has a metastable state at $q = q_0$ defined by $V'(q_0) = 0$. However, if f is increased and takes a critical value f_c, the metastable state disappears. The critical value f_c is calculated as

$$f_c = \frac{4\varepsilon}{3\sqrt{3}\pi} \simeq 0.245\varepsilon (\ll 1). \tag{2.25}$$

When the external current f is taken as $f = f_c - \eta$ ($\eta > 0$), the potential energy has a barrier V_0 as shown in Fig. 2.3. To observe quantum tunneling in the laboratory, V_0 must be small. Hence, we assume $\eta \ll f_c$. The potential is approximated by the quadratic-plus-cubic potential around a metastable state as

$$V(x) = -\frac{16\varepsilon}{9\sqrt{3}}x^3 + \sqrt{\frac{32\pi\varepsilon\eta}{3\sqrt{3}}}x^2, \tag{2.26}$$

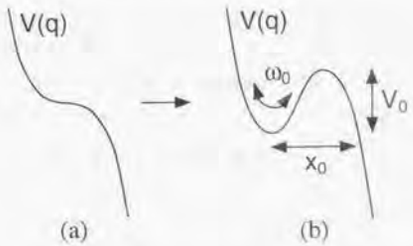

Figure 2.3: The potential form $V(q)$ for a fluxon (a) when the external current f is taken as the critical value f_c, and (b) when f is taken as a slightly smaller value $f = f_c - \eta(\eta > 0)$ than f_c.

where the origin of the coordinate x is located at a metastable state ($q = q_0 + x$). From this approximated potential, the potential barrier height V_0 is calculated as

$$V_0 = \sqrt{\frac{8\pi^3\eta^3}{\sqrt{3}\varepsilon}} \simeq 12.0\varepsilon^{-1/2}\eta^{3/2}. \tag{2.27}$$

The frequency of small oscillations around the metastable minimum defined by $\omega_0 = (V''(0)/m)^{1/2}$ is also obtained as

$$\omega_0 = \left(\frac{2\pi\varepsilon\eta}{3\sqrt{3}}\right)^{1/4} \simeq 1.05\varepsilon^{1/4}\eta^{1/4}, \tag{2.28}$$

where the fluxon mass $m = 8$ has been substituted. Note that V_0 and ω_0 are normalized by E_0 and the plasma frequency ω_p, respectively.

The quantum decay rate from the metastable state at $T = 0$ can be calculated by applying Langer's method to the effective action (2.10). The tunneling rate Γ takes the form

$$\Gamma = A\exp(-B). \tag{2.29}$$

The exponent B is determined by the action of the bounce path $q_B(\tau)$ which minimizes the effective action (2.10). The explicit forms of A and B are obtained only for the limiting cases. In actual experiments, the damping coefficient $\alpha + \beta/3$ in Eq.(2.4) is small (< 0.1 in the present estimate). Then, the estimate in the weak damping limit, (1.37)-(1.38) can

be used. The parameters A and B are then estimated as

$$\begin{aligned} A &= \sqrt{60}\omega_0\omega_p\left(\frac{B}{2\pi}\right)^{1/2}(1+\mathcal{O}(a)), && (2.30)\\ B &= \frac{36V_0E_0}{5\hbar\omega_0\omega_p}\left(1+1.74a+\mathcal{O}(a^2)\right) \\ &\simeq \frac{82.2\eta^{5/4}\varepsilon^{-3/4}}{g^2}(1+1.74a+\mathcal{O}(a^2)), && (2.31)\end{aligned}$$

where $a = (\alpha + \beta/3)/2\omega_0$. Since the predominant effect of the dissipation appears in the exponent of the decay rate, the correction for the prefactor due to the dissipation may be neglected.

Since g^2 takes a small value as given in Sec. 2.1.3, the exponent B takes a fairly large value. To observe MQT of a fluxon in a time scale of the laboratory, we need to take a small value of the parameter η to increase the decay rate. For example, if we take $\eta = 5\times10^{-4}$, $\varepsilon = 0.1$, then the values of V_0 and $\hbar\omega_0$ are estimated from (2.27) and (2.28) as

$$\begin{aligned} V_0E_0 &\sim 0.82W\,[\mathrm{K}], && (2.32)\\ \hbar\omega_0\omega_p &\sim 0.34\,[\mathrm{K}], && (2.33)\end{aligned}$$

in the original unit. We note that $\eta = 5\times10^{-4}$ and $\varepsilon = 0.1$ are not difficult to be realized experimentally. When $W = 1[\mu\mathrm{m}]$ and dissipation effects are neglected ($\alpha = \beta = 0$), the tunneling rate Γ is estimated from (2.29) with (2.30)-(2.31) as

$$\Gamma \sim 2\times10^4[1/\mathrm{s}]. \tag{2.34}$$

Even for the strongly damped case ($\alpha = 0.088, \beta = 0.01$), if η is reduced to 2×10^{-5}, the tunneling rate is estimated as

$$\Gamma \sim 4\times10^6[1/\mathrm{s}]. \tag{2.35}$$

These results indicate that it is possible to observe the MQT in controlled experiments. Actually, a proper apparatus to observe MQT in LJJs efficiently has been proposed in Ref. [2].

2.1.5 Quantum tunneling in two-state systems

In this subsection, we study a two-state system made by two microresisters. In classical mechanics, a fluxon may stay at either of two stable states at zero temperature. In quantum

mechanics, however, quantum tunneling through the energy barrier is possible. When the energy levels of the ground state at each well is the same and dissipation is neglected, the quantum tunneling makes an energy splitting and generates oscillation of a fluxon between the two wells retaining the coherence. This macroscopic effect is called quantum macroscopic coherence (MQC).

When there exists no external current ($f = 0$), we obtain the potential made by two microresisters as

$$V(q) = -\frac{2\varepsilon}{\cosh^2(q - l/2)} - \frac{2\varepsilon}{\cosh^2(q + l/2)}, \tag{2.36}$$

where the origin of q is taken at the midpoint of the resistors, and the distance between the resistors is denoted with l. The potential $V(q)$ has only one stable state for small l, while the potential has a double well structure, when $l > l_0$. The critical length l_0 is given by

$$l_0 = \ln\left(\frac{\sqrt{3}+1}{\sqrt{3}-1}\right) \simeq 1.317. \tag{2.37}$$

We only consider the case where the potential barrier is small. In this situation, we may assume $l = l_0 + a$ with $a \ll 1$. The potential term can be expanded around $q = 0$ as

$$V(q) = \frac{32}{27}\varepsilon q^4 - \frac{16}{3\sqrt{3}}\varepsilon a q^2. \tag{2.38}$$

From this potential, the position of the stable states is obtained as $q = \pm q_0$ where

$$q_0 = \sqrt{\frac{3\sqrt{3}}{4}a} \simeq 1.14a^{1/2}. \tag{2.39}$$

When $a \ll 1$, we obtain $q_0 \ll 1$ and the expansion in the form of the potential (2.38) is valid around the two stable states.

The amplitude of the dissipation is determined by a dimensionless quantity K as

$$K = m\left(\alpha + \frac{\beta}{3}\right)\frac{(2q_0)^2}{2\pi g^2}. \tag{2.40}$$

Here $m = 8$ is the mass of a fluxon. By using the estimated values of g^2, we estimate K as

$$K \sim 3.3 \times 10^3\left(\alpha + \frac{\beta}{3}\right)aW. \tag{2.41}$$

Note that K is independent of details of the potential form and determined by the distance between potential minima $2q_0$ and the width of the junction W.

To estimate K, we assume that the ratio between α and β is temperature independent [104, 107]. Then, because β is not dominant in the dissipation amplitude $\alpha + \beta/3$ at relatively high temperatures as is observed experimentally [105], we expect that β is not dominant also at low temperatures. Hence we neglect the β-term, and estimate the value of K roughly as

$$K \sim 3 \times 10^2 aW\frac{\alpha}{\alpha_0} = 3 \times 10^2 aW\frac{r_n}{r_{qp}}. \tag{2.42}$$

Here, we inserted the dissipation coefficient $\alpha_0 = 0.088$ estimated in Sec. 2.1.3. The ratio between the normal resistance r_n and the quasiparticle resistance r_{qp} can be obtained experimentally.

The condition to observe MQC is given as [30, 64]

$$K \ll 1 \quad \text{and} \quad k_B T \ll \hbar\Gamma/K. \tag{2.43}$$

If $a = 0.1$, $W = 1$, and $r_n/r_{qp} = 10^{-3}$ can be realized, the estimated value of $K(\sim 0.03)$ seems to satisfy the first conditions in (2.43). Although the estimate of the ratio $r_n/r_{qp} = 10^{-3}$ is very rough, it seems to be attainable at low temperatures of the order of mK [105]. Hence, we expect that the observation of MQC in LJJs appears to be possible within the Caldeira Leggett theory.

Recently the incoherent tunneling has been reported in a SQUID system [72]. In the experiment, it has been observed that the tunneling rate follows a power law as a function of temperature. The dissipation strength K has been determined from the power as $K = 1.44$. This dissipation strength is larger than the damping on a fluxon in LJJs. Hence, it is expected that MQC may be observed more easily in LJJs. Here, however, we should be careful that the origin of damping has not been understood clearly yet [66, 72]. Hence, we cannot comment on the possibilities to observe MQC in LJJs further.

2.1.6 Concluding remarks of this section

In this section, we have studied two kinds of quantum tunneling for a single fluxon. We have found that the quantum tunneling from a metastable state may be observed at low temperatures (mK order), and that the junction width should be as small as possible. If the junction width is taken as $\sim 1[\mu m]$, the required accuracy of current measurement seems attainable in the laboratory. We have also found that the observation of MQC in a two-state system in LJJs appears to be possible, because dissipation due to the quasiparticle

tunneling is strongly suppressed at low temperatures. It should be noted, however, that the damping amplitude may increase by other dissipation sources. In the experiment on SQUIDs [72], the observed damping amplitude is larger than the one estimated by quasiparticle resistance.

The most characteristic feature of LJJs is that the phase difference ϕ has a spatial dependence. In other words, ϕ is a field variable with infinite degrees of freedom. This opens the possibility of studying combined effects of macroscopic quantum phenomena and many-body effects. In this section, however, dynamics of only one degree of freedom, i. e., the center position of the fluxon has been considered as the first attempt. Other infinite degrees of freedom of the field appear in the form of plasmons. They do not play an important role in quantum dynamics of a fluxon because of two reasons: (i) plasmon excitations have an energy gap, and plasmons are suppressed at low temperatures; (ii) in the lowest order of g^2, plasmons are decoupled from the fluxon. Hence, within the present study, characteristic features of the field with infinite degrees of freedom do not appear. To study many-body effects of the field variable, we must consider different situations. Fortunately, it is rather easy to devise LJJs compared with other systems described by field theories. New and rich quantum phenomena may appear by such devices, and it will be a challenging subject to study the interplay of many-body interactions and the macroscopic quantum effects.

2.2 Vortices in 0-π-0 Josephson Junctions

2.2.1 Introduction

In this section, we consider a long Josephson junction including a so-called π junction, which has negative critical current. In such junctions, the phase difference shows more complicated properties than traditional LJJs. Hence, we expect new phenomena characteristic of the sine-Gordon field with infinite degrees of freedom. Macroscopic quantum tunneling (MQT) in these junctions is also discussed.

The negative critical current has been discussed first in Josephson junctions, which have an insulator layer with magnetic impurities [108, 109]. More recently, it has been proposed that π junctions can be made by unconventional superconductors with non-s-wave symmetry. Geshkenbein *et al.* [110] have discussed π junctions formed in heavy electron

systems, whereas π junctions in high-T_c superconductors have been proposed to explain the positive paramagnetic Meissner effect [111, 112]. In order to probe the symmetry of the superconducting gap, a number of experiments have been performed, including interference measurements in single crystal $YBa_2Cu_3O_{7-\delta}$-Pb SQUIDs [113, 114], and direct imaging of magnetic flux in a tricrystal ring geometry [115, 116]. These measurements indicate that π junctions can be realized at grain boundaries of high-T_c superconductors, and that the d-wave symmetry is realized in high-T_c superconductors.

Static behavior of LJJs with both 0 and π junctions (0-π junctions) has been studied theoretically by several authors [108, 117, 118]. They have shown that a half vortex appears spontaneously at a boundary between 0 junction and π junction in sufficiently long junctions. Further, Kuklov *et al.* have proposed that the half vortex can change its orientation by applying an external current to the junction [119]. They have also conjectured that the half-vortex can be utilized in superconducting memory and logic devices.

Here, let us explain experimental situations. In Ref. [116], a half vortex has been observed in grain-boundary Josephson junctions of d-wave superconductors as shown in Fig. 2.2.1 (a). These samples have been made from thin films of the high-temperature superconductor $YBa_2Cu_3O_{7-\delta}$ 120 nm thick grown epitaxially on c-axis upon tricrystal substrates of $SrTiO_3$. The tricrystal substrates have been fabricated from the crystals that were reoriented, polished, and fused together to form three bicrystals that meet at a single point. In a similar way, it is expected to be possible to make grain-boundary Josephson junctions as shown in Fig. 2.2.1 (b). This Josephson junction consists of normal junction with positive critical current, and π junction with negative critical current. Thus, the 0-π long Josephson junctions are expected to be fabricated in this way.

In this section, we consider a 0-π-0 long Josephson junction, which has a positive critical current at $|x| > a$, and a negative critical current at $|x| < a$. This junction is realized in the grain-boundary Josephson junctions as shown in Fig. 2.2.1 (c). This junction would be made in the way used in ref. [116], though the fabrication would be rather difficult when the length of the π junction becomes small. The 0-π-0 long Josephson junctions are also realized in the grain-boundary junction as shown in Fig. 2.2.1 (d). In this figure, the dashed lines show the grain-boundary Josephson junctions with much larger critical current j_c' than the ones shown as the thick lines. These grain-boundaries shown as the dashed lines can be neglected for the studies of junction properties because the energy of

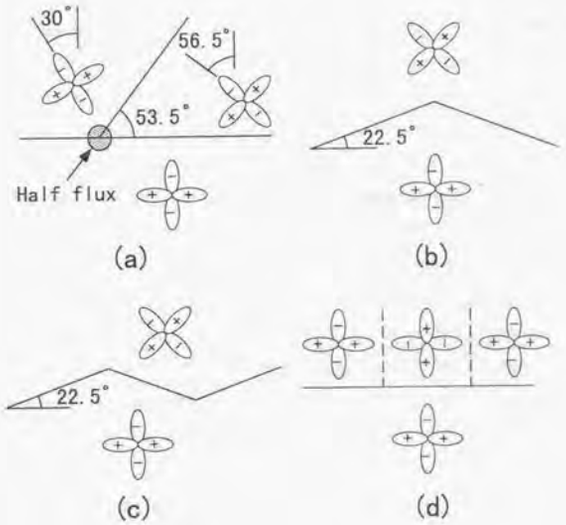

Figure 2.4: (a) The experimental configuration in the observation of a half vortex by Kirtley *et. al*, and (b) one possible configuration of 0-π grain-boundary Josephson junctions are shown. Two possible ways to fabricate 0-π-0 Josephson junctions are also shown in (c) and (d). The thick lines show grain-boundary junctions with relatively small critical current density j_c, while the dashed lines show grain-boundary junctions with large critical current density $j_c' \gg j_c$ which can be neglected for studies of the properties of the junctions.

the flux through them is larger, and the flux avoids penetrating the grain-boundary shown as the thick lines. Also in this configuration, the fabrication would become more difficult when the length of the π-junction becomes small. Additionally, the 0-π-0 long Josephson junctions may be fabricated by introducing magnetic impurities in insulator layers without high-T_c superconductors.

First, we study static properties of the junction in Sec. 2.2.2. After that, we consider MQT in this junction to study quantum effects in Sec. 2.2.3. A summary is given in Sec. 2.2.4.

2.2.2 Hamiltonian and static properties

Hamiltonian

The Hamiltonian of the 0-π-0 Josephson junction with an external current is given by

$$H = \int_{-\infty}^{\infty} \left(\frac{1}{2}\phi_x^2 + \Theta(|x| - a)(1 - \cos\phi) + f\phi \right) \mathrm{d}x. \tag{2.44}$$

Here, x is scaled by the Josephson length λ_J, $f = I/I_0$ is the external current, and $\Theta(x)$ is the step function. Note that the Hamiltonian is scaled by an energy scale of the junction E_0. Here, to simplify the situation, we assume that the absolute value of the critical current is uniform along the junction. Static behavior of ϕ is given by $\delta H/\delta\phi(x) = 0$. From (2.44), we obtain the sine-Gordon equation [120]

$$\phi_{xx} = \Theta(x)\sin\phi + f. \tag{2.45}$$

This equation is also obtained from (2.1) by taking $\phi_t = 0$. It should be noted that dissipation does not affect static properties.

First, we consider the case with $f = 0$. In stable solutions minimizing (2.44), the system prefers to have a uniform phase difference ϕ at $2\pi n$ for $x \gg |a|$, while $\phi = (2n+1)\pi$ is preferred for $|x| \ll a$, where n is an integer. As a result, we obtain two types of solutions, $\phi_1(x)$ and $\phi_2(x)$ as schematically shown in Fig. 2.5. Here, we assumed without losing generality that both solutions satisfy $\phi(\pm\infty) = 0$.

The physical meaning of these solutions is clear in case of $a \gg 1$. For example, we consider the situation described by $\phi_1(x)$ shown in Fig. 2.5. The induced magnetic field in the junction is proportional to ϕ_x. Hence, a vortex and an antivortex appear at $x = -a$ and at $x = a$, respectively. The magnetic flux carried by these vortices is $\pm\Phi_0/2$, where

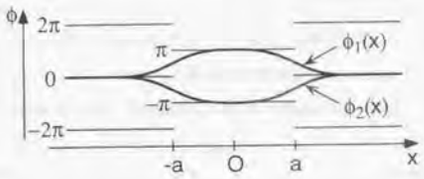

Figure 2.5: Two types of solutions of the sine-Gordon equation are drawn for sufficiently large a. The minima of the potential for ϕ is given as $(2n+1)\pi$ at $|x| < a$, and as $n\pi$ at $|x| > a$.

$\Phi_0 = h/2e$ is the unit flux. These induced vortices are called half vortices. The other solution $\phi_2(x)$ has the same vortices, except that the orientations of the vortices are reversed from those in $\phi_1(x)$.

Magnetic flux

The induced magnetic flux is proportional to $\Delta\phi = \phi_1(0) - \phi_1(\infty)$. In the case of $a \gg 1$, we obtain $\Delta\phi = \pi$, where the magnetic flux carried by the vortices is $\pm\Phi_0/2$. The magnetic flux defined by $\Delta\phi$, however, decreases as we put a vortex and an antivortex closer to each other. We have calculated $\phi(x)$ from (2.45) numerically, and obtained $\Delta\phi$ as a function of a. The result is shown in Fig. 2.6. For $a \leq \pi/4 \approx 0.79$, we obtain $\Delta\phi = 0$. This means that the vortices disappear when the distance between vortices is too small. As shown later, the critical value $\pi/4$ can be obtained analytically. For $a \geq \pi/4$, the value of $\Delta\phi$ increases quickly as the value of a becomes large, and approaches π for $a \gg 1$.

We expect that this behavior of the flux carried by the vortices may be applied to accurate measurements of λ_J. When we change the length of the π junction or the Josephson penetration length λ_J by an external magnetic field, the measurement of the magnetic flux carried by vortices will gives us the information about the value of λ_J. The measurement of λ_J using direct imaging by scanning SQUIDs has already been reported by Kirtley *et. al.* [116] Compared with this, we expect that the measurement using the 0-π-0 Josephson junction is more accurate, because the magnetic flux is sensitive to the ratio $a = d/2\lambda_J$, where d is a length of the π junction.

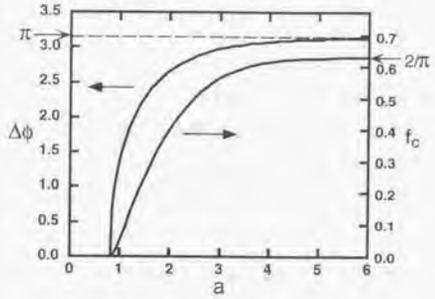

Figure 2.6: $\Delta\phi = \phi_1(0) - \phi_1(\infty)$ is shown as a function of a, which is one half of the distance between two vortices scaled by λ_J. The critical current f_c necessary for vortices to change their orientation is also shown. Both vanish at $a = \pi/4 \approx 0.79$ as a decreases.

External current

Next, we study static behavior of the solution in the presence of the external current f. We assume that the initial state is described by $\phi_1(x)$. As the external current f adiabatically increases from zero, the form of $\phi_1(x)$ is modified. The modified solution is denoted as $\phi_1(x, f)$. When the external current takes a critical value f_c, the solution $\phi_1(x, f)$ becomes unstable. Then, a transition from $\phi_1(x, f)$ to the other stable solution $\phi_2(x, f)$ occurs. Here, $\phi_2(x, f)$ is a solution modified adiabatically from the initial solution $\phi_2(x)$ by the external current f. During the transition, a voltage pulse across the junction is generated. This transition is intuitively understood easily as follows: the vortices exchange their locations each other. After that, the system remains the state described by $\phi_2(x, f)$, as long as $f > 0$. When a negative external current is applied to the junction, a transition from $\phi_2(x, f)$ to $\phi_1(x, f)$ occurs at $f = -f_c$.

The critical current f_c is calculated from (2.45) numerically. The result is shown also in Fig. 2.6. For $a > \pi/4$, the critical current f_c increases as a becomes large, and is saturated toward $2/\pi$, which can be obtained analytically as shown later. Note that the critical value f_c is smaller than 1. This means that the exchange of a vortex and an antivortex occurs before the whole junction is driven to a voltage state.

Limiting cases

Next, we consider two limiting cases: (i) $a = \pi/4 + \lambda$ ($\lambda \ll 1$), and (ii) $a \gg 1$. In these cases, we can perform an analytical calculation.

In the case (i), the phase difference $\phi(x)$ satisfies $|\phi(x)| \ll 1$ for all x. Then, the Hamiltonian (2.44) for $f = 0$ up to ϕ^2 is reduced to

$$H[\phi(x)] = \int_{-\infty}^{\infty} \mathrm{d}x\, \varphi(x) \frac{1}{2} \left(-\frac{\mathrm{d}^2}{\mathrm{d}x^2} + \Theta(|x| - a) \right) \varphi(x), \tag{2.46}$$

where φ represents fluctuations around the trivial solution and is defined by $\phi(x) = 0 + \varphi(x)$. The eigenmodes of the fluctuation are obtained by solving the 'Schödinger equation'

$$-\frac{\mathrm{d}^2\varphi_n}{\mathrm{d}x^2} + \Theta(|x| - a)\varphi_n = \varepsilon_n \varphi_n, \tag{2.47}$$

under the normalization condition

$$\int_{-\infty}^{\infty} \mathrm{d}x\, \varphi_n(x)\varphi_m(x) = \delta_{nm}. \tag{2.48}$$

Here, $\Theta(|x| - a)$ can be regarded as a well-shaped potential with the width $2a$. When $a \leq \pi/4$, the lowest energy ε_0 is positive, and the trivial solution $\phi = 0$ is stable. However, when $a = \pi/4 + \lambda$ ($0 < \lambda \ll 1$), there exists a negative eigenmode ϕ_0, which means that the trivial solution $\phi(x) = 0$ is unstable. Hence, when we expand the static solution

$$\phi(x) = \sum_{n=0}^{\infty} C_n \varphi_n(x), \tag{2.49}$$

the coefficients C_n become 0 for $n \geq 1$, and only C_0 is nonzero. For $a = \pi/4 + \lambda$ ($\lambda \ll 1$), the ground state energy ε_0 is close to zero. By taking $\varepsilon_0 = 0$, the form of the unstable mode $\varphi_0(x)$ is obtained approximately from (2.47) and (2.48) as

$$\varphi_0(x) = \begin{cases} \sqrt{\dfrac{4}{\pi + 4}} \cos x & (|x| < a), \\ \sqrt{\dfrac{4}{\pi + 4}} \cos a\, e^{-(|x| - a)} & (|x| > a). \end{cases} \tag{2.50}$$

To determine C_0, we derive an effective Hamiltonian for C_0 by substituting $\phi(x) = C_0\varphi_0(x)$ and (2.50) in the Hamiltonian (2.44). By assuming that C_0 is small, a simple analysis gives

$$H = -\frac{\varepsilon_0}{2} C_0^2 + \frac{\pi + 2}{8(\pi + 4)^2} C_0^4 - \sqrt{\frac{32}{\pi + 4}} f C_0 \tag{2.51}$$

to the fourth order of C_0. Here, $\varepsilon_0 = 8\lambda/(\pi + 4)$. From (2.51), $\Delta\phi$ and f_c are calculated analytically as

$$\Delta\phi = \sqrt{\frac{64}{\pi + 4}} \lambda^{1/2}, \quad f_c = \frac{128}{27(\pi + 2)} \lambda^{3/2}. \tag{2.52}$$

In the case (ii), i.e., for $a \gg 1$, we can regard the junction as two independent 0-π junctions. Then, a half vortex and a half antivortex appear at $x = \pm a$. We notice only the half vortex at $x = a$. The behavior of a half vortex in 0-π junctions in the presence of an external current has already been studied by Kuklov *et.al.* [119]. They have studied a critical current f_c, at which a half vortex changes its orientation with an integer flux being created. In order to study the stability of the static solution $\phi_1(x, f)$, we expand $\phi(x)$ around $\phi_1(x, f)$

$$\phi(x) = \phi_1(x, f) + \sum_{n=0}^{\infty} C'_n \varphi_n(x) \tag{2.53}$$

with eigenmodes of small fluctuation defined by

$$-\frac{\mathrm{d}^2\varphi_n}{\mathrm{d}x^2} + U''\varphi_n = E_n\varphi_n, \quad U'' \equiv \frac{\partial^2 U}{\partial\phi^2}(\phi_1(x, f)). \tag{2.54}$$

Here, $U(\phi) = \Theta(|x| - a)(1 - \cos\phi)$. At $f = f_c$, the lowest energy E_0 becomes zero as in the case (i). It can easily be checked that $\varphi_0 = C\partial_x\phi_1(x, f)$ always satisfies the equation (2.54) with $E_0 = 0$. Here, the constant C is determined by solving the normalization condition (2.48). This mode is called the translational mode, because this modulation translates the half vortex along the junction. We should note, however, that both $\varphi_0(x)$ and $\partial_x\varphi_0(x)$ must be continuous at $x = a$. This condition and (2.45) leads to $\phi_1(a, f_c) = 0$. Further, from the first integral of (2.45), we obtain

$$0 - \cos\phi(0) - f\phi(0) = \frac{1}{2}\phi_x(a)^2 - \cos\phi(a) - f\phi(a), \tag{2.55}$$

$$0 + \cos\phi(\infty) - f\phi(\infty) = \frac{1}{2}\phi_x(a)^2 + \cos\phi(a) - f\phi(a). \tag{2.56}$$

From these equations and $\phi_1(a, f_c) = 0$, the critical current for $a \gg 1$ is calculated as $f_c = 2/\pi$ [121]. For the critical solution $\phi(x, f_c)$, the normalization constant in φ_0 is numerically calculated as $C \approx 0.5468$.

As well as in the case (i), only the lowest energy mode $\varphi_0(x)$ becomes unstable for $f > f_c$. The effective Hamiltonian in the case (ii) can be written by substituting $\phi = \phi_1(x, f_c) + C'_0\varphi_0(x)$ to (2.44) as

$$H = \pi\delta C C'_0 - \alpha(C C'_0)^3, \tag{2.57}$$

Figure 2.7: Sketches of the transition from $\phi_1(x)$ to $\phi_2(x)$ in two limiting cases: (a) $a = \pi/4 + \lambda$ ($\lambda \ll 1$), and (b) for $a \gg 1$. The gray lines represent intermediate configurations during the transition. The transition occurs symmetrically in the case (a), while the integer flux is generated at either side in the case (b).

to the third order of C_0'. Here, $\delta = f_c - f$ denotes the difference between the critical current and the external current, and α is a constant calculated by

$$\begin{aligned} \alpha &= \frac{1}{6}\int_{-\infty}^{\infty} \mathrm{d}x\, \Theta(|x| - a) \sin\phi_1(x, f_c)(\partial\phi_1(x, f_c))^3 \\ &= \frac{2}{3}(\phi_\infty \sin\phi_\infty + \cos\phi_\infty - 1) \approx 0.1403, \end{aligned} \tag{2.58}$$

where $\phi_\infty = \phi(\infty) = -\sin^{-1} f_c$. From the effective Hamiltonian (2.57), it is shown that there exists a metastable state for $\delta > 0$. Note that (2.57) is valid only for a small C_0'. Hence, (2.57) can be used only for $\delta \ll 1$ case, where the value of C_0' at a metastable state is small.

Crossover region

It should be noted that the way to exchange the location of a vortex and an antivortex each other is different in the two limiting cases. In the case (i), the transition from ϕ_1 to ϕ_2 occurs by keeping the symmetry $\phi(-x) = \phi(x)$ as shown in Fig. 2.7(a), because the most unstable mode $\varphi_0(x)$ is symmetric. In the case (ii), the transition occurs symmetrically in the original model (2.44) as well as in the case (i). However, in the presence of even small spatial inhomogeneities, either of the two half vortices begins to move at a lower external current as shown in Fig. 2.7(b). Then, this half vortex changes its orientation first and creates an integer vortex in the region $|x| < a$. This integer flux propagates along the π junction toward the other half vortex, and combines to it to change its orientation.

To study the transition process for an intermediate value of a, we focus on the Schrödinger

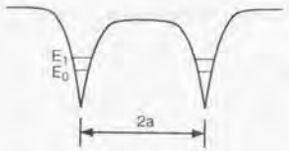

Figure 2.8: A sketch of the potential $U''(\phi_1(x))$ in the Schrödinger equation for fluctuations $\varphi(x)$. Here, E_0 is the ground state energy, and E_1 is the first excited state energy.

equation for fluctuations $\varphi(x)$,

$$-\frac{\mathrm{d}^2\varphi_n}{\mathrm{d}x^2} + U''\varphi_n = E_n\varphi_n, \quad U'' \equiv \frac{\partial^2 U}{\partial\phi^2}(\phi(x)). \tag{2.59}$$

The potential term $U''(\phi(x))$ has two minima at $x = \pm a$ as shown in Fig. 2.8. The ground state energy E_0 and the first excited state energy E_1 are also drawn in Fig. 2.8. As a increases, the wave function of the ground state is modified by keeping the symmetry $\varphi_0(-x) = \varphi_0(x)$ and its nodeless form. Hence, the most unstable mode $\varphi_0(x)$ is connected smoothly from the case (i) to the case (ii).

When the distance between two wells $2a$ increases, the energy splitting $\Delta = E_1 - E_0$ is suppressed exponentially. For $a \gg 1$, the lowest two eigenstates become almost degenerate, and we can constitute wave functions localized at each well as

$$\varphi_{\mathrm{R(L)}} = (\varphi_0(x) \pm \varphi_1(x))/\sqrt{2}. \tag{2.60}$$

In the presence of spatial inhomogeneities, the potential energy is modified, and the energy difference between two wells appears. This effect can be studied by the effective Hamiltonian on the two-dimensional Hilbert space spanned by φ_{R} and φ_{L}:

$$H_{\mathrm{eff}} = \Delta\sigma_x + \varepsilon\sigma_z. \tag{2.61}$$

Here, ε is the energy difference between wells due to inhomogeneities, and σ_x and σ_z are Pauli's matrices. When the energy splitting Δ is much larger than ε, the wave function of the ground state is symmetric, and given by φ_0 approximately. Hence, the transition from ϕ_1 to ϕ_2 occurs symmetrically as shown in Fig. 2.7(a). On the other hand, Δ becomes smaller than ε when a is large. Then, the wave function of the ground state is localized in

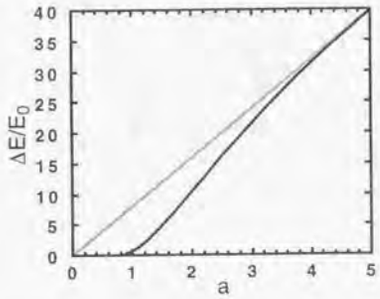

Figure 2.9: The solid line represents $\Delta E = H[\phi_1(x, f_c)] - H[\phi_2(x, f_c)]$ as a function of a. Here, E_0 is an energy scale of the junction. The curve for $\Delta E/E_0$ approaches $8a$(gray line) for $a \gg 1$.

either well, and given by φ_R (or φ_L) approximately. As a result, the transition begins from either side as shown in Fig. 2.7(b). The qualitative change which is expected to occur in the intermediate region of a is not a transition but a crossover.

Voltage pulse

In order to estimate the voltage of the pulse, we have calculated numerically the energy difference ΔE defined as

$$\Delta E/E_0 = H[\phi_1(x, f_c)] - H[\phi_2(x, f_c)], \tag{2.62}$$

where $E_0 = \Phi_0 I_0 \lambda_J / 2\pi L$ is the energy scale of the junction, and L is the junction length. The result is shown in Fig. 2.9. The energy difference increases monotonically for $a \geq \pi/4$. When a is large, the curve for $\Delta E/E_0$ approaches $8a$, which is obtained analytically by neglecting the spatial distribution of vortices around the boundary between the 0 junction and the π junction. The electric power of the pulse P is estimated as $P = \Delta E/\Delta t$, where δt is the time scale of the transition from ϕ_1 to ϕ_2 or *vice versa*. An accurate estimate of δt is difficult, because we have to solve the sine-Gordon equation (2.1) dynamically. For $a \gg 1$, however, it is inferred that δt is determined by the time for an integer vortex to propagate from $x = a$ to $x = -a$ or *vice versa*, and is estimated as $\delta t \sim 2a\lambda_J/\bar{c}$ in

the original unit. Here, $\bar{c} = \lambda_J \omega_c$ is a characteristic velocity of the integer vortex, and $\omega_c \sim \omega_p \times \max(1, \alpha + \beta/3)$ is a characteristic frequency of the junction. Thus, the pulse voltage V is estimated as

$$V \sim \frac{P}{I} \sim \frac{\Phi_0 \omega_c \lambda_J}{L}, \tag{2.63}$$

where L is the junction length. Here we used the critical current $f_c = I/I_0 = 2/\pi$. From Fig. 2.9, it is expected that the pulse voltage is suppressed as a decreases. Hence, the estimate (2.63) is expected to give an upper limit for V.

2.2.3 Macroscopic quantum tunneling

In this subsection, we consider the transition due to macroscopic quantum tunneling (MQT) from the metastable state ϕ_1 to the stable state ϕ_2. We study only limiting cases, which allow us to perform an analytical calculation on the basis of the effective Hamiltonian (2.51) and (2.57).

We first consider the case $a = \pi/4 + \lambda (\lambda \ll 1)$. We assume that $\delta = f_c - f \ll 1$, and that (2.51) can be approximated as a cubic potential. For the dissipationless case ($\alpha = \beta = 0$), the tunneling rate Γ is calculated as

$$\Gamma = A \exp(-B), \quad B = \frac{7.2V}{\hbar\omega_0}. \tag{2.64}$$

Here, V is the energy barrier, and ω_0 is the frequency of small oscillations around the metastable state. The prefactor A is of the order of ω_p, where ω_p is the plasma frequency of the junction. From (2.51), we can estimate the exponent for $a = \pi/4 + \lambda$ as

$$B \approx \frac{121}{g^2} \lambda^{-3/8} \delta^{5/4}, \tag{2.65}$$

where $g^2 = \hbar\omega_p/E_0$.

In a similar way, the exponent B is estimated for the case $a \gg 1$ from the effective Hamiltonian (2.57) as

$$B \approx \frac{99}{g^2} \delta^{5/4}. \tag{2.66}$$

Note that the exponent B is proportional to $\delta^{5/4}$ in both cases as seen in (2.65) and (2.66). Therefore, we expect that the δ-dependence in B does not change qualitatively in all the ranges of a.

The value of g^2 can be related to experimental parameters as

$$g^2 = \frac{16\pi}{137}\left(\frac{2\lambda_L d}{W^2 \varepsilon_r}\right)^{1/2}, \tag{2.67}$$

where λ_L is the London length, ε_r/d is the capacitance per area, and W is the junction width. The typical experimental value for g is very small ($\sim 10^{-3}$) [2]. Therefore, MQT can be observed only for $\delta \ll 1$, because the tunneling rate Γ must be large enough to be observed in the laboratory. For example, assuming $a \gg 1$, $\beta = 10^{-3}$, and $A = 10^{10}$[1/s], we obtain $\Gamma \sim 2 \times 10^2$[1/s] for $\delta = 10^{-3}$.

The quantum effects were treated here on the basis of the effective Hamiltonians including only one degree of freedom for the field. Other degrees of freedom appear only in the form of plasmons in the semiclassical approximation, while the plasmons do not affect the tunneling rate at sufficiently low temperatures [2]. The semiclassical approximation is justified for $g \ll 1$. Then, many-body effects characteristic of the sine-Gordon fields do not appear in this junction.

In the above calculation, we have neglected dissipation effects due to quasiparticles. It is, however, expected that damping effect on the junction remains even at sufficiently low temperatures, and strongly affects the tunneling rate, when there exist gapless nodes for quasiparticle excitations in non-s-wave superconductors. The damping effect can be estimated phenomenologically in the Caldeira-Leggett theory. From the result for weak-damping (1.37)-(1.38) and $a \gg 1$, the exponent is calculated as

$$B \approx \frac{99}{g^2}\delta^{5/4}(1 + \mathcal{O}(\alpha, \beta)), \tag{2.68}$$

where α and β are damping parameters of the classical equation of motion (2.1). Thus, the exponent increases, and the tunneling rate is suppressed by dissipation. In real π junctions, the microscopic estimate of α and β is difficult, and a very rough estimate seems to suggest that they are usually large enough to prevent us from observing tunneling effects, because of low quality of realistic junctions. Hence, for observation of MQT in this system, fabrication of high-quality π-junctions is necessary. Additionally, the estimate of the tunneling rate beyond the Caldeira-Leggett phenomenological theory remains for further studies.

2.2.4 Summary of this section

In summary, we studied static properties of magnetic fluxes and their macroscopic quantum tunneling in the 0-π-0 Josephson junction, where two half vortices are formed if the π junction region is long. We calculated the magnetic flux of spontaneously induced vortices, and the critical current needed to make a transition between two degenerate vortex configurations. We also studied the quantum tunneling rate for this transition. This MQT may be observed in high-T_c superconductors under appropriate conditions.

Chapter 3

Study of a Dissipative Tight Binding Model

In this chapter, we consider dissipative dynamics of a quantum particle in the tight-binding model through thermodynamics and transport properties. Dynamics of this model has already been discussed by the real-time path integral method in Sec. 1.2.6, while the model is studied by the imaginary-time path integral method in this chapter. This model for the ohmic damping is directly relevant to the dissipative motion of small Josephson junctions [66] (see Sec. 1.3.2).

This chapter is organized as follows. An introduction is given in Sec. 3.1, and a general formulation is given in Sec. 3.2. The detailed calculation for the ohmic damping case is given in Sec. 3.3, and a summary is given in Sec. 3.4.

3.1 Introduction

In Chapter 2, long Josephson junctions have been studied. Here, as an introduction to this chapter, let us study small Josephson junctions. Small resistance-shunted Josephson junctions can be well described by the classical equation of motion as

$$C\frac{d^2}{dt^2}\left(\frac{\Phi_0}{2\pi}\phi\right)+\frac{1}{R}\frac{d}{dt}\left(\frac{\Phi_0}{2\pi}\phi\right)+I_0\sin\phi=I, \tag{3.1}$$

where C, R, I_0 are a capacitance, a shunted resistance, and a critical current of the Josephson junctions, I is an external current, and $\Phi_0=2e/h$ is the unit of flux. (For details, see

Sec. 1.3.2.) The voltage of the junction is determined by the phase dynamics as

$$V=\frac{\hbar}{2e}\langle\dot{\phi}\rangle. \tag{3.2}$$

This description is connected to the dissipative tight-binding model in the following way. We can take $q=\Phi_0\phi/2\pi$ as the spatial coordinate of the particle with the mass C and damping coefficient $1/R$. The equation of motion of this particle is obtained as

$$C\ddot{q}+\frac{1}{R}\dot{q}+\frac{\partial U}{\partial q}=0, \tag{3.3}$$

$$U(q)=-Iq-E_J\cos\left(\frac{2\pi}{\Phi_0}q\right), \tag{3.4}$$

where $E_J=\Phi_0 I_0/2\pi$ is the Josephson coupling energy. Here, $U(q)$ is a biased periodic potential. The frequency of the oscillations of the potential minima ω_p is calculated for $I=0$ as

$$\omega_p=\left(\frac{2\pi I_0}{C\Phi_0}\right)^{1/2}, \tag{3.5}$$

which is called the plasma frequency of the junction. Then, the dissipative tight-binding model is obtained in the limit $\omega_p,\varepsilon\ll E_J$, where ε is the energy difference between neighboring wells defined by $\varepsilon=I\Phi_0$. Thus, the resistance-shunted Josephson junction system can be mapped to the dissipative tight-binding model with the ohmic damping. (see sec. 1.2.6 for detail.) This dissipative tight-binding model can describe nontrivial quantum phenomena in small Josephson junctions as discussed in sec. 3.3.4.

Besides the small Josephson junction system, the dissipative tight-binding model is also relevant to heavy particles in metals at least in the high-temperature limit, though the Caldeira-Leggett model may be problematic at low temperatures. (See Sec. 1.4.1) Moreover, the dissipative tight-binding model has possibilities to describe damping of carrier in solids, because this model captures a basic and fundamental feature of damping. Based on this argument, we use the Caldeira-Leggett formalism to calculate the optical conductivity is calculated to see the transport properties of the carrier.

The behavior of the dissipative tight-binding model is well understood in two regions: the incoherent hopping region and the continuum limit. In the high temperature and/or strong damping case, the particle motion becomes incoherent, and is described by the classical master equation. The tunneling rate takes the same value as for two-state systems [54], and the optical conductivity shows an unusual ω-dependence. On the other hand, in the

continuum limit, which corresponds to the low-temperature and weak-damping limit, we recover the Drude form derived by the equation of motion

$$\tilde{M}\ddot{q}(t) + \tilde{M}\gamma\dot{q}(t) + \frac{\partial V}{\partial q} = \xi(t), \tag{3.6}$$

where $\tilde{M}$ is the effective mass defined by the curvature at the bottom of the particle band. In this chapter, we study the crossover behavior between these two regions by constructing a formalism valid in the weak-coupling region. We also speculate that this study may contribute to the understanding of non-Drude forms of the conductivity observed in various strongly correlated systems [122].

In this chapter, the main aim is to study the crossover behavior from the incoherent motion at high temperatures to the quantum motion at low temperatures through the specific heat and optical conductivity $\sigma(\omega)$. The linear optical mobility is also obtained by $\mu(\omega) = \sigma(\omega)/e^2$. The thermodynamics of the system is formulated by the imaginary-time path integral, and transport properties are studied in the framework of the linear response theory, i. e., the Kubo formula [123].

This chapter is organized as follows. In Sec. 3.2 we derive exact formal expressions for the partition function and the optical conductivity for arbitrary form of $J(\omega)$. For analytical calculations, $J(\omega)$ is taken as

$$J(\omega) = \frac{2\pi\delta_s}{a^2}\left(\frac{\omega}{\bar{\omega}}\right)^{s-1}\omega f(\omega;\omega_c), \tag{3.7}$$

where δ_s is a dimensionless coupling coefficient, and $\bar{\omega}$ is a reference frequency. Here, $f(\omega;\omega_c)$ is a cutoff function usually taken as $f(\omega,\omega_c) = e^{-\omega/\omega_c}$, while we use a sharp cutoff, $f(\omega,\omega_c) = \Theta(\omega_c - \omega)$ in Sec. 3.2.3, where $\Theta(\omega)$ is a step function. In any case, the low-frequency ($\omega \ll \omega_c$) behavior of the dissipative particle is not influenced by the detailed form of the cut-off function. The exponent s in (3.7) mainly determines the properties of the heat bath. In Sec. 3.3 we study the case $s = 1$ called 'ohmic damping', where the coupling constant δ_s agrees with K. A summary of this chapter is given in Sec. 3.4.

3.2 Formulation

In this section, we give formal expressions for the partition function (Sec. 3.2.1) and the optical conductivity (Sec. 3.2.2). We also discuss the continuum limit of the tight binding model (Sec. 3.2.3). To deal with this model analytically, we focus on two limiting regions: an incoherent tunneling regime (Sec. 3.2.4) and a weak damping region (Sec. 3.2.5). In this section, the derived expressions are applicable to arbitrary form of $J(\omega)$.

3.2.1 Partition function

The exact formal expression for the partition function Z is given in the imaginary-time functional-integral representation. The integrals over the heat-bath variables are Gaussian and they can be evaluated exactly [1, 12]. After integrating out the degrees of freedom for the environment, the partition function is expressed as

$$Z = Z_R \oint \mathcal{D}q(\tau)\exp(-S[q(\tau)]). \tag{3.8}$$

Here, Z_R is the partition function of the heat bath, and in following calculation, Z_R is removed in order to focus only on the damping effects on the particle. The paths $q(\tau)$ satisfy the periodic boundary condition $q(\beta) = q(0)$, where $\beta = 1/T$. The effective action $S[q(\tau)]$ has been calculated in (1.10), and it may be modified as

$$S[q(\tau)] = \int_0^\beta \mathrm{d}\tau\left(\frac{1}{2}M\dot{q}^2 + V(q)\right) - \frac{1}{a^2}\int_0^\beta \mathrm{d}\tau\mathrm{d}\tau'\,\phi(\tau-\tau')\dot{q}(\tau)\dot{q}(\tau'). \tag{3.9}$$

Damping effects due to the heat bath are described by the last term, which takes a nonlocal form for τ. The kernel $\phi(\tau)$ is calculated as

$$\phi(\tau) = \frac{a^2}{\pi}\int_0^\infty \mathrm{d}\omega\frac{J(\omega)}{\omega^2}(D_\omega(0) - D_\omega(\tau)), \tag{3.10}$$

$$D_\omega(\tau) = \frac{1}{\beta}\sum_{n=-\infty}^{\infty}\frac{2\omega}{\nu_n^2+\omega^2}e^{-i\nu_n\tau} \tag{3.11}$$

$$= \frac{\cosh[\omega(\beta/2 - |\tau|)]}{\sinh(\beta\omega/2)}, \tag{3.12}$$

where $\nu_n = 2\pi n/\beta$ are the Matsubara frequencies. In a tight binding model, each path $\dot{q}(\tau)$ is expressed as the sum of the delta functions as

$$\dot{q}(\tau)/a = \sum_{l=1}^{2m}\xi_l\delta(\tau-\tau_l). \tag{3.13}$$

Here, $\xi_l = \pm 1$ specifies the direction of the l-th hopping at $\tau = \tau_l$. Substituting (3.13) to (3.9), the exact formal expression of the partition function is obtained as

$$Z = \sum_{m=0}^{\infty}\Delta^{2m}\sum_{\{\xi_l\}}\int_0^\beta \mathrm{d}\tau_{2m}\int_0^{\tau_{2m}}\mathrm{d}\tau_{2m-1}\cdots\int_0^{\tau_2}\mathrm{d}\tau_1\exp\left[\sum_{k<l}^{2m}\xi_k\xi_l\phi(\tau_l-\tau_k)\right]$$

$$= \sum_{m=0}^{\infty} \frac{\Delta^{2m}}{2m!} \sum_{\{\xi_l\}'} \prod_{n=1}^{2m} \int_0^\beta \mathrm{d}\tau_n \exp\left[\sum_{k<l}^{2m} \xi_k \xi_l \phi(\tau_l - \tau_k)\right]. \tag{3.14}$$

Here, the prime in $\{\xi_l\}'$ denotes summation in accordance with the constraint

$$\sum_{l=1}^{2m} \xi_l = 0. \tag{3.15}$$

The expression (3.14) may be interpreted as the statistical model of the classical particles interacting in the τ-direction with the potential $-\phi(\tau)$ [49]. From this point of view, Δ and ξ_l are regarded as the chemical potential and the charge of the classical particle. The inverse temperature $\beta = 1/T$ in the original model corresponds to the system length in the τ direction. At the same time, the constraint (3.15) is interpreted as the condition for the charge neutrality. The mapping to the classical statistical mechanics is useful for constituting the weak coupling theory. Actually, the 'screening effect' by the charged particles in the mapped model is important to describe transport properties of the original model at low temperatures (see Sec. 3.2.5).

3.2.2 Optical conductivity

We formulate the optical conductivity $\sigma(\omega)$ in one dimension using the Kubo formula [123]

$$\sigma(\omega) = -e^2 a^2 \frac{\langle -\mathcal{K}\rangle - \Lambda(\omega)}{\mathrm{i}(\omega + \mathrm{i}\delta)}, \tag{3.16}$$

where δ is an adiabatic constant, and $\mathcal{K}$ is the kinetic energy

$$\mathcal{K} = -\Delta \sum_n \left(c_{n+1}^\dagger c_n + c_n^\dagger c_{n+1}\right), \tag{3.17}$$

and the current-current correlation function $\Lambda(\omega)$ is defined by

$$\Lambda(\omega) = \tilde{\Lambda}(\mathrm{i}\omega_m \to \omega + \mathrm{i}\delta), \tag{3.18}$$

$$\tilde{\Lambda}(\mathrm{i}\omega_m) = \int_0^\beta \mathrm{d}\tau\, \mathrm{e}^{\mathrm{i}\omega_m \tau} \langle j(\tau) j(0)\rangle. \tag{3.19}$$

Here, the current operator $j(\tau) = \mathrm{e}^{\tau H} j \mathrm{e}^{-\tau H}$ is defined by

$$j = \mathrm{i}\Delta \sum_n \left(c_{n+1}^\dagger c_n - c_n^\dagger c_{n+1}\right). \tag{3.20}$$

The real part of $\sigma(\omega)$ contains a coherent part expressed by a delta function as [124, 125]

$$\mathrm{Re}\,\sigma(\omega) = D\delta(\omega) + \sigma_{\mathrm{res}}(\omega). \tag{3.21}$$

Here, D is called the Drude weight, and $\sigma_{\mathrm{res}}(\omega)$ is the residual incoherent part. From (3.16), we obtain

$$\frac{D}{\pi e^2 a^2} = \langle -\mathcal{K}\rangle - \mathrm{Re}\,\Lambda(\omega \to 0), \tag{3.22}$$

$$\sigma_{\mathrm{res}}(\omega) = e^2 a^2 \frac{\mathrm{Im}\,\Lambda(\omega)}{\omega}. \tag{3.23}$$

To evaluate $\Lambda(\omega)$, we consider the imaginary-time correlation function $\tilde{\Lambda}(\tau) = \langle j(\tau) j(0)\rangle$ for $\tau > 0$. The correlation function is formulated by the imaginary-time path integral as

$$\tilde{\Lambda}(\tau) = \frac{\Delta^2}{Z} \oint \mathcal{D}' q(\tau') \exp\left[-S[q(\tau')]\right]. \tag{3.24}$$

Here, the path integral is performed over all the possible paths $q(\tau)$ with two jumps at $\tau' = 0, \tau$ as

$$\dot{q}(\tau')/a = \sum_{l=1}^{2m} \xi_l \delta(\tau' - \tau_l) + \sigma\delta(\tau') + \sigma'\delta(\tau' - \tau), \tag{3.25}$$

where $2m + 2$ is the number of transitions, and $\xi_l, \sigma, \sigma' = \pm 1$ denote the directions of hopping at $\tau' = \tau_l, 0, \tau$, respectively. Then, the path integral is expressed as

$$\oint \mathcal{D}' q(\tau')(\cdots) = \sum_{m=0}^{\infty} \sum_{\{\xi_l, \sigma, \sigma'\}'} (-\sigma\sigma') \frac{1}{2m!} \prod_{l=1}^{2m} \int_0^\beta \mathrm{d}\tau_l (\cdots). \tag{3.26}$$

Here, the prime in $\{\xi_l, \sigma, \sigma'\}'$ denotes the summation in accordance with the constraint

$$\sum_{l=1}^{2m} \xi_l + \sigma + \sigma' = 0, \tag{3.27}$$

which comes from the periodic boundary condition for $q(\tau')$. Here, we divide $\Lambda(\omega)$ into two parts as

$$\tilde{\Lambda}(\tau) = \tilde{\Lambda}_1(\tau) - \tilde{\Lambda}_2(\tau), \tag{3.28}$$

where $\tilde{\Lambda}_1(\tau)$ and $\tilde{\Lambda}_2(\tau)$ denote the contribution of paths which satisfy $\sigma = -\sigma'$ and $\sigma = \sigma'$, respectively. From (3.24)-(3.26) we obtain

$$\tilde{\Lambda}_1(\tau) = \frac{2\Delta^2}{Z} \sum_{m=0}^{\infty} \frac{\Delta^{2m}}{2m!} \sum_{\{\xi_l\}'} \int_0^\beta \prod_{l=1}^{2m} \mathrm{d}\tau_l$$

$$\times \exp\left(\sum_{k<l}^{2m}\xi_k\xi_l\phi(\tau_l-\tau_k)+\sum_{l=1}^{2m}\xi_l\phi(\tau_l)-\sum_{l=1}^{2m}\xi_l\phi(\tau_l-\tau)-\phi(\tau)\right). \quad (3.29)$$

$$\bar{\Lambda}_2(\tau) = \frac{2\Delta^2}{Z}\sum_{m=0}^{\infty}\frac{\Delta^{2m}}{2m!}\sum_{\{\xi_l\}''}\int_0^\beta\prod_{l=1}^{2m}\mathrm{d}\tau_l$$

$$\times \exp\left(\sum_{k<l}^{2m}\xi_k\xi_l\phi(\tau_l-\tau_k)+\sum_{l=1}^{2m}\xi_l\phi(\tau_l)+\sum_{l=1}^{2m}\xi_l\phi(\tau_l-\tau)+\phi(\tau)\right). \quad (3.30)$$

Here, the prime in $\{\xi_l\}'$ and the double prime in $\{\xi_l\}''$ denote the summations in accordance with (3.15) and the condition

$$\sum_{l=1}^{2m}\xi_l+2=0, \quad (3.31)$$

respectively. From (3.29) and (3.30), $\bar{\Lambda}_1(\tau)$ and $\bar{\Lambda}_2(\tau)$ can be interpreted as the partition functions with fixed charges at $\tau'=0,\tau$ in terms of the classical partition function (3.14).

We can calculate $\sigma_{res}(\omega)=e^2a^2\mathrm{Im}\Lambda(\omega)/\omega$ without the Wick rotation (3.18). We introduce the real-time correlation function as

$$\begin{aligned}\Lambda(t) &= \mathrm{i}\Theta(t)\langle j(t)j(0)-j(0)j(t)\rangle\\ &= -2\mathrm{Im}\,\bar{\Lambda}(\tau\to\mathrm{i}t),\end{aligned} \quad (3.32)$$

where $j(t)=\mathrm{e}^{\mathrm{i}Ht}j\mathrm{e}^{-\mathrm{i}Ht}$. Then, the correlation function $\Lambda(\omega)$ is calculated by

$$\Lambda(\omega)=\int_0^\infty \mathrm{d}t\,\Lambda(t)\mathrm{e}^{\mathrm{i}\omega t}. \quad (3.33)$$

The above expressions, (3.32) and (3.33), are used for the calculation in the incoherent region and the weak-coupling region. We should note that the causality, $\Lambda(t)=0$ for $t<0$, gives the frequency sum-rule [126]

$$\int_{-\infty}^{\infty}\mathrm{d}\omega\,\mathrm{Re}\,\sigma(\omega)=\pi e^2a^2\langle-\mathcal{K}\rangle. \quad (3.34)$$

The sum rule is always satisfied in the approximations adopted in this chapter, since the causality is always satisfied.

3.2.3 Continuum limit

In the dissipationless case, the energy dispersion is given by

$$\varepsilon_k=-2\Delta\cos ka, \quad (3.35)$$

where k is the momentum. The lattice model is reduced to the continuum model in the limit $a\to 0$ ($\Delta\to\infty$) by keeping $\bar{M}=1/2\Delta a^2$ constant. In this limit, the energy dispersion is approximated as

$$\varepsilon_k\simeq-2\Delta+\frac{k^2}{2\bar{M}}. \quad (3.36)$$

Note that the mass $\bar{M}$ is not necessarily the same as the bare mass M in the original Hamiltonian. In the continuum limit $\Delta\to\infty$, thermal fluctuations may be neglected compared with the band width ($T/\Delta\to 0$). Hence, the continuum limit corresponds to the zero-temperature limit.

Next, we consider the dissipative case. In the continuum limit, the classical equation of motion for the average position $\langle q(t)\rangle$ is obtained by virtue of Ehrenfest's theorem as

$$\langle\ddot{q}(t)\rangle+\int_{-\infty}^{t}dt'\gamma(t-t')\langle\dot{q}(t')\rangle=\frac{e}{\bar{M}}E(t), \quad (3.37)$$

where $E(t)$ is the external electric field. The damping kernel $\gamma(t)$ is determined by the spectral density $J(\omega)$ as [1, 14]

$$\gamma(t) = \int_{-\infty}^{\infty}\frac{\mathrm{d}\omega}{2\pi}\mathrm{e}^{-\mathrm{i}\omega t}\tilde{\gamma}(z\to-\mathrm{i}\omega+\delta), \quad (3.38)$$

$$\tilde{\gamma}(z) = \frac{2z}{\pi\bar{M}}\int_0^\infty\mathrm{d}\omega'\frac{J(\omega')}{\omega'(\omega'^2+z^2)}. \quad (3.39)$$

From the classical equation (3.37), the Fourier transformation of the current $j(t)=e\langle\dot{q}(t)\rangle$ gives $\tilde{j}(\omega)=\sigma(\omega)\tilde{E}(\omega)$, and the optical conductivity $\sigma(\omega)$ is given by

$$\sigma(\omega)=\left.\frac{e^2}{\bar{M}(z+\tilde{\gamma}(z))}\right|_{z\to-\mathrm{i}\omega+\delta}. \quad (3.40)$$

The above result is valid for any form of the spectral density $J(\omega)$. Here, we take $J(\omega)$ as

$$J(\omega)=\bar{M}\gamma_s\left(\frac{\omega}{\tilde{\omega}}\right)^{s-1}\omega\Theta(\omega_c-\omega), \quad (3.41)$$

where $\gamma_s=2\pi\delta_s/a^2\bar{M}=4\pi\delta_s\Delta$ is the damping frequency, and the cut-off function $f(\omega;\omega_c)$ in (3.7) is taken as the step function $\Theta(\omega_c-\omega)$ for convenience. The characteristic damping frequency $\tilde{\gamma}$ is given by $\tilde{\gamma}=(\gamma_s\tilde{\omega}^{1-s})^{1/(2-s)}$. To keep $\tilde{\gamma}$ constant in the continuum limit $\Delta\to\infty$, the dimensionless coupling coefficient $\delta_s=\gamma_s/4\pi\Delta$ must be suppressed to zero. Hence, the continuum limit corresponds to the weak coupling limit $\delta_s\to 0$.

From (3.41), the damping kernel $\tilde{\gamma}(\omega)$ in (3.39) is calculated analytically. The leading term is given by [14]

$$\tilde{\gamma}(z) = \begin{cases} \dfrac{\gamma_s z}{\sin(\pi s/2)\tilde{\omega}} \left|\dfrac{z}{\tilde{\omega}}\right|^{s-2} \left[1 + \mathcal{O}\left(z/\omega_c, (z/\omega_c)^{2-s}\right)\right], & (0 < s < 2), \\ \dfrac{\gamma_s z}{\pi\tilde{\omega}} \ln\left(1 + \dfrac{\omega_c^2}{z^2}\right), & (s = 2), \\ \dfrac{2\gamma_s}{\pi(s-2)} \left(\dfrac{\omega_c}{\tilde{\omega}}\right)^{s-2} \dfrac{z}{\tilde{\omega}} \left(1 + \mathcal{O}(z^2/\omega_c^2, (z/\omega_c)^{s-2})\right), & (s > 2). \end{cases} \tag{3.42}$$

From (3.40) and (3.42), it is proved that the delta function disappears at $\omega = 0$ in $\mathrm{Re}\,\sigma(\omega)$ for $0 < s < 2$. This result strongly indicates that the Drude weight D in (3.21) vanishes for $0 < s < 2$ at all temperatures and damping coefficients. This is because the continuum limit describes the low-temperature and weak-coupling limit, $T, \delta_s \to 0$, while this limit should give the most coherent result in the parameter space. On the other hand, the Drude weight exists for $s > 2$, and the damping effects appears only in the mass renormalization

$$\tilde{M} \to \tilde{M}\left(1 + \frac{2}{\pi(s-2)} \frac{\gamma_s}{\tilde{\omega}} \left(\frac{\omega_c}{\tilde{\omega}}\right)^{s-2}\right). \tag{3.43}$$

In this case, the residual conductivity for $\omega > 0$ vanishes. The above result is related to the Brownian motion caused by a heat bath, where the long time behavior of $\langle (q(t) - q(0))^2 \rangle$ at finite temperatures is proportional to t^2 for $s > 2$, and t^s for $s < 2$. The transition at $s = 2$ can be understood by a simple discussion on the mass renormalization expressed in general as [13, 14]

$$\tilde{M} \to \tilde{M} + \frac{2}{\pi} \int_0^\infty \mathrm{d}\omega \frac{J(\omega)}{\omega^3}. \tag{3.44}$$

When this integral is convergent, the particle motion becomes coherent in the continuum limit. (See also Sec. 1.2.2.)

Let us investigate the s dependence in more detail. The residual part $\sigma_{res}(\omega)$ appears only for the case $s \leq 2$. From (3.40) and (3.42), we obtain

$$\sigma_{res}(\omega) = \frac{e^2}{\tilde{M}\tilde{\gamma}} \frac{\left(\dfrac{\omega}{\tilde{\gamma}}\right)^{s-1}}{\left(\dfrac{\omega}{\tilde{\gamma}} - \cot\dfrac{\pi s}{2}\left(\dfrac{\omega}{\tilde{\gamma}}\right)^{s-1}\right)^2 + \left(\dfrac{\omega}{\tilde{\gamma}}\right)^{2(s-1)}}, \tag{3.45}$$

where $\tilde{\gamma} = (\gamma_s \tilde{\omega}^{1-s})^{1/(2-s)}$. In this case, $\sigma_{res}(\omega)$ behaves qualitatively as

$$\sigma_{res}(\omega) \sim \begin{cases} \omega^{1-s} & (\omega < \tilde{\gamma}), \\ \omega^{s-3} & (\omega > \tilde{\gamma}). \end{cases} \tag{3.46}$$

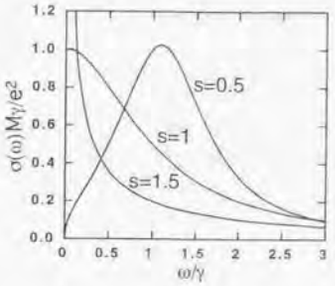

Figure 3.1: The optical conductivity $\sigma(\omega)$ in the continuum limit for $s = 0.5, 1, 1.5$. Particularly, for the ohmic damping $s = 1$, $\sigma(\omega)$ takes a simple Drude form.

The ω-dependence of $\sigma_{res}(\omega)$ for $s = 0.5, 1, 1.5$ is shown in Fig. 3.1. For subohmic damping $0 < s < 1$, the conductivity is reduced to zero as ω decreases. On the other hand, in the superohmic case $1 < s < 2$, the conductivity diverges for $\omega \to 0$. For the ohmic damping $s = 1$, the optical conductivity $\sigma_{res}(\omega)$ takes a simple Drude form.

As s increases toward 2, the curve of $\sigma_{res}(\omega)$ approaches the $1/\omega$ form. The case of $s = 2$ is marginal, and we obtain

$$\sigma_{res}(\omega) = \frac{e^2\gamma_s}{\tilde{M}\omega\tilde{\omega}} \frac{1}{\left(1 + \dfrac{\gamma_s}{\pi\tilde{\omega}} \log\left|\dfrac{\omega_c^2}{\omega^2} - 1\right|\right)^2 + \left(\dfrac{\gamma_s}{\tilde{\omega}}\right)^2}, \quad (\omega < \omega_c). \tag{3.47}$$

The optical conductivity $\sigma_{res}(\omega)$ behaves nearly as $1/\omega$ for $\omega \ll \omega_c$. For $s > 2$, the incoherent part vanishes, and the delta function appears in $\mathrm{Re}\,\sigma(\omega)$.

3.2.4 Incoherent tunneling regime

In the limit of high temperatures and/or strong damping, the particle moves incoherently to the neighboring sites. In this regime, the occupation probabilities obey a simple master equation [50, 54], and the hopping rate is formulated by Fermi's golden rule, where the incoherent motion of the particle is described by the term of order of Δ^2 in the correlation function. From (3.28)-(3.30), the relevant term is given by

$$\bar{\Lambda}(\tau) = 2\Delta^2 \exp\left[-\phi(\tau)\right]. \tag{3.48}$$

From (3.32), the real-time correlation function $\Lambda(t)$ is derived as

$$\Lambda(t) = 4\Delta^2 \sin R(t) \exp(-S(t)), \tag{3.49}$$

where $S(t)$ and $R(t)$ are real functions defined by $\phi(\tau = it) = S(t) + iR(t)$. The explicit form of $S(t)$ and $R(t)$ is given from (3.10) and (3.12) as

$$S(t) = \frac{a^2}{\pi}\int_0^\infty d\omega \frac{J(\omega)}{\omega^2}(1-\cos\omega t)\coth\frac{\beta\omega}{2}, \tag{3.50}$$

$$R(t) = \frac{a^2}{\pi}\int_0^\infty d\omega \frac{J(\omega)}{\omega^2}\sin\omega t. \tag{3.51}$$

The Fourier transformation of (3.49) gives

$$\mathrm{Im}\,\Lambda(\omega) = 4\Delta^2 \int_0^\infty dt\, \sin\omega t \sin R(t)\exp(-S(t)). \tag{3.52}$$

Thus, the optical conductivity is calculated from $\sigma_{res}(\omega) = e^2a^2\mathrm{Im}\,\Lambda(\omega)/\omega$. The formulation of the incoherent region is valid only when the integral (3.52) is convergent.

The above formulation is quite similar to the calculation of the nonlinear mobility in biased periodic-potential systems [56]. Actually, the hopping rate k^+ (k^-) to the right(left) well can be calculated. Then, the tunneling rate $\Gamma(\varepsilon) = k^+ + k^-$ and the nonlinear mobility $\mu(\varepsilon) = (k^+ - k^-)a^2/\varepsilon$ with a finite bias ε are obtained in the tight-binding model as

$$\Gamma(\varepsilon) = 4\Delta^2 \int_0^\infty dt \cos\varepsilon t \sin R(t)\exp(-S(t)), \tag{3.53}$$

$$\mu(\varepsilon) = \frac{4a^2\Delta^2}{\varepsilon}\int_0^\infty dt \sin\varepsilon t \sin R(t)\exp(-S(t)). \tag{3.54}$$

Comparing (3.54) with (3.52), the optical conductivity is obtained as $\sigma_{res}(\omega) = e^2\mu(\varepsilon \to \omega)$. Further, it is proved that $\mu(\varepsilon)$ is related to $\Gamma(\varepsilon)$ through the relation [56]

$$\mu(\varepsilon) = a^2 \tanh(\beta\varepsilon/2)\Gamma(\varepsilon)/\varepsilon. \tag{3.55}$$

Thus, we can obtain the optical conductivity from the tunneling rate $\Gamma(\varepsilon)$ as

$$\sigma_{res}(\omega) = e^2a^2\frac{\tanh(\beta\omega/2)}{\omega}\Gamma(\varepsilon \to \omega). \tag{3.56}$$

In order to calculate $\Gamma(\varepsilon)$ in the incoherent regime, we can utilize the results of two-state systems obtained in Ref. [30], where the tunneling rate is formulated in the same form as (3.53), and is calculated for a few regions in the parameter space. For ohmic damping, it is

proved that the expansion in terms of Δ gives the systematic high-temperature expansion. We consider the lowest contribution of order of Δ^2 in Sec. 3.3. In the subohmic case ($0 < s < 1$) and in the superohmic case ($1 < s < 2$), the calculation is so complicated that analytical treatment is possible only in the limiting cases. The results are given in Appendix 3·A, and we do not discuss the other cases in this chapter. It should be noted that the result (3.52) is also related to the transition rate of the photo-induced tunneling in the two-level systems [31].

In the incoherent tunneling regime, the partition function (3.14) is also approximated as

$$Z = 1 + 2\beta\Delta^2 \int_0^\beta d\tau \exp[-\phi(\tau)]. \tag{3.57}$$

This form corresponds to the partition function of dissipative two-state systems apart from a difference of a factor of 2 which comes from two possible transitions to neighboring sites [34].

3.2.5 Weak coupling theory

For weak damping ($\delta_s \ll 1$), analytical calculation is possible for all temperatures. However, we should be careful to constitute the weak coupling theory, because we must deal with screening effects of interacting classical particles described in (3.14). In order to treat the screening effects, we adopt the 'ring approximation', which is proved to be equivalent to the Debye-Hückel theory. Since this approximation is believed to be valid in the weak coupling region, we expect that reliable results are obtained in the weak damping region by this approximation. Detailed discussions about the validity of the ring approximation are summarized in Appendix 3·D. In this subsection, we derive the partition function and the optical conductivity based on the ring approximation. Since details of the calculation are straightforward, but rather tedious, we show only the results here. Details of the calculation are given in Appendix 3·B and 3·C.

Partition function

First, we define a Fourier transformation of the potential $\phi(\tau)$ as

$$\phi(i\omega_m) = \int_0^\beta d\tau\, e^{i\omega_m\tau}\phi(\tau), \tag{3.58}$$

where $\omega_m = 2\pi m/\beta$ are the Matsubara frequencies. By comparing (3.10)-(3.11) with (3.39), $\phi(\mathrm{i}\omega_m)$ can be related to the damping kernel $\tilde{\gamma}(z)$ defined in (3.39) for $\omega_m \neq 0$ as

$$\phi(\mathrm{i}\omega_m) = -\frac{Ma^2}{\omega_m}\tilde{\gamma}(z=\omega_m). \tag{3.59}$$

To avoid unphysical divergence, we shift the potential $\phi(\tau)$ by the zero frequency component $\phi_0 = \phi(\mathrm{i}\omega_m = 0)$ as

$$\phi(\tau) \to \phi(\tau) + \phi_0. \tag{3.60}$$

By the potential shift, the transition amplitude Δ is renormalized as

$$\bar{\Delta} = \Delta \exp\left(-\frac{1}{2}\phi_0\right), \tag{3.61}$$

where the factor $\exp(-\phi_0/2)$ corresponds to the Frank-Condon factor. Details of the calculation for ϕ_0 are given in Appendix 3-B.

From the approximate calculation given in Appendix 3-C, the analytical form of the partition function is obtained as

$$Z = \int_0^{2\pi} \frac{\mathrm{d}\theta}{2\pi} \exp\left[U(n)\right], \tag{3.62}$$

$$U(n) = n + \int_0^n \mathrm{d}n'\, Q(n') - nQ(n), \tag{3.63}$$

$$Q(n) = \frac{1}{\beta^2}\sum_{\omega_m>0} \frac{n\phi(\mathrm{i}\omega_m)^2}{1 - n\phi(\mathrm{i}\omega_m)/\beta}, \tag{3.64}$$

where $n = n(\theta)$ is determined by the equation

$$2\beta\bar{\Delta}\cos\theta = n\mathrm{e}^{-Q(n)}. \tag{3.65}$$

From Eqs. (3.62)-(3.65), the partition function Z is calculated analytically at least for the ohmic damping (See Sec. 3.3.2) .

Optical conductivity

The ring approximation is also applicable to the conductivity $\sigma(\omega)$. When we define a screened potential $\varphi(\tau;\theta)$ as

$$\varphi(\tau;\theta) = \frac{1}{\beta}\sum_{\mathrm{i}\omega_m} \frac{\phi(\mathrm{i}\omega_m)}{1 - n(\theta)\phi(\mathrm{i}\omega_m)/\beta}\mathrm{e}^{-\mathrm{i}\omega_m\tau}, \tag{3.66}$$

the correlation functions are expressed as

$$\bar{\Lambda}(\tau) = \bar{\Lambda}_1(\tau) - \bar{\Lambda}_2(\tau), \tag{3.67}$$

$$\bar{\Lambda}_1(\tau) = \frac{1}{2Z}\int_0^{2\pi} \frac{\mathrm{d}\theta}{2\pi}\frac{n^2}{\beta^2\cos^2\theta}\exp\left[U(\theta) - \varphi(\tau;\theta)\right], \tag{3.68}$$

$$\bar{\Lambda}_2(\tau) = \frac{1}{2Z}\int_0^{2\pi} \frac{\mathrm{d}\theta}{2\pi}\frac{n^2}{\beta^2\cos^2\theta}\exp\left[U(\theta) + 2\mathrm{i}\theta + \varphi(\tau;\theta)\right]. \tag{3.69}$$

After the replacement $\tau \to it$, the screened potential is expressed by

$$\varphi(it;\theta) = S(t;\theta) + \mathrm{i}R(t;\theta), \tag{3.70}$$

where $S(t;\theta)$ is the real part, and $R(t;\theta)$ is the imaginary part. Using this notation, the real-time correlation function in (3.32) is written as

$$\Lambda(t) = \frac{1}{Z}\int_0^{2\pi} \frac{\mathrm{d}\theta}{2\pi}\frac{n^2}{\beta^2\cos^2\theta}\mathrm{e}^{U(\theta)}\left[\mathrm{e}^{-S(t;\theta)} + \mathrm{e}^{S(t;\theta)}\cos 2\theta\right]\sin R(t;\theta). \tag{3.71}$$

Thus, the optical conductivity is calculated from (3.23) and (3.33).

In the high-temperature limit ($\beta \to \infty$), the screened potential (3.66) agrees with the unscreened potential $\phi(\tau)$, because the second term of the denominator in (3.66) is suppressed. Therefore, the expressions of the weak coupling region are consistently connected to the formulation in the incoherent regime (3.48).

In the limit $T, \delta_s \to 0$, weak coupling must correspond to the continuum limit. To see the relation, it is convenient to study the imaginary-time correlation function $\bar{\Lambda}(\tau)$. In the continuum limit, the dimensionless coupling coefficient δ_s is reduced to zero. Therefore, the screened potential $\varphi(\tau)$ becomes small, and the approximation

$$\exp(\pm\varphi(\tau)) \simeq 1 \pm \varphi(\tau) \tag{3.72}$$

is justified. From (3.67)-(3.69), the imaginary-time correlation function is calculated approximately as

$$\bar{\Lambda}(\mathrm{i}\omega_m) = -\frac{1}{2Z}\int_0^{2\pi} \frac{\mathrm{d}\theta}{2\pi}\frac{n^2}{\beta^2\cos^2\theta}\mathrm{e}^{U(\theta)}\left(1 + \mathrm{e}^{2\mathrm{i}\theta}\right)\frac{\phi(\mathrm{i}\omega_m)}{1 - n(\theta)\phi(\mathrm{i}\omega_m)/\beta}. \tag{3.73}$$

The continuum limit ($\Delta \to \infty$) corresponds also to the low-temperature limit ($T/\Delta \to 0$), where the contribution at $\theta = 0$ is dominant in the integral (3.73), and n is evaluated by $n = 2\beta\Delta$ from (3.65). Thus, we obtain

$$\bar{\Lambda}(\mathrm{i}\omega_m) = \frac{1}{Ma^2}\frac{\tilde{\gamma}(\omega_m)}{\omega_m + \tilde{\gamma}(\omega_m)}, \tag{3.74}$$

where $\tilde{M} = 1/2\Delta a^2$ and the relation (3.59) is used. From (3.74), the optical conductivity in the continuum limit is obtained as

$$\sigma_{\rm res}(\omega) = e^2 a^2 {\rm Im} \frac{\tilde{\Lambda}(i\omega_m \to \omega + i\delta)}{\omega} \tag{3.75}$$

$$= \frac{e^2}{\tilde{M}} {\rm Re} \left. \frac{1}{z + \tilde{\gamma}(z)} \right|_{z \to -i\omega + \delta}. \tag{3.76}$$

This expression corresponds to the optical conductivity in the continuum limit (3.40).

3.3 Ohmic Damping

3.3.1 General review of ohmic damping

In this section we consider the ohmic damping case, in which the spectral density is described as

$$J(\omega) = \frac{2\pi K}{a^2} \omega e^{-\omega/\omega_c}. \tag{3.77}$$

Here, K is a dimensionless coupling constant. The Fourier component of the potential in (3.10) is calculated as

$$\phi(i\omega_m) = \begin{cases} -\dfrac{2\pi K}{|\omega_m|}, & (0 < |\omega_m| \ll \omega_c), \\ 2K \log \dfrac{\beta\omega_c}{2\pi}, & (\omega_m = 0). \end{cases} \tag{3.78}$$

The calculation of $\phi_0 = \phi(i\omega_m = 0)$ is given in Appendix 3-B. From (3.78), the renormalized hopping amplitude $\tilde{\Delta}$ in (3.61) is given by

$$\tilde{\Delta} = \Delta \left(\frac{\beta\omega_c}{2\pi} \right)^{-K}. \tag{3.79}$$

In the following subsections, we calculate the specific heat and the optical conductivity for ohmic dissipation. Before showing the results, we briefly review previous works on the properties of ohmic dissipation.

For two-state systems, the nonequilibrium behavior of the dissipative particle has been studied by Leggett *et. al.* [30]. They have calculated the real-time evolution of the expectation of the particle position with the non-interacting blip approximation (NIBA). The properties of the system are determined by the damping strength K and the temperature T, where the phase diagram obtained by NIBA is given in Fig. 3.2. There exist two regions

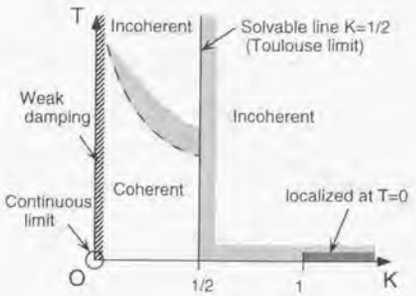

Figure 3.2: The phase diagram of dissipative two-state systems for the ohmic damping. This phase diagram has been obtained by the non-interacting blip approximation. In the 'coherent' region, the expectation value of the position $\langle q(t) \rangle$ shows oscillations, while in the 'incoherent' region, $\langle q(t) \rangle$ shows exponential decay. The regions which allow analytical treatment are also shown: the weak coupling regime and the solvable line ($K = 1/2$). The localization-delocalization transition at $T = 0$ is also drawn.

in the phase diagram. In the 'incoherent' region, the particle moves incoherently, and the expectation value of the position $\langle q(t) \rangle$ decays exponentially to the thermal equilibrium state. On the other hand, in the 'coherent' region, $\langle q(t) \rangle$ shows damped oscillation. We should note that several different definitions of the terms 'coherent' and 'incoherent' are possible [127]. For example, in the numerical study of equilibrium properties of dissipative two-state systems [45, 46], the term 'incoherence' is defined by the disappearance of the inelastic peak of the response function, which is observed at $K > 0.33$.

In this chapter, we mainly consider two limiting regions in the phase diagram. The first one is the weak damping region $K \ll 1$, which allows analytical treatment at all temperatures. The formulation of the weak damping theory can connect the low-temperature 'coherent' region to the high-temperature 'incoherent' region in a natural way. The result obtained in this narrow region will also be useful to understand properties in the other region. The second region is the high-temperature and/or strong damping region. In this limit, the dissipative particle moves incoherently with the hopping rate determined mainly

	Low-temperature and weak-damping region	High-temperature and/or strong damping
Specific heat C	$\propto T/K$	$\propto \begin{cases} T^{-2+2K} & (K < 3/2) \\ T & (K > 3/2) \end{cases}$
Optical conductivity $\sigma(\omega)$	$\propto \begin{cases} \omega^{-2+2K} & (\omega \gg \gamma_0) \\ \text{const.} & (\omega \ll \gamma_0) \end{cases}$	$\propto \begin{cases} \omega^{-2+2K} & (\omega \gg KT) \\ T^{-2+2K} & (\omega \ll KT) \end{cases}$
DC conductivity $\sigma_{\rm DC}$	$\propto 1 - \text{const.}T^2$	$\propto T^{-2+2K}$

Table 3.1: Summary of the results. Here, K is the dimensionless damping coefficient, and γ_0 is the damping frequency defined in the text.

by Fermi's golden rule. Especially, in the region $K > 1$, the high temperature expansion is convergent, and Fermi's golden rule gives the leading term at all temperatures. On the other hand, for $K < 1$, the high temperature expansion fails below the Kondo temperature $T_{\rm K}$. The summary of the results of these two regions is given in Table 3.1.

With regard to the optical conductivity, the result of the continuum limit is also useful to understand the general behavior. The continuum limit corresponds to the low-temperature and weak-coupling limit ($K, T \to 0$), and the particle is expected to move coherently. From (3.45), the optical conductivity in the continuum limit is calculated as a simple Drude form

$$\sigma_{\rm res}(\omega) = \frac{e^2\gamma}{\bar{M}(\omega^2+\gamma^2)}. \tag{3.80}$$

When finite damping is introduced, the optical conductivity deviates from the Drude form (3.80). This behavior is studied in detail in Sec. 3.3.3.

In addition to the above regions, it is expected that the calculation at $K = 1/2$ is tractable analytically by following Ref. [57], though we do not deal with that case in this chapter. In the other regions (particularly for $0 < K < 1$), the analytical method cannot be used. Hence, the dynamical properties of these regions will have to be studied by numerical calculation, which has not been performed before for the lattice model to our knowledge.

Finally, we comment on the renormalization of Δ due to the damping. For ohmic damping, the relevant frequency of the system is given by

$$\Delta_{\rm eff} = \Delta\left(\frac{\Delta}{\omega_c}\right)^{K/(1-K)}, \tag{3.81}$$

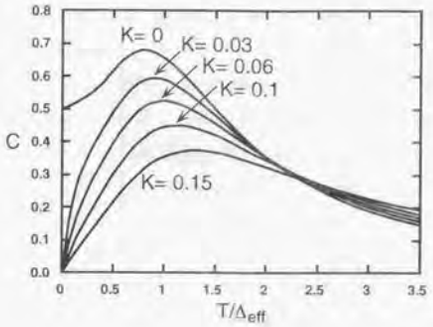

Figure 3.3: The specific heat for weak damping ($K = 0.03, 0.06, 0.1, 0.15$). The specific heat is suppressed to zero as the temperature decreases. This behavior is quite different from the dissipationless case ($K = 0$), where the specific heat approaches a nonzero constant at low temperatures.

for $0 < K < 1$. The frequency gives the scale of the Kondo temperature $T_{\rm K}$. By rewriting $\Delta_{\rm eff}$ as Δ, the final results can be expressed without the cutoff frequency ω_c [30]. (See also (1.47).) In this chapter, all the results are expressed by $\Delta_{\rm eff}$ finally.

3.3.2 Specific heat

In this subsection, we consider the specific heat of the system coupled to the ohmic heat bath. At high temperatures, we can obtain the specific heat C from (3.57). This result is exactly twice as large as the one obtained in dissipative two-state systems. As a result, the specific heat is proportional to T^{2K-2} for $0 < K < 3/2$, and proportional to T for $K > 3/2$. For details of the calculation, see Ref. [34].

Next, we focus on the weak damping region $K \ll 1$. From eqs.(3.62)-(3.65), we obtain

$$Z = \int_0^{2\pi} \frac{d\theta}{2\pi} e^{U(n)}, \tag{3.82}$$

$$U(n) = n + \log\Gamma(Kn+1) - Kn\psi(Kn+1), \tag{3.83}$$

$$Q(n) = K(\psi(Kn+1) + \tilde{\gamma}), \tag{3.84}$$

$$2\beta\bar{\Delta}\cos\theta = ne^{-Q(n)}, \tag{3.85}$$

where $\bar{\gamma}$ is the Euler's constant, and $\psi(z)$ is the polygamma function. From this expression, the specific heat is obtained as shown in Fig. 3.3 by numerical integration. We can see that even for weak damping, the specific heat is suppressed at low temperatures, and goes to zero in the limit $T \to 0$. This behavior is different from the dissipationless case $K = 0$, where C approaches a nonzero constant value at low temperatures. In the dissipationless case, the partition function is classical in the momentum in the sense that the Hamiltonian is diagonalized in the momentum space. Note that the quantization of the momentum due to a boundary condition is not taken in this formalism so that the specific heat approaches a classical nonzero value for $K = 0$.

The asymptotic expansion of Z for $\beta = 1/T(\gg 1)$ gives

$$\ln Z = 2(1-K)\beta c\Delta_{\rm eff} + \frac{1}{2}\ln K + \frac{1}{24K\beta c\Delta_{\rm eff}} + \mathcal{O}(\beta^{-2}), \tag{3.86}$$

where c is a renormalization factor defined by $c = (4\pi K e^{\bar{\gamma}})^{K/(1-K)}$, and takes $c \sim 1$ for weak damping $K \ll 1$. Details of the derivation are given in Appendix 3-E. From the partition function, we obtain the low-temperature behavior of the system energy E and the specific heat C as

$$E = -\frac{\partial}{\partial\beta}(\ln Z) = -2(1-K)c\Delta_{\rm eff} + \frac{1}{24K\beta^2 c\Delta_{\rm eff}} + \mathcal{O}(\beta^{-3}), \tag{3.87}$$

$$C = \frac{\partial E}{\partial T} = \frac{T}{12Kc\Delta_{\rm eff}} + \mathcal{O}(T^2). \tag{3.88}$$

We can see that the specific heat is proportional to the temperature T, and the coefficient depends on the damping strength as $C \simeq T/K\Delta_{\rm eff}$. We denote the relevant energy scale with $\gamma = 4\pi Kc\Delta_{\rm eff}$. As shown later, γ expresses the relevant energy scale in the optical conductivity in the weak coupling region. Then, we can write the specific heat as

$$C \simeq \pi T/3\gamma \tag{3.89}$$

at low temperatures.

Next, we discuss the density of states $D(\omega)$ of the dissipative particle. From the partition function, $D(\omega)$ is calculated by

$$Z(\beta) = \int_{-\delta}^{\infty} d\omega\, D(\omega) e^{-\beta\omega}. \tag{3.90}$$

Here, the energy is shifted in order that the ground state energy becomes zero, and the infinitesimal quantity δ is introduced for convenience. In the dissipationless case, the

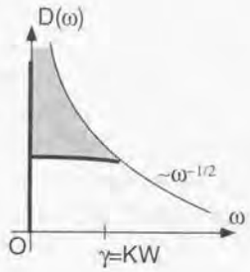

Figure 3.4: The density of states in the dissipative case (thick line) and the free case (thin line). By introducing dissipation, it seems that the states expressed by the patched area moves to the weight of the delta function at $\omega = 0$.

density of states of 1D lattice systems is calculated as

$$D(\omega) = \frac{1}{\pi\sqrt{\left(\frac{W}{2}\right)^2 - \left(\frac{W}{2} - \omega\right)^2}}, \tag{3.91}$$

where W is the band width. Particularly, for low-energy states, $D(\omega)$ behaves as

$$D(\omega) \simeq \frac{1}{\pi W}\left(\frac{\omega}{W}\right)^{-1/2}. \tag{3.92}$$

In the presence of dissipation, the density of low-energy states is strongly modified. To see this, we rewrite the partition function (3.86) by using the effective band width $W = 2c\Delta_{\rm eff}$ as

$$\begin{aligned} Z &\simeq \sqrt{K} e^{1/12K\beta W} \\ &\simeq \sqrt{K}\left(1 + \frac{1}{12K\beta W} + \mathcal{O}(\beta^{-2})\right). \end{aligned} \tag{3.93}$$

Then, the low-energy form of $D(\omega)$ is obtained from (3.90) as

$$D(\omega) \simeq \sqrt{K}\delta(\omega) + \frac{1}{12K^{1/2}W} + \mathcal{O}(\omega). \tag{3.94}$$

The difference between (3.92) and (3.94) is schematically shown in Fig. 3.4. We can see that the dissipative environment strongly modifies the low-energy states. Roughly speaking,

because of dissipation, some parts of low-energy states up to $\omega \sim KW$ (the patched region in Fig. 3.4) gathers to $\omega = 0$ in the form of the delta function. Although we cannot discuss the details of this change until the one-particle Green's function is obtained, it can be conjectured that the dispersion is modified to be flat by dissipation, and the wave function of the low-energy states is localized in space.

We note that similar behavior has been shown in two-state systems, where the Schottky form of the specific heat is modified to the T-linear behavior at the low temperatures [34]. (See also Sec. 1.2.4.) Also in this case, the T-linear behavior of the specific heat is induced by the modification of the density of states caused by the environment.

3.3.3 Optical conductivity

The limit of high temperatures and/or strong dissipation

For ohmic damping, $S(t)$ and $R(t)$ in (3.50)-(3.51) are obtained as

$$S(t) = 2K \log \left| \frac{\beta\omega_c}{\pi} \sinh\left(\frac{\pi t}{\beta}\right) \right|, \tag{3.95}$$

$$R(t) = \pi K \mathrm{sign}(t). \tag{3.96}$$

From (3.52) we obtain the optical conductivity $\sigma_{\rm res}(\omega) = e^2 a^2 \mathrm{Im}\Lambda(\omega)/\omega$ as

$$\sigma_{\rm res}(\omega) = 2e^2 a^2 \frac{\Delta^2}{\omega_c} \left(\frac{\beta\omega_c}{2\pi}\right)^{1-2K} \frac{|\Gamma(K + \mathrm{i}\beta\omega/2\pi)|^2}{\Gamma(2K)} \frac{\sinh \beta\omega/2}{\omega} \tag{3.97}$$

$$= 2e^2 a^2 \Delta_{\rm eff} \left(\frac{\beta\Delta_{\rm eff}}{2\pi}\right)^{1-2K} \frac{|\Gamma(K + \mathrm{i}\beta\omega/2\pi)|^2}{\Gamma(2K)} \frac{\sinh \beta\omega/2}{\omega}. \tag{3.98}$$

The temperature and frequency dependencies of $\sigma_{\rm res}(\omega)$ are shown in Fig. 3.5. In the low-frequency side ($\omega \ll KT$), $\sigma_{\rm res}(\omega)$ depends on the temperature. The DC conductivity $\sigma_{DC} = \sigma_{\rm res}(\omega \to 0)$ is calculated as

$$\sigma_{DC} = 2\pi e^2 a^2 \left(\frac{\beta\Delta_{\rm eff}}{2\pi}\right)^{2-2K} \frac{\Gamma(K)^2}{\Gamma(2K)}, \tag{3.99}$$

which is proportional to T^{2K-2}. On the other hand, in the high-frequency limit, $\sigma_{\rm res}(\omega)$ takes a temperature-independent form

$$\sigma_{\rm res}(\omega) = \frac{2\pi e^2 a^2}{\Gamma(2K)} \left(\frac{\Delta_{\rm eff}}{\omega}\right)^{2-2K}. \tag{3.100}$$

On the high-frequency side, $\sigma_{\rm res}(\omega)$ is proportional to ω^{-2+2K}, and deviates from the Drude form (3.80).

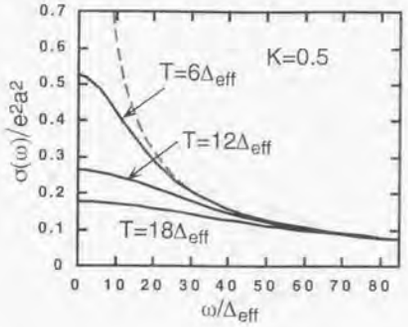

Figure 3.5: The optical conductivity $\sigma_{\rm res}(\omega)$ at high temperatures ($T = 6\Delta_{\rm eff}, 12\Delta_{\rm eff}, 18\Delta_{\rm eff}$) for $K = 0.5$. The dashed gray line represents the asymptotic behavior ($\propto 1/\omega$) at $\omega/\Delta_{\rm eff} \gg 1$. The characteristic energy at which the optical conductivity deviates from the asymptotic form is estimated as KT.

Weak coupling region

Next, we consider the weak damping region $K \ll 1$. For ohmic damping, the screened potential defined by (3.66) is calculated as

$$\varphi(\tau;\theta) = \frac{1}{\beta} \sum_{\omega_m} \frac{-2\pi K}{|\omega_m| + \gamma(\theta)} e^{-\mathrm{i}\omega_m \tau}, \tag{3.101}$$

where $\gamma(\theta)$ is the inverse of the screening length in the τ-direction given by

$$\gamma(\theta) = 2\pi K n(\theta)/\beta. \tag{3.102}$$

Following the usual way, the sum over the Matsubara frequencies in (3.101) is replaced by an integral form. As a result, $\varphi(\mathrm{i}t;\theta) = S(t;\theta) + \mathrm{i}R(t;\theta)$ is obtained as

$$R(t;\theta) = \pi K e^{-\gamma(\theta)t}, \tag{3.103}$$

$$S(t;\theta) = 2K \int_0^\infty \mathrm{d}\omega \frac{\omega}{\omega^2 + \gamma(\theta)^2} \left[\frac{2}{\beta\omega} - \coth\frac{\beta\omega}{2} \cos\omega t\right]$$
$$+ 2\pi K \Theta(-\gamma) \left[\frac{2}{\beta\omega} - \coth\frac{\beta\omega}{2} \cos\omega t\right], \tag{3.104}$$

where $\Theta(x)$ is a step function. For the no damping case $\gamma \to 0$, the above expressions become unscreened potentials, $S(t)$ and $R(t)$ in (3.50)-(3.51). Analytical expressions for

$S(t;\theta)$ are obtained only for two limiting cases. At high temperatures $\beta \to 0$, $S(t;\theta)$ is calculated as

$$S(t;\theta) = \frac{2\pi K}{\beta\gamma(\theta)}(1 - e^{-\gamma(\theta)t}). \tag{3.105}$$

On the other hand, at low temperatures, $S(t;\theta)$ is expanded by the temperature $T = 1/\beta$ as

$$S(t;\theta) = S_0(t;\theta) + \frac{2\pi KT}{\gamma(\theta)} + \mathcal{O}(T^2), \tag{3.106}$$

$$S_0(t;\theta) = K\left[e^{\gamma(\theta)t}\mathrm{Ei}(-\gamma(\theta)t) + e^{-\gamma(\theta)t}\mathrm{Ei}(\gamma(\theta)t)\right], \tag{3.107}$$

where $\mathrm{Ei}(z)$ is the exponential integral function, and $S_0(t)$ is a temperature-independent part. In both cases, the limiting value at $t \to \infty$ is given by

$$S(t \to \infty;\theta) = \frac{2\pi KT}{\gamma(\theta)}. \tag{3.108}$$

Although we can calculate $\sigma(\omega)$ by the expressions (3.103)-(3.104) for all temperatures, we only consider zero temperature in this chapter. At zero temperature, the dominant contribution comes from $\theta = 0$ in the integral (3.71). The real-time correlation function for $K \ll 1$ is obtained by using the asymptotic form $n = 2\beta c\Delta_{\mathrm{eff}}$ as

$$\Lambda(\omega) = \frac{\gamma_0}{2\pi K}\int_0^\infty dt\, e^{i\omega t - \gamma_0 t}\cosh\left[S_0(t)\right]. \tag{3.109}$$

Here, $\gamma_0 = \gamma(\theta = 0)$ is the damping frequency at $T = 0$ given by

$$\gamma_0 = 4\pi K c\Delta_{\mathrm{eff}}, \tag{3.110}$$

where $c = (4\pi K e^{\bar{\gamma}})^{K/(1-K)}$. The optical conductivity can be calculated by numerical Fourier transformation of (3.109). The result for $\sigma_{\mathrm{res}}(\omega)$ is shown in Fig. 3.6. The Drude formula (3.80) in the continuum limit is also shown. At the high frequency side, the optical conductivity of the dissipative system deviates from the Drude form.

The qualitative behavior of $\sigma(\omega)$ is obtained by considering the limiting from of $S_0(t)$:

$$S_0(t) = \begin{cases} 2K\log(e^{\bar{\gamma}}\gamma_0 t) & (t \to 0), \\ \dfrac{2K}{(\gamma_0 t)^2} & (t \to \infty), \end{cases} \tag{3.111}$$

where $\bar{\gamma}$ is the Euler's constant. From (3.109) and (3.111), the limiting behavior of the optical conductivity is obtained as

$$\sigma(\omega) = \begin{cases} \dfrac{2\pi e^2 a^2}{\Gamma(2K)}\left(\dfrac{\Delta_{\mathrm{eff}}}{\omega}\right)^{2-2K}, & (\omega \gg \omega^*), \\ \dfrac{e^2 a^2}{2\pi K}\dfrac{\gamma_0^2}{\gamma_0^2 + \omega^2}, & (\omega \ll \omega^*), \end{cases} \tag{3.112}$$

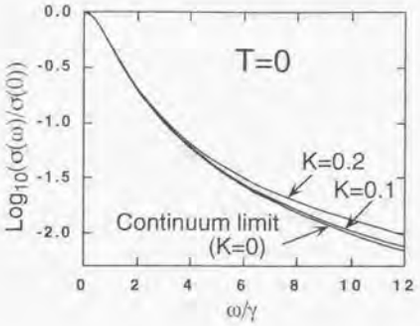

Figure 3.6: The optical conductivity $\sigma(\omega)$ at zero temperature for weak damping ($K = 0, 0.1, 0.2$). As the damping increases, $\sigma(\omega)$ deviates from the Drude form ($K = 0$). At high frequencies, $\sigma(\omega)$ is proportional to ω^{2K-2}.

where $\omega^* = (2c)^{1/K}\Delta_{\mathrm{eff}}$ is the crossover frequency at which the two expressions take the same value. The high-frequency behavior of $\sigma(\omega)$ agrees with the result of the high temperature limit (3.100). This indicates that the high-frequency side is independent of the temperature at *any* damping strength, since (3.100) is valid at any value of K. On the other hand, the low-frequency side coincides with the Drude form (3.80) obtained in the continuum limit. It is interesting that the asymptotic form in the limit $\omega \to \infty$ of the Drude form (the first equation in (3.112)) deviates from the high frequency form (the second equation in (3.112)) shown in the lower equation of (3.112) by a factor of 2. At first glance, one might be suspicious about this difference. However, this difference indeed exists: When we take the limit $K \to 0$, the crossover frequency ω^* in (3.112) goes to infinity. Then, the region $\omega \gg \omega^*$ disappears and the lower expression in (3.112) governs even the high-frequency region, which reproduces (3.80).

On the high frequency side $\omega \gg \omega^*$, the particle moves by using the heat-bath excitations. Therefore, the particle moves incoherently even at zero temperature. These results are relevant to photo-assisted tunneling [31].

DC conductivity

We consider the DC conductivity $\sigma_{\rm DC}$ of the lattice model for the weak coupling region ($K \ll 1$). The low-temperature behavior is obtained by the asymptotic expansion over $\beta = 1/T$ as

$$\sigma_{\rm DC}/\sigma^0_{\rm DC} = 1 - \frac{1}{8}\left(\frac{T}{e\Delta_{\rm eff}}\right)^2 + \mathcal{O}(T^4), \tag{3.113}$$

where $\sigma^0_{\rm DC} = e^2a^2/2\pi K$. (See Appendix 3-E.) Thus, the thermal fluctuations suppress $\sigma_{\rm DC}$. The T^2-suppression at low temperatures is consistent to the general study of the linear mobility $\mu_l = \sigma_{\rm DC}/e^2$ [56]. In the previous work, the linear mobility has not been obtained correctly even in the weak damping $K \ll 1$ [128]. The high-temperature limit of $\sigma_{\rm DC}$ for $K \ll 1$ is obtained from (3.99) as

$$\sigma_{\rm DC}/\sigma^0_{\rm DC} = 8\pi^2\left(\frac{\beta\Delta_{\rm eff}}{2\pi}\right)^{2-2K}. \tag{3.114}$$

For the special value of $K = 1/2$, the mobility is calculated for all temperatures [56]. Let us compare the result with the one obtained in the weak damping region. For $K = 1/2$, the linear mobility is calculated as

$$\mu_l = \frac{\mu_0\Delta_{\rm eff}}{2T}\psi'(\Delta_{\rm eff}/2T + 1/2), \tag{3.115}$$

where $\psi'(z)$ is the trigamma function, and $\mu_0 = a^2/2\pi K$. At low temperatures, the DC conductivity $\sigma_{\rm DC} = \mu_l/e^2$ behaves for $K = 1/2$ as

$$\sigma_{\rm DC}/\sigma^0_{\rm DC} \simeq 1 - \frac{T^2}{3\Delta^2_{\rm eff}}, \tag{3.116}$$

and shows the T^2-suppression. This strongly indicates that the T^2-suppression appears for any value of $0 < K \leq 1/2$. At high temperatures, the DC conductivity for $K = 1/2$ shows a $1/T$ behavior as

$$\sigma_{\rm DC}/\sigma^0_{\rm DC} \simeq \frac{\pi^2\Delta_{\rm eff}}{4T}, \tag{3.117}$$

which agrees with (3.99) for $K = 1/2$.

3.3.4 Application to small Josephson junctions

As discussed in Sec. 3.1, the dissipative dynamics in a periodic potential can be directly connected to the I-V characteristics of small resistance-shunted Josephson junctions. In this subsection, we apply the results of the ohmic damping to the Josephson junction systems. In this subsection, the Plank constant $\hbar$ is revived to clarify the discussion.

The dimensionless coupling constant K of the ohmic damping is related to the shunted resistance R as

$$K = \frac{R_{\rm Q}}{R}. \tag{3.118}$$

Here, $R_{\rm Q} = \hbar/(2e)^2 = 6.5[{\rm k}\Omega]$ is the quantum resistance. In this chapter, the weak coupling region $K \ll 1$ has been studied mainly, and this condition is easily satisfied if R is taken much larger than $R_{\rm Q}$.

The I-V characteristics is obtained from (3.2) within the linear response theory as

$$V = \mu_{\rm DC} I, \tag{3.119}$$

where $\mu_{\rm DC} = \sigma_{\rm DC}/e^2$ is the mobility of the particle. From this relation, the results obtained in the previous subsection can be connected to the I-V characteristic of the resistance-shunted small Josephson junctions. The temperature dependence of the mobility in the weak damping region $K \ll 1$ is calculated by the junction parameters as

$$\mu_{\rm DC} = \begin{cases} R\left(1 - \left(\frac{T}{8\Delta_{\rm eff}}\right)^2 + \mathcal{O}(T^4)\right), \\ 8\pi^2 R\left(\frac{\Delta_{\rm eff}}{2\pi T}\right)^{2-2K}. \end{cases} \tag{3.120}$$

Here, $\Delta_{\rm eff}$ is the fitting parameter which should be determined experimentally. At high temperatures, the mobility increases as the temperature decreases, while at low temperatures ($T < \Delta_{\rm eff}$), the mobility saturates to R.

Let us discuss the physical meaning of the above result based on the conservation law of the current:

$$C\dot{V} + \frac{V}{R} + I_0 \sin\phi = I. \tag{3.121}$$

At zero temperature, $\mu_{\rm DC}$ saturates to R, and the generated voltage becomes $V = IR$. From (3.121), this means that the junction behaves just as the Josephson coupling vanishes ($I_0 \to 0$). In this situation, the whole external current flows through the shunted resistance as the normal current. As the temperature increases, the generated voltage decreases, and the voltage vanishes in the high temperature limit. In this situation, the whole external current flows as the super current through the Josephson coupling between superconductors, and no current flows through the resistance.

We can associate this temperature-dependence of μ_{DC} with the results in the Kondo problem in a qualitative level. As discussed in Sec. 1.2.4, the dissipative two-state systems can be mapped to the Kondo Hamiltonian. Then, the Kondo temperature T_K is scaled by Δ_{eff}, and determines the characteristic energy scale of the system. Also in the dissipative multi-state systems, $T_K \sim \Delta_{eff}$ is thought to determine the characteristic energy scale. At high temperatures ($T \gg T_K$), the particle hops between periodic wells incoherently, and is described by the classical master equation. On the other hand at low temperatures ($T \ll T_K$), more complicated quantum dynamics occurs, and causes the saturation of the mobility. This behavior is thought to be related to the Kondo problem where the impurity spin shows the Curie law at high temperatures, and the spin-singlet state is constituted at low temperatures.

At zero temperature, the optical mobility $\mu(\omega) = \sigma(\omega)/e^2$ is evaluated in the previous subsection as

$$\mu(\omega) = \begin{cases} \dfrac{R}{\Gamma(2K-1)}\left(\dfrac{\Delta_{eff}}{\omega}\right)^{2-2K}, & (\omega > \omega^*), \\ R\dfrac{\gamma_0^2}{\gamma_0^2+\omega^2}, & (\omega < \omega^*), \end{cases} \tag{3.122}$$

where $\gamma_0 \simeq 4\pi K\Delta_{eff}$ gives the damping energy in the Lorentzian form. The crossover frequency between the Lorentzian from and the asymptotic form proportional to ω^{2K-2} is given as $\omega^* \sim 2^{1/K}\gamma_0$. For $K \ll 1$, this frequency ω^* is much larger than γ_0. Note that the expression (3.122) is valid for $\omega \ll \omega_p$.

At high temperatures, the optical mobility is calculated as

$$\mu(\omega) = 4\pi KR\Delta_{eff}\left(\frac{\beta\Delta_{eff}}{2\pi}\right)^{2-2K}\frac{|\Gamma(K+i\beta\omega/2\pi)|^2}{\Gamma(2K)}\frac{\sinh\beta\omega/2}{\omega}. \tag{3.123}$$

The characteristic frequency is given by $\omega \sim KT$. When the temperature decrease, the expression (3.122) becomes wrong below a crossover temperature. This crossover temperature is estimated as $\Delta_{eff} \sim T_K$ where the characteristic frequencies in (3.122) and (3.123) take the same order ($\gamma_0 = 4\pi K\Delta_{eff} \sim KT$). Thus, it is expected that the optical properties also change at the Kondo temperature T_K.

Let us estimate experimental parameters which allows comparison with the theory. For simplicity, the junction parameters are taken as those adopted in Sec. 2.1.3. The plasma frequency ω_p is independent of the area of the Josephson junction, and estimated as $\omega_p \sim 5 \times 10^{11}$[1/s]. To realize the tight-binding limit, the Josephson coupling energy E_J must

be sufficiently large as compared with ω_p. Additionally, the effective hopping amplitude must be large enough to observe the behavior of the mobility at the crossover temperature, which is of the order of Δ_{eff}. Although the estimate of Δ_{eff} is difficult, the upper limit is evaluated by the bare tunneling matrix Δ calculated by the Langer's WKB method when $E_J \gg \omega_p$. The tunneling matrix Δ is controlled by E_J as

$$\Delta \sim \omega_p \exp\left(-\frac{8E_J}{\hbar\omega_p}\right). \tag{3.124}$$

From this equation, E_J must be small enough for Δ not to be too small. Since the Josephson energy E_J is proportional to the area of the junction, the ratio between E_J and ω_p can be controlled by the area of the junction. Unfortunately, in the WKB condition $E_J \gg \omega_p$, the tunneling amplitude Δ becomes so small that the crossover behavior calculated in (3.120) cannot be observed experimentally. To make Δ a realistic value, E_J must be order of ω_p. The area of the junction to satisfy this condition is estimated as $\sim 0.05[\mu m^2]$ from the parameters given in Sec. 2.1.3. In this case, the WKB condition is not satisfied, and the WKB result (3.124) is expected to give only a rough estimate of Δ. The tunneling amplitude is estimated as

$$\Delta \sim 1.3[\text{mK}]. \tag{3.125}$$

Thus, the crossover behavior (3.120) may be observed when the temperature is controlled as $T \sim 1$[mK].

The behavior of the optical mobility calculated in (3.122) is also expected to be observed when $T \ll 1$[mK]. The characteristic frequency γ_0 in (3.122) is estimated as $\gamma_0 \sim 30$[MHz], which seems to be attainable in the presently available experimental techniques.

Finally, we summarize the results about the Josephson junction systems. At high temperatures, classical 2π-phase slips due to the tunneling effects are dominant , where the mobility is determined by the tunneling rate. On the other hand at low temperatures ($T \ll T_K$), more complicated quantum dynamics occurs, and μ_{DC} saturates to R. This crossover behavior can never be obtained within the classical or semiclassical treatment. Thus, it would be a basic and nontrivial experiment to study the low-temperature properties of small resistance-shunted Josephson junctions. Additionally, there may be possibilities to observe new quantum effects by studying non-linear responses or by studying other situations. This problem remains for future studies.

3.4 Summary of this Chapter

We have studied the thermodynamics and transport properties of the dissipative particle in the tight-binding model. By utilizing the imaginary-time path integral, the specific heat and the optical conductivity have been formulated for arbitrary form of the spectral density. A systematic approximation has been considered to treat the weak-coupling region at all temperatures. We have obtained an analytical form which can connect the high-temperature region to the low-temperature region.

The actual calculation has been performed for the ohmic damping case. The specific heat at weak damping shows T-linear behavior at low temperatures, and the density of low-energy states is modified by dissipation. The optical conductivity shows non-Drude from even at zero temperature, and behaves as ω^{2K-2} on the high-frequency side, where K is the dimensionless damping strength. At high temperatures, the high-frequency side does not change the non-Drude form, and only the low-frequency side depends on the temperature T. Particularly, the DC conductivity is proportional to T^{2K-2}.

In this chapter, we have focused only on ohmic damping. The detailed calculation for the non-ohmic damping and the solvable line $K = 1/2$ remains for future studies. We expect that the simple model considered in this chapter may contribute to the understanding of transport properties of a particle coupled to other degrees of freedom, and wish that the results of this chapter may be directly observed in a properly fabricated experiment.

Appendix of Chapter 3

3·A Non-ohmic Damping in the Incoherent Tunneling Regime

In this appendix, we study the optical conductivity $\sigma(\omega)$ for the non-ohmic damping case in the incoherent regime following the formulation in Sec. 3.2.4. The results of the tunneling rate $\Gamma(\varepsilon)$ obtained in ref. [30] are utilized to obtain $\sigma(\omega)$. We only consider a few limiting cases which allow analytical treatment.

We begin with superohmic damping $1 < s < 2$. Under the strong bias $\varepsilon \gg \tilde{\Delta}$ and the

weak coupling condition $\delta_s(\varepsilon/\tilde{\omega})^{s-1} \ll 1$, the tunneling rate $\Gamma(\varepsilon)$ is calculated as

$$\Gamma(\varepsilon) = \frac{a^2}{2}\left(\frac{2\tilde{\Delta}}{\varepsilon}\right)^2 J(\varepsilon)\coth(\beta\omega/2). \tag{3.126}$$

By using (3.7) and (3.56), we obtain the optical conductivity as

$$\sigma(\omega) = 4\pi\delta_s\left(\frac{\tilde{\Delta}}{\omega}\right)^2\left(\frac{\omega}{\tilde{\omega}}\right)^{s-1}. \tag{3.127}$$

which is temperature-independent at all temperatures. Hence, the optical conductivity behaves as $\sigma(\omega) \propto \omega^{s-3}$. This behavior corresponds to the result (3.46) in the continuum limit $(T, \delta_s \to 0)$ on the high frequency side, except for a difference by a factor of 2. The same difference appears also in the case of ohmic damping, and the origin of the factor 2 is expected to be the same. (See (3.112) and the following text.)

The tunneling rate for $\varepsilon = 0$ is calculated as follows:

$$\Gamma = \left(\frac{(2-s)\sin(\pi s/2)}{2\delta_s\Gamma(s-1)\sin\pi(s-1)}\right)^{1/(2-s)}\Gamma\left(\frac{3-s}{2-s}\right)\frac{\tilde{\Delta}^2}{\tilde{\omega}}\left(\frac{\tilde{\omega}}{T}\right)^{1/(2-s)}. \tag{3.128}$$

This result is valid at high temperatures $T^* \ll T (\ll \omega_c)$, where T^* is given by

$$T^* = \frac{\tilde{\Delta}}{\delta_s\Gamma(s-1)}\left(\frac{\tilde{\omega}}{\tilde{\Delta}}\right)^{s-1}. \tag{3.129}$$

The DC conductivity is obtained from (3.128) by $\sigma_{\rm DC} = e^2a^2\Gamma/2T$, and behaves as $\sigma_{\rm DC} \propto T^{-\frac{3-s}{2-s}}$ at high temperatures. The exponent of T decreases from -2 to $-\infty$ by increasing s from 1 to 2.

Next, we consider subohmic damping $0 < s < 1$. At zero temperature, the tunneling rate is calculated under the condition $\delta_s(\varepsilon/\tilde{\omega})^{s-1} \gg 1$ as

$$\begin{aligned}\Gamma(\varepsilon) &= \frac{(B\Delta)^2}{4\tilde{\omega}}\left(\frac{2\pi[2\delta_s\Gamma(s)]^{1/2}}{s}\right)^{1/2}\left(\frac{\tilde{\omega}}{\varepsilon}\right)^{(1+s)/2s} \\ &\quad\times\exp\left[-\frac{s}{1-s}[2\delta_s\Gamma(s)]^{1/s}\left(\frac{\tilde{\omega}}{\varepsilon}\right)^{(1-s)/s}\right],\end{aligned} \tag{3.130}$$

where $B = \exp[\delta_s|\Gamma(s-1)|(\tilde{\omega}/\omega_c)^{1-s}]$. This result cannot be related to the result of the continuum limit because of the strong coupling condition $\delta_s(\varepsilon/\tilde{\omega})^{s-1} \gg 1$. The optical conductivity is obtained by $\sigma(\omega) = a^2e^2\Gamma(\omega)/\omega$, and behaves as $\sigma(\omega) \sim \omega^{-(1+3s)/2s}\exp(-\text{const.}\omega^{-(1-s)/s})$. Notice that the optical conductivity vanishes with an essential singularity as $\omega \to 0$.

The tunneling rate for $z = 0$ for the condition $\delta_s(\bar{\omega}/T)^{1-s} \gg 1$ is given by

$$\Gamma = \frac{(B\Delta)^2}{2\bar{\omega}}\left(\frac{\bar{\omega}}{T}\right)^{(1+s)/2}\left(\frac{\pi}{2(1+s)^2\Gamma(s)\zeta(1+s)\delta_s}\right)^{1/2} \times \exp\left[-\frac{1+s}{1-s}\Gamma(s)\left(\frac{1}{2(1+s)\zeta(1+s)}\right)^{(1-s)/(1+s)}\delta_s\left(\frac{\bar{\omega}}{T}\right)^{1-s}\right]. \quad (3.131)$$

From (3.131), the DC conductivity is obtained by $\sigma_{\rm DC} = a^2e^2\Gamma/2T$, and behaves as $\sigma_{\rm DC} \sim T^{-(3+s)/2}\exp(-\text{const.} \times T^{s-1})$. The DC conductivity vanishes with an essential singularity as $T \to 0$, and this result is consistent with the continuum limit, where $\sigma_{\rm reg}(\omega \to 0) = 0$. Note that the power law $\sigma_{\rm DC} \sim T^{2K-2}$ for the ohmic case $s = 1$ is obtained from (3.131) by carefully considering the limit $s \to 1^-$.

3·B Calculation of ϕ_0

In this appendix, we evaluate the zero frequency component $\phi_0 = \phi(\mathrm{i}\omega_m = 0)$. From (3.58) and (3.10)-(3.11), ϕ_0 is explicitly given as

$$\phi_0 = \frac{a^2}{\pi}\int_0^\infty \mathrm{d}\omega\frac{J(\omega)}{\omega^2}\left(\coth\frac{\beta\omega}{2} - \frac{2}{\beta\omega}\right). \quad (3.132)$$

We consider the analytical form of the spectral density

$$J(\omega) = \frac{2\pi\delta_s}{a^2}\left(\frac{\omega}{\bar{\omega}}\right)^{s-1}\omega\mathrm{e}^{-\omega/\omega_c}, \quad (3.133)$$

where the exponential cut-off is adopted, and the cutoff frequency ω_c is taken as $\Delta, 1/\beta \ll \omega_c$. By substituting (3.133) to (3.132), we obtain

$$\phi_0 = 2\delta_s\left(\frac{\omega_c}{\bar{\omega}}\right)^z\Gamma(z)\left[\frac{2}{(\beta\omega_c)^z}\zeta(z, 1/\beta\omega_c) - 1 - \frac{2}{z-1}\frac{1}{\beta\omega_c}\right] \quad (3.134)$$

$$\simeq 2\delta_s\left(\frac{\omega_c}{\bar{\omega}}\right)^z\Gamma(z)\left[1 + \frac{2\zeta(z)}{(\beta\omega_c)^z} + \mathcal{O}(1/\beta\omega_c)\right], \quad (3.135)$$

where $z = s - 1$, and $\zeta(z, a)$ is the generalized zeta function, and $\zeta(z)$ is the zeta function. In the second equation, we have left only the leading terms under the condition $\beta\omega_c \gg 1$. For the superohmic case $z > 0$, the first term in the bracket is dominant, and ϕ_0 is temperature independent. Further, the result is expressed generally by the Frank-Condon factor calculated as

$$\phi_0 = \frac{a^2}{\pi}\int_0^\infty \frac{J(\omega)}{\omega^2}\mathrm{d}\omega. \quad (3.136)$$

On the other hand, for subohmic damping $z = s - 1 < 0$, the second term in the bracket in (3.135) is dominant. Hence, ϕ_0 depends on the temperature. For the ohmic case $s = 1$, the expression (3.135) fails, and careful treatment of (3.134) is required. As a result, the leading term in ϕ_0 depends logarithmically on the temperature as

$$\phi_0 \simeq 2K\log\frac{\beta\omega_c}{2\pi}, \quad (3.137)$$

where $K = \delta_1$. In this case, the renormalized matrix element (3.61) is given by

$$\bar{\Delta} = \Delta\left(\frac{\beta\omega_c}{2\pi}\right)^{-K}. \quad (3.138)$$

At a first glance, one might regard this result as unphysical, because the matrix element is reduced to zero as the temperature decreases even for the weak coupling region $K \ll 1$. We, however, show that the renormalization factor $(\beta\omega_c/2\pi)^{-K}$ is canceled by other factors for observables in the weak coupling theory.

3·C Ring Approximation

In this appendix, we give details of the calculation in the weak coupling theory (§ 3.2.5) for the arbitrary form of $J(\omega)$. We first study the partition function based on the cluster expansion of classical imperfect gas [129]. The partition function and the optical conductivity are formulated by the ring approximation.

We begin with the partition function (3.14). After the potential shift (3.60), we obtain

$$Z = \sum_{m=0}^{\infty}\frac{\bar{\Delta}^{2m}}{m!m!}\prod_{l=1}^{m}\int_0^\beta \mathrm{d}\tau_l\int_0^\beta \mathrm{d}\rho_l \times \exp\left[\sum_{k<l}^{m}\{\phi(\tau_l - \tau_k) + \phi(\rho_l - \rho_k)\} - \sum_{l=1}^{m}\sum_{k=1}^{m}\phi(\tau_l - \rho_k)\right\}, \quad (3.139)$$

where $\bar{\Delta}$ is the renormalized transition amplitude defined by (3.61). Here, new integral variables $\{\tau_l\}$ and $\{\rho_l\}$ describe the positions of positive ($\xi_l = +1$) and negative ($\xi_l = -1$) charges. Note that the partition function is multiplied by the factor $2m!/m!m!$. This factor comes from the number of the ways in which $2m$ charges are divided into two groups consisting of m charges to guarantee the electroneutrality condition (3.15). Then, we consider the cluster expansion for the partition function (3.139). To simplify the expansion,

we rewrite it in the following form

$$Z = \sum_{m=0}^{\infty} \frac{(\beta\tilde{\Delta})^{2m}}{m!m!} \langle \prod_{k<l}^{m} (1 + f_{kl}^{++})(1 + f_{kl}^{--}) \prod_{k=1}^{m}\prod_{l=1}^{m} (1 + f_{kl}^{+-}) \rangle, \tag{3.140}$$

Here, the potential $\phi(\tau)$ is replaced by Mayer's functions

$$f_{kl}^{++} = e^{\phi(\tau_k - \tau_l)} - 1, \tag{3.141}$$

$$f_{kl}^{--} = e^{\phi(\rho_k - \rho_l)} - 1, \tag{3.142}$$

$$f_{kl}^{+-} = e^{-\phi(\tau_k - \rho_l)} - 1, \tag{3.143}$$

and $\langle \cdots \rangle$ denotes the average

$$\langle \cdots \rangle = \frac{1}{\beta^{2m}} \prod_{l=1}^{m} \int_0^\beta d\tau_l \int_0^\beta d\rho_l \, (\cdots). \tag{3.144}$$

Each term in the expansion on f_{kl} in (3.140) is expressed by a product of integrals of clusters. We introduce cluster integrals

$$b_{l,k} = \frac{1}{l!k!} \sum_{\text{clusters}} \langle \prod_{i,j} f_{ij}^{\sigma_i \sigma_j} \rangle, \tag{3.145}$$

where $\sum_{\text{clusters}}$ denotes the sum of all clusters including k positive charges and l negative charges. The products are taken over all bonds combining i-th and j-th charges in each cluster, where σ_i and σ_j are the signs of the charges. For example, the explicit form of $b_{l,k}$ for small k, l is given by

$$b_{0,0} = 0, \quad b_{10} = b_{01} = 1, \tag{3.146}$$

$$b_{2,0} = \frac{1}{2} \langle f_{12}^{++} \rangle, \tag{3.147}$$

$$b_{1,1} = \langle f_{12}^{+-} \rangle, \tag{3.148}$$

$$b_{3,0} = \frac{1}{6} \langle f_{12}^{++} f_{23}^{++} f_{31}^{++} + 3 f_{12}^{++} f_{23}^{++} \rangle, \tag{3.149}$$

$$b_{2,1} = \frac{1}{2} \langle f_{12}^{++} f_{23}^{+-} f_{13}^{+-} + 2 f_{12}^{++} f_{23}^{+-} + f_{13}^{+-} f_{23}^{+-} \rangle, \tag{3.150}$$

and so on. The above integrals can be depicted by graphical representations as shown in Fig. 3.7. The partition function is expressed by the cluster integrals $b_{l,k}$ as

$$Z = \sum_{m=0}^{\infty} \frac{(\beta\tilde{\Delta})^{2m}}{m!m!} \sum_{\{m_{l,k}\}'} \frac{m!}{\prod_{l,k} m_{l,k}! (l!)^{m_{l,k}}}$$

$$\times \frac{m!}{\prod_{l,k} m_{l,k}! (k!)^{m_{l,k}}} \times \prod_{l,k} (l!k! b_{l,k})^{m_{l,k}} \times \prod_{l,k} m_{l,k}!, \tag{3.151}$$

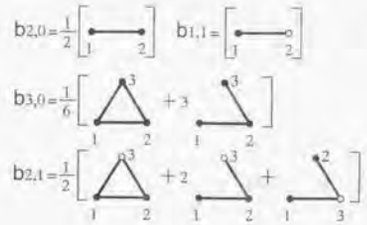

Figure 3.7: The diagrams representing the integrals $b_{l,m}$. The closed (open) circles denote the positive (negative) charges. Note that $b_{l,m} = b_{m,l}$.

where $m_{l,k}$ is the number of clusters including l positive charges and k negative charges. The sums and products are taken over l and k except for the case $(l,k) = (0,0)$. The prime in $\{m_{l,k}\}'$ denotes the summation in accordance with the conditions

$$\sum_{l,k} l m_{l,k} = m, \tag{3.152}$$

$$\sum_{l,k} k m_{l,k} = m. \tag{3.153}$$

The first (second) factor in the sum $\sum_{\{m_{l,k}\}'}$ in (3.151) gives the number of ways in which m positive (negative) charges can be distributed into the clusters. The third part is the relevant cluster integral, and the forth part is the number of ways to combine $m_{l,k}$ groups of positive charges to $m_{l,k}$ groups of negative charges.

From (3.152)-(3.153), we obtain the constraint on the total number of charges as

$$\sum_{l,k} (l + k) m_{l,k} = 2m, \tag{3.154}$$

and this constraint can be removed by the sum over m. On the other hand, the electroneutrality condition

$$\sum_{l,k} (l - k) m_{l,k} = 0, \tag{3.155}$$

remains. To remove the constraint (3.155), we introduce an integral over a new variable θ as

$$\sum_{m=0}^{\infty} \sum_{\{m_{l,k}\}'} (\cdots) = \sum_{\{m_{l,k}\}} \int_0^{2\pi} \frac{d\theta}{2\pi} \exp\left(i \sum_{l,k} (l - k) m_{l,k} \right) (\cdots). \tag{3.156}$$

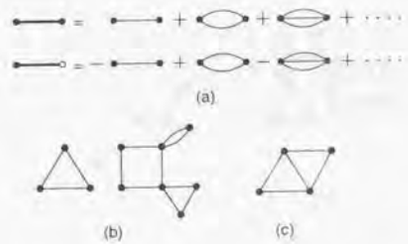

Figure 3.8: The diagrammatic graphs representing the expansion are drawn in (a). The graphs in both (b) and (c) are representative cluster integrals: (b) each charge has even bonds, while (c) includes charges with odd bonds.

From (3.151) and (3.156), the partition function Z is obtained as

$$Z = \int_0^{2\pi} \frac{\mathrm{d}\theta}{2\pi} \exp\left(\sum_{l,k} b_{l,k} (\beta\bar{\Delta})^{l+k} \mathrm{e}^{\mathrm{i}(l-k)\theta} \right). \tag{3.157}$$

For the dissipationless case ($K = 0, \bar{\Delta} = \Delta$), $b_{l,k}$ vanishes for $l + k \geq 2$ and the partition function is exactly calculated as

$$Z = \int_0^{2\pi} \frac{\mathrm{d}\theta}{2\pi} \exp(2\beta\Delta\cos\theta) = I_0(2\beta\Delta), \tag{3.158}$$

where $I_0(z)$ is the Modified Bessel function. Of course, this result is also obtained by usual the treatment for the tight-binding model of a free particle.

So far, the obtained expression for Z is exact. In the following discussion, the so-called 'ring approximation' is introduced. First, we expand $f_{ij}^{\sigma_i\sigma_j}$ as

$$f_{ij}^{++} = f_{ij}^{--} = \sum_{n=1}^{\infty} \frac{\{\phi(\tau_i - \tau_j)\}^n}{n!}, \tag{3.159}$$

$$f_{ij}^{+-} = \sum_{n=1}^{\infty} \frac{\{-\phi(\tau_i - \tau_j)\}^n}{n!}. \tag{3.160}$$

Graphical representations of the expansion are given in Fig. 3.8(a), where the bond denoted with n thin lines denotes $\phi(\tau_i - \tau_j)^n$. Here, we assume that (I) the dominant contribution comes from the clusters in which each charge is combined by 'even' bonds to other charges. Based on the assumption (I), we neglect other clusters which do not satisfy this condition.

For example, we consider the graphs as shown in Fig. 3.8(b), and neglect the graphs as shown in Fig. 3.8(c). At this stage, however, in order to avoid confusion, we do not justify the assumption (I). We mention this point after introducing the ring approximation.

The diagrams as shown in Fig. 3.8(b) have the crucial property that the cluster integral on the graphs remains constant when the sign of each charge is reversed. As a result, the cluster integral $l!k!b_{l,k}$ depends only on the total charge number $l + k$. In this situation, $l!k!b_{l,k}$ can be denoted with $(l+k)!b_{l+k}$, and the sum over l, k under the constraint $l+k = m$ in the partition function (3.157) gives

$$Z = \int_0^{2\pi} \frac{\mathrm{d}\theta}{2\pi} \exp\left(\sum_{m=1}^{\infty} b_m \xi^m \right). \tag{3.161}$$

Here $\xi = 2\beta\bar{\Delta}\cos\theta$ is regarded as a fugacity of 'one-component' classical charges. Because the remaining calculation follows the usual procedure of the classical imperfect gas as given in Ref. [129], we briefly note the results next. The diagrams, in which all charges are more than singly connected, are called irreducible diagrams. The irreducible integrals β_l are defined on the irreducible diagrams with the size $(l + 1)$ as

$$\beta_l = \frac{1}{l!} \sum_{\substack{\text{irreducible} \\ \text{clusters}}} \langle \prod_{i,j} (\phi(\tau_i - \tau_j))^{n_{i,j}} \rangle, \tag{3.162}$$

where the product is taken over all bonds in a cluster, and $n_{i,j}$ is the number of bonds combining i-th and j-th charges. Every cluster integral b_l can be expressed as a sum of terms, each of which is a numerical coefficient multiplied by a product of powers of the reduced integrals β_l as

$$\begin{aligned} b_1 &= 1, \quad & b_3 &= \tfrac{1}{2}\beta_1^2 + \tfrac{1}{3}\beta_2, \\ b_2 &= \tfrac{1}{2}\beta_1, \quad & b_4 &= \tfrac{2}{3}\beta_1^3 + \beta_1\beta_2 + \tfrac{1}{4}\beta_3. \end{aligned} \tag{3.163}$$

In general, it is proved that the equation for b_l is

$$b_l = \frac{1}{l^2} \sum_{\{m_k\}'} \prod_k \frac{(l_k\beta_k)^{m_k}}{m_k!}, \tag{3.164}$$

where the prime in $\{m_k\}'$ denotes the summation subject to the constraint

$$\sum_{k=1}^{l-1} k m_k = l - 1. \tag{3.165}$$

We also define the particle density n by

$$n = \sum_{m=1}^{\infty} m b_m \xi^m. \tag{3.166}$$

This value corresponds to the average of the hopping number in the imaginary-time path $q(\tau)$ in the original action, and qualitatively gives an effective hopping amplitude through $\Delta_{\rm eff}^{-1} \simeq \beta/n$. By using β_l and n, the partition function Z can be expressed in a closed form. To see this, we expand ξ by n as

$$\xi = a_1 n + a_2 n^2 + \cdots, \tag{3.167}$$

and determine $a_1, a_2, \cdots$ so that (3.166) is satisfied. Thus, we obtain

$$\begin{aligned} a_1 &= b_1^{-1} = 1, \quad a_3 = 8b_2^2 - 3b_3, \\ a_2 &= -2b_2, \qquad a_4 = -40b_2^3 + 30b_2 b_3 - 4b_4. \end{aligned} \tag{3.168}$$

From (3.163), these results can be rewritten in terms of the β_l's as

$$\begin{aligned} a_1 &= 1, \qquad a_3 = -(\beta_2 - \tfrac{1}{2}\beta_1^2), \\ a_2 &= -\beta_1, \quad a_4 = -(\beta_3 - \beta_1\beta_2 + \tfrac{1}{6}\beta_1^3). \end{aligned} \tag{3.169}$$

In general, ξ is expressed by the particle density n as

$$\xi = 2\beta\bar{\Delta}\cos\theta = n\exp\left(-\sum_{l=1}^{\infty}\beta_l n^l\right). \tag{3.170}$$

It can be checked easily that the first four terms in the expansion of (3.170) gives (3.169). The partition function (3.161) is expressed in terms of β_l and n by utilizing (3.167) and (3.169). As a result we obtain

$$Z = \int_0^{2\pi}\frac{\mathrm{d}\theta}{2\pi}\exp[U(n)], \tag{3.171}$$

$$U(n) = n\left(1 - \sum_{l=1}^{\infty}\frac{l}{l+1}\beta_l n^l\right). \tag{3.172}$$

When we introduce

$$Q = \sum_{l=1}^{\infty}\beta_l n^l, \tag{3.173}$$

the relation (3.170) and the exponent $U(n)$ is expressed in simple forms as

$$\xi = n\mathrm{e}^{-Q(n)}, \tag{3.174}$$

$$U = n + \int_0^n \mathrm{d}n\, Q - nQ. \tag{3.175}$$

Figure 3.9: The ring irreducible graphs considered in the ring approximation.

At this stage, we introduce the approximation by assuming that only the ring irreducible diagrams as shown in Fig. 3.9 are dominant. This approximation is called the 'ring approximation'. Then, the irreducible integrals β_l are expressed by the Fourier component $\phi(\mathrm{i}\omega_m)$ as

$$\beta_l = \frac{1}{2\beta^{l+1}}\sum_{\mathrm{i}\omega_m}\phi(\mathrm{i}\omega_m)^{l+1}, \tag{3.176}$$

and thus we obtain

$$Q = \frac{1}{\beta^2}\sum_{\omega_m>0}\frac{n\phi(\mathrm{i}\omega_m)^2}{1 - n\phi(\mathrm{i}\omega_m)/\beta}. \tag{3.177}$$

Here, the sum is taken over the Matsubara frequencies, $\omega_m = 2\pi m/\beta$. The justification of the ring approximation is not clear. However, it can be proved that this approximation is equivalent to the Debye-Hückel theory, which has been considered to calculate thermodynamic quantities in strong electrolytes [130]. In the Debye-Hückel theory, the screening effects due to the other charges are described by a screening potential $\varphi(\tau)$. (The explicit form of the screening potential is given in (3.66).) These screening effects are essential to study thermodynamic quantities at low-temperatures in the original model. In the ring approximation, the assumption (I) adopted in the previous discussion is automatically satisfied, because the neglected diagrams by the assumption (I) are also removed in the ring approximation.

Next, we calculate the optical conductivity. The correlation function $\tilde{\Lambda}_1(\tau)$ in (3.29) is expressed by the cluster integrals as

$$\begin{aligned} \tilde{\Lambda}_1(\tau) &= \frac{2\bar{\Delta}^2}{Z}\int_0^{2\pi}\frac{\mathrm{d}\theta}{2\pi}\exp\left(\sum_{l,k} b_{l,k}(\beta\bar{\Delta})^{l+k}\mathrm{e}^{\mathrm{i}\theta(l-k)}\right) \\ &\quad\times \sum_{l,k} B_{l,k}(\beta\bar{\Delta})^{l+k}\mathrm{e}^{\mathrm{i}\theta(l-k)}. \end{aligned} \tag{3.178}$$

Here, $B_{l,k}$ is the cluster integral of the diagram including two 'fixed' charges at $\tau' = 0, \tau$, and l and k are the numbers of additional positive and negative charges. Note that diagrams in which the two 'fixed' charges are separated into two clusters do not contribute to the optical conductivity, because such terms are independent of τ.

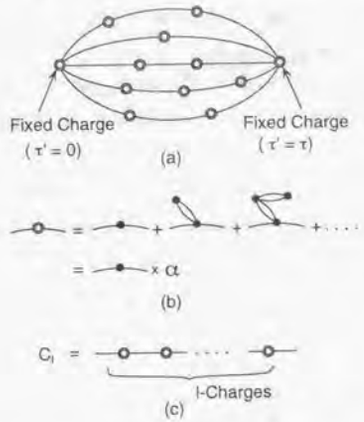

Figure 3.10: (a) The representative diagram relevant to the optical conductivity in the ring approximation. The renormalization of the fugacity ξ is denoted with the sum of diagram (b). The diagram (a) can be divided into the lines with l charges as shown in Fig. (c).

In the ring approximation, (3.178) is reduced to the partition function of one-component charged particles. Thus, we obtain

$$\widetilde{\Lambda}_1(\tau) = \frac{1}{2\beta^2 Z}\int_0^{2\pi}\frac{\mathrm{d}\theta}{2\pi}\frac{\xi^2}{\cos^2\theta}\exp\left(\sum_{m=1}^{\infty} b_m\xi^m\right)\sum_{m=1}^{\infty} B_m\xi^m, \tag{3.179}$$

where $\xi = 2\beta\tilde{\Delta}\cos\theta$. Since the sum of $b_m\xi^m$ gives U as shown in (3.161) and (3.171)-(3.172), the remaining problem is the summation of $B_m\xi^m$, which comes from the cluster integrals of the diagrams including two fixed charges. In the ring approximation, only the diagrams shown in Fig. 3.10 (a) are relevant. The double circle in the diagram denotes the sum of the diagrams as shown in Fig. 3.10 (b), and renormalize the fugacity ξ as

$$\xi \to \xi\sum_{m=0}^{\infty} m b_m \xi^{m-1} = \xi\frac{\mathrm{d}U}{\mathrm{d}\xi}. \tag{3.180}$$

By using (3.172), it is proved that the renormalization is given by $\xi \to n$, where n is the particle density.

Finally, we consider the sum of the diagrams represented by Fig. 3.10 (a). The cluster integrals including two 'fixed' charges are summed up as

$$\sum_{m=0}^{\infty} B_m n^m = \sum_{m=0}^{\infty}\frac{n^m}{m!}\sum_{\{m_l\}'}\frac{m!}{\prod_{l=0}^{m} m_l!(l!)^{m_l}}\prod_{l=0}^{m}(C_l l!)^{m_l}\times(-1)^{m_l}m_l! \tag{3.181}$$

$$= \exp\left(-\sum_{l=0}^{\infty} C_l n^l\right). \tag{3.182}$$

Here, C_l denotes the sum shown in Fig. 3.10(c), and is obtained as

$$C_l = \frac{1}{l!}\times\frac{l!}{\beta^{l+1}}\sum_{\mathrm{i}\omega_m}\phi(\mathrm{i}\omega_m)^{l+1}e^{-\mathrm{i}\omega_m\tau}. \tag{3.183}$$

From (3.179) and (3.182)-(3.183), the equation (3.68) is derived. Similarly, $\widetilde{\Lambda}_2(\tau)$ is derived by removing the last term $(-1)^{m_l}$ in (3.181), and by replacing the electroneutrality condition (3.15) with (3.31).

3-D Validity of the Ring Approximation

In this chapter, the ring approximation has been used to study the dissipative tight-binding model. In this appendix, we discuss the validity of the ring approximation, and the condition to justify this approximation is evaluated.

The concept of this approximation has first been considered by Debye and Hückel [131]. Later, Mayer has shown that the Debye-Hückel theory can be reproduced from the ring approximation in the classical cluster expansion [132]. Since then, the corrections to the Debye-Hückel theory have been studied for the problem of interacting plasma.

Let us consider the 3D classical Coulomb gas with the particle density n. In the ring approximation, the two-body distribution function is calculated as

$$\rho_2(r) = n^2\exp\left(-\frac{\phi_{\mathrm{D}}(r)}{T}\right). \tag{3.184}$$

Here, T is the temperature, and $\phi_{\mathrm{D}}(r)$ is the screened potential

$$\phi_{\mathrm{D}}(r) = e^2\frac{e^{-\kappa_{\mathrm{D}}r}}{r}, \tag{3.185}$$

where $1/\kappa_{\mathrm{D}}$ is the Debye screening length given by

$$\kappa_{\mathrm{D}} = \left(\frac{4\pi n e^2}{T}\right)^{1/2}. \tag{3.186}$$

Note that the two-body distribution function can be written in a simple form as

$$\rho_2(r) = n^2 \exp\left(-\varepsilon \frac{e^{-x}}{x}\right), \tag{3.187}$$

where $x = \kappa_D r$ is the dimensionless spatial coordinate, and $\varepsilon = e^2\kappa_D/T$ is the plasma parameter. Beyond the ring approximation, it is possible to sum the graphs up to the order of ε^2 in the cluster expansion [133, 134]. The result is given as

$$\rho_2(r) = n^2 \exp\left(-\varepsilon \frac{e^{-x}}{x} - \varepsilon^2 f(x)\right), \tag{3.188}$$

where $f(x)$ is the complex function of x. From this result, if the series of ε is convergent, then the ring approximation is justified for $\varepsilon \ll 1$. Also the results by the Monte Carlo simulations [135, 136] have confirmed Eq. (3.188). Thus, the ring approximation is thought to be valid in the weak coupling limit $\varepsilon \ll 1$ for the 3D classical Coulomb gas.

Next, let us discuss the 1D classical Coulomb gas. The Hamiltonian is given as

$$H = \frac{1}{2}\sum_i p_i^2 - 2\pi e^2 \sum_{i<j} \sigma_i\sigma_j |q_i - q_j|, \tag{3.189}$$

where p_j, q_j, and $\sigma_j = \pm 1$ are the momentum, position, and sign of the j-th charged particle. Among 2N particles, N particles are charged positively and N negatively. Fortunately, this model can be solved exactly [137]. We take the dimensionless parameter as $\gamma = P/2\pi e^2$, where P is the pressure. In this model, the system behaves as ideal gas in the high-pressure limit $\gamma \to \infty$. The energy per particle u is calculated for $\gamma \gg 1$ in the expansion from as

$$u = \frac{\theta}{2} + \frac{\theta}{2}\left\{1 + \frac{1}{(2\gamma)^{1/2}} - \frac{1}{8\gamma} + \frac{1}{128\sqrt{2}\gamma^{3/2}} + \cdots\right\}. \tag{3.190}$$

It can easily be checked that the Debye-Hückel theory gives the exact result (3.190) up to the order of $1/\gamma^{1/2}$. It can also be checked that the ring approximation gives the Debye-Hückel theory for 1D Coulomb gas. Thus, the ring approximation is applicable to the 1D classical Coulomb gas for the weak coupling region $\gamma \gg 1$.

From the above discussions, the ring approximation is thought to be applicable to general classical plasma models in the condition

$$(\text{the Debye length} \quad 1/\kappa_D) \gg (\text{the averaged particle distance} \quad \bar{l}). \tag{3.191}$$

Hence, the ring approximation is expected to be valid also for the dissipative tight-binding model in the condition (3.191). At this time, this expectation has not be proved explicitly.

To clarify the validity of the ring approximation, other methods such as Monte Carlo simulations are needed.

To study the dissipative tight-binding model, 1D classical particles interacting with the potential $\phi(\tau)$ in the τ direction have been considered. The potential is formulated as

$$\phi(\tau) = \frac{1}{\beta}\sum_{\omega_m} \phi(\mathrm{i}\omega_m) e^{-\mathrm{i}\omega_m\tau}, \tag{3.192}$$

$$\phi(\mathrm{i}\omega_m) = -\frac{\tilde{M}a^2}{\omega_m}\tilde{\gamma}(z = \omega_m). \tag{3.193}$$

From the expression (3.42) of $\gamma(z)$, the potential $\phi(\mathrm{i}\omega_m)$ is evaluated as

$$\phi(\mathrm{i}\omega_m) = \begin{cases} -\dfrac{2\pi\delta_s}{\sin(\pi s/2)\tilde{\omega}}\left|\dfrac{\omega_m}{\tilde{\omega}_m}\right|^{s-2}, & (0 < s < 2), \\ -\dfrac{4\delta_s}{(s-2)\tilde{\omega}}\left(\dfrac{\omega_c}{\tilde{\omega}}\right)^{s-2}, & (2 < s), \end{cases} \tag{3.194}$$

for $0 < |\omega_m| \ll \omega_c$, while the potential vanishes for $\omega_m > \omega_c$. From these expression, it is shown that the potential is long-ranged for $0 < s < 2$, while short-ranged for $s > 2$. We restrict ourselves the case $0 < s < 2$. The potential $\phi(\tau)$ is calculated at zero temperature as

$$\phi(\tau) = \begin{cases} -\dfrac{\delta_s\Gamma(s-1)}{(\tilde{\omega}\tau)^{s-1}} + \text{const.}, & (0 < s < 1, \text{ or } 1 < s < 2), \\ 2K\ln(\omega_c\tau), & (s = 1), \end{cases} \tag{3.195}$$

for $\omega_c\tau \gg 1$. The condition (3.191) to justify the ring approximation can be evaluated for the tight-binding model as follows. In the ring approximation, the screened potential $\varphi(\mathrm{i}\omega_m)$ is calculated as

$$\varphi(\mathrm{i}\omega_m) = \frac{\phi(\mathrm{i}\omega_m)}{1 - n\phi(\mathrm{i}\omega_m)/\beta}. \tag{3.196}$$

The screening effects appears when the second term of the denominator in (3.196) is dominant. Hence ,the Debye screening length $1/\kappa_D$ can be defined as $n\phi(\omega_m = \kappa_D)/\beta \sim 1$. Then, the condition (3.191) is evaluated for $0 < s < 2$ as

$$\delta_s\left(\frac{\Delta_{\mathrm{eff}}}{\tilde{\omega}}\right)^{s-1} \ll 1. \tag{3.197}$$

In the ohmic damping case ($s = 1$, $\delta_s = K$), this condition is nothing but the weak-damping condition $K \ll 1$, where we expect the ring approximation gives reliable results in the weak-damping region.

We summarize the consistency of the ring approximation by comparing the results with the ones obtained by other methods. As discussed in Sec. 3.2.5, the ring approximation reproduces the results obtained in the continuum limit ($K \to 0$, $\Delta \to \infty$ with $\gamma = 4\pi\delta_s\Delta$ fixed). This agreement is understood from the fact that the optical conductivity $\sigma(\omega)$ can be expressed in the series of δ_s as

$$\sigma(\omega) = \sigma^{(0)}(\omega;\gamma) + \delta_s\sigma^{(1)}(\omega;\gamma) + \mathcal{O}(\delta_s^2), \tag{3.198}$$

where $\sigma^{(0)}(\omega;\gamma)$ is obtained by the sum of the ring-shaped graphs, and $\sigma^{(1)}(\omega;\gamma)$ by the sum of the other graphs of the order of δ_s. Assumed that the series of δ_s is convergent, the optical conductivity calculated based on the ring approximation becomes exact in the limit $\delta_s \to 0$.

Also, in the high temperature and/or strong damping region, the ring approximation reproduces the results calculated from the hopping rate of the incoherent particle from Fermi's golden rule (see Sec. 3.2.5).

For the ohmic damping case, the DC conductivity at zero temperature for $K < 1$ is obtained from the discussion of the duality mapping and renormalization group analysis as [1, 50]

$$\sigma_{\rm DC}(T=0) = e^2a^2/\pi K. \tag{3.199}$$

The ring approximation also reproduces this result at zero temperature.

In this chapter, the specific heat and density of states for the weak damping have been calculated based on the ring approximation. Hence, the results obtained in Sec. 3.3.3 (Fig. 3.3 and Fig. 3.6) depend on the ring approximation. However, the discussion about the existence of the Drude weight D is based on the continuum limit. The results of the Drude weight given in Sec. 3.2.3 do not depend on the ring approximation.

3·E Low-Temperature Expansions

In this appendix, we discuss the low-temperature expansions for the specific heat and the DC conductivity in the case of ohmic damping. This expansion is obtained by asymptotic expansions in terms of the inverse temperature $\beta = 1/T$. We begin with the partition function Z expressed by

$$Z = \int_{-\pi}^{\pi} \frac{d\theta}{2\pi} e^{U(\theta)}. \tag{3.200}$$

Here, $U(\theta) = U(n(\theta))$ is given by

$$U(n) = n + \log\Gamma(Kn+1) - Kn\psi(Kn+1), \tag{3.201}$$

where $\Gamma(z)$ is the gamma function, and $\psi(z)$ is the polygamma function. At low temperatures, the integral in (3.200) is determined by the contribution around $\theta = 0$. We expand $U(\theta)$ as

$$U(\theta) \simeq U(0) + \frac{1}{2}U''(0)\theta^2 + \mathcal{O}(\theta^4), \tag{3.202}$$

and the integral (3.200) is replaced with the Gaussian integral by (3.202), approximately. By using $U''(0) = -n_0$ and asymptotic forms of $\Gamma(z)$ and $\psi(z)$, we obtain

$$Z = (1-K)n_0 + \text{const.} + \frac{1}{6Kn_0} + \mathcal{O}(n_0^{-2}), \tag{3.203}$$

where $n_0 = n(\theta = 0)$. We should note that the asymmetry part $U''''(0)$ also gives a term of the order of $1/n_0$. However, this term takes a finite value for $K \to 0$, and for weak damping ($K \ll 1$), and this contribution is less than the third term of (3.203). From (3.84) and (3.85), n_0 is determined by

$$2\beta\bar{\Delta} = n_0 e^{-Q(n_0)} \tag{3.204}$$

$$Q(n_0) = K(\psi(Kn_0+1) + \bar{\gamma}). \tag{3.205}$$

Next, we calculate the asymptotic form of (3.204). By using $\bar{\Delta} = \Delta(\beta\omega_c/2\pi)^{-K}$ and $\Delta_{\rm eff} = \Delta(\Delta/\omega_c)^{K/(1-K)}$, the lefthand side of (3.204) is represented as $4\pi(\beta\Delta_{\rm eff}/2\pi)^{1-K}$. For $\beta \to \infty$ ($n \to \infty$), the righthand side of (3.204) is expanded as

$$n_0 e^{-Q(n_0)} = (Ke^{\bar{\gamma}})^{-K} n_0^{1-K}\left(1 - \frac{1}{2n_0} + \frac{1}{12Kn_0^2} + \mathcal{O}(n_0^{-3})\right). \tag{3.206}$$

We substitute $n_0 = a_1\beta + a_0 + a_{-1}/\beta + \cdots$ to (3.206), and determine the constants a_1, a_0, a_{-1} so that (3.206) gives the lefthand side of (3.204). Thus, we obtain

$$n_0 = 2\beta c\Delta_{\rm eff} + \frac{1}{2(1-K)} - \frac{1}{24K\beta c\Delta_{\rm eff}} + \mathcal{O}(\beta^{-2}), \tag{3.207}$$

where $c = (4\pi Ke^{\bar{\gamma}})^{K/(1-K)}$. From (3.203) and (3.207), we obtain the low-temperature expansion of the partition function (3.86).

In order to calculate $\sigma_{\rm DC}$, it is sufficient to consider the long-time behavior of $S(t;\theta)$ and $R(t;\theta)$ defined in (3.103)-(3.104). From (3.104) and (3.108), we obtain for $t \to \infty$

$$S(t;\theta) = \frac{2\pi KT}{\gamma(\theta)} = \frac{1}{n(\theta)}, \tag{3.208}$$

$$R(t;\theta) = \pi K e^{-\gamma(\theta)t}. \tag{3.209}$$

Here, we have used $\gamma(\theta) = 2\pi K n(\theta)/\beta$. From (3.71), the real-time correlation function in the long-time limit is obtained as

$$\Lambda(t) = \frac{e^2 a^2}{Z} \int_{-\pi}^{\pi} \frac{\mathrm{d}\theta}{2\pi} \frac{n^2}{\beta^2 \cos^2\theta} \mathrm{e}^{U(\theta)} \left[\mathrm{e}^{-1/n} + \mathrm{e}^{1/n} \cos 2\theta\right] \pi K \mathrm{e}^{-\gamma(\theta)t}. \tag{3.210}$$

Then, the DC conductivity is calculated as

$$\begin{aligned} \sigma_{\mathrm{DC}} &= \lim_{\omega \to 0} \frac{1}{\omega} \mathrm{Im} \int_0^{\infty} \mathrm{d}t\, \mathrm{e}^{\mathrm{i}\omega t} \Lambda(t) \\ &= \frac{\sigma_{\mathrm{DC}}^0}{2Z} \int_{-\pi}^{\pi} \frac{\mathrm{d}\theta}{2\pi} \mathrm{e}^{U(\theta)} \left[\frac{\mathrm{e}^{-1/n} - \mathrm{e}^{1/n}}{\cos^2\theta} + 2\mathrm{e}^{1/n}\right], \end{aligned} \tag{3.211}$$

where $\sigma_{\mathrm{DC}}^0 = e^2 a^2 / 2\pi K$. The low-temperature expansion is obtained by expanding (3.211) over $1/n (\ll 1)$ as

$$\sigma_{\mathrm{DC}} = \frac{\sigma_{\mathrm{DC}}^0}{Z} \int_{-\pi}^{\pi} \frac{\mathrm{d}\theta}{2\pi} \left[1 + \frac{1}{2n^2} - \frac{1}{n}\theta^2 + \mathcal{O}(n^{-2}, \theta^4)\right] \mathrm{e}^{U(0) + U''(0)\theta^2/2}. \tag{3.212}$$

By using the Gaussian integral formulas and an asymptotic form of the partition function

$$Z = \int_{-\infty}^{\infty} \frac{\mathrm{d}\theta}{2\pi} \mathrm{e}^{U(0) + U''(0)\theta^2/2}, \tag{3.213}$$

we obtain

$$\sigma(\omega) = \sigma_{\mathrm{DC}}^0 \left(1 - \frac{1}{2n^2} + \mathcal{O}(n^4)\right). \tag{3.214}$$

From (3.207) and (3.214), we obtain(3.113).

Chapter 4

Summary

In this thesis, several dissipative quantum systems have been studied theoretically within the Caldeira-Leggett model. In the first part (Chapter 2), macroscopic Quantum phenomena in long Josephson junctions have been studied, while in the latter part (Chapter 3), a dissipative tight-binding model has been studied, and applications to small Josephson junctions has been discussed.

In Chapter 2, macroscopic quantum tunneling (MQT) for a single fluxon moving along a long Josephson junction has been studied theoretically. To introduce a fluxon-pinning force, we have considered inhomogeneities made by modifying the thickness of an insulating layer locally. Two different situations have been studied: one is quantum tunneling from a metastable state caused by a single inhomogeneity, and the other one is quantum tunneling in a two-state system formed by two inhomogeneities. In the quantum tunneling from a metastable state, the decay rate has been estimated within the WKB approximation. Dissipation effects on fluxon dynamics have been taken into account by the Caldeira-Leggett theory. Required experimental resolutions to observe MQT of a fluxon seem attainable within the presently available micro-fabrication technique. For the two-state system, we have studied quantum resonance between two stable states, i.e., macroscopic quantum coherence (MQC). From the estimate of the dissipation coefficients due to quasiparticle tunneling, the observation of MQC appears to be possible within the Caldeira-Leggett theory.

In Chapter 2, we have also studied a current-biased 0-π-0 Josephson junction made by high-T_c superconductors, theoretically. When the length of the π junction is large enough, this junction contains a vortex-antivortex pair at both ends of the π junction. Magnetic

flux carried by the vortices has been calculated using the sine-Gordon equation. The result shows that the magnetic flux of the vortices is suppressed to zero as the distance between the vortices is reduced. By applying an external current, the orientation of the vortices is reversed, and a voltage pulse is generated. The current needed for this transition and the generated pulse energy have been calculated. Macroscopic quantum tunneling (MQT) in this transition has also been studied. The tunneling rate has been evaluated by an effective Hamiltonian with one degree of freedom with ohmic damping.

In Chapter 3, thermodynamics and transport properties of a dissipative particle in a tight-binding model have been studied through specific heat and optical conductivity. A weak coupling theory has been constituted to study the crossover behavior between the low-temperature region and the high-temperature region analytically. We have found that the coherent part around zero frequency in the optical conductivity disappears for $0 < s < 2$, where s is the exponent of the spectral function of the environment. A detailed calculation has been performed for ohmic damping ($s = 1$). In this case, the specific heat shows an unusual T-linear behavior at low temperatures, which indicates that the environment strongly influences the particle motion, and changes the low-energy states of the dissipative particle. The optical conductivity $\sigma(\omega)$ takes a non-Drude form even at zero temperature, and the high-frequency side behaves as ω^{2K-2}, where K is a dimensionless damping strength. The high frequency side of the optical conductivity is independent of the temperature T, while the low frequency side depends on the temperature, and behaves as T^{2K-2} at high temperatures. The application of this model to small resistance-shunted Josephson junctions has also been discussed.

In these studies, experimental parameters have been estimated to observe various dissipative quantum phenomena. I hope that these experiments will be performed in future, and a comparison with the theoretical results obtained in this thesis will become possible. I also hope that these studies help to clarify basic properties of quantum dissipative systems.

References

[1] U. Weiss: *Quantum Dissipative Systems* (World Scientific, Singapore, 1993).

[2] T. Kato and M. Imada: J. Phys. Soc. Jpn. **65** (1996) 2963.

[3] T. Kato and M. Imada: J. Phys. Soc. Jpn. **66** (1997) 1445.

[4] T. Kato: Master Thesis (University of Tokyo, 1996)

[5] T. Kato and M. Imada: J. Phys. Soc. Jpn. **67** (1998) 2828.

[6] R. Zwanzig: J. Chem. Phys. **33** (1960) 1338.

[7] H. Mori: Progr. Theor. Phys. **33** (1965) 423.

[8] R. P. Feynman and F. L. Vernon: Ann. Phys. (N. Y.) **24** (1963) 118.

[9] P. Ullersma: Physica (Utrecht) **32** (1966) 27, 56, 74, 90.

[10] A. O. Caldeira and A. J. Leggett: Phys. Rev. Lett. **46** (1981) 211.

[11] A. O. Caldeira and A. J. Leggett: Ann. Phys. (N. Y.) **149** (1983) 374 [Errata; **153** (1984) 445].

[12] R. P. Feynman: *Statistical Mechanics* (Benjamin, New York, 1972)

[13] V. Hakim and V. Ambegaokar: Phys. Rev. A **32** (1985) 423.

[14] H. Grabert, P. Schramm and G. -L. Ingold: Phys. Rep. **168** (1988) 115.

[15] S. Arrhenius: Z. Phys. Chem. (Leipzig) **4** (1889) 226.

[16] H. A. Kramers: Physica (Utrecht) **7** (1940) 284.

[17] P. Hänggi, P. Talkner and M. Borkovec: Rev. Mod. Phys. **62** (1990) 251.

[18] Affleck: Phys. Rev. Lett. **46** (1981) 388.

[19] A. I. Larkin and Yu. N. Ovchinnikov: Sov. Phys.-JETP **59** (1984) 420.

[20] H. Grabert and U. Weiss: Phys. Rev. Lett. **53** (1984) 1787.

[21] H. Grabert, P. Olschowski and U. Weiss: Phys. Rev. B **36** (1987) 1931.

[22] J. S. Langer: Ann. Phys. (N. Y.) **41** (1967) 108.

[23] C. G. Callan and S. Coleman: Phys. Rev. D **16** (1977) 1762.

[24] S. Coleman: *Aspects of Symmetry* (Cambridge University Press, 1985)

[25] E. Freidkin, P. S. Riseborough, and P. Hänggi: Z. Phys. B **64** (1987) 193.

[26] J. W. Trompt and W. H. Miller: J. Phys. Chem. **90** (1986) 3482

[27] G. A. Voth, D. Chandler and W. H. Miller: J. Chem. Phys. **91** (1989) 7749.

[28] G. A. Voth: J. Phys. Chem. **97** (1993) 8365.

[29] K. Takatsuka and H. Ushiyama: Phys. Rev. A **51** (1995) 4353.

[30] A. J. Leggett, S. Chakravarty, A. T. Dorsey, M. P. A. Fisher, A. Garg and W. Zwerger: Rev. Mod. Phys. **59** (1987) 1;*ibid.* **67** (1995) 725(E).

[31] S. Chakravarty and S. Kivelson: Phys. Rev. B **32** (1985) 76.

[32] A. T. Dorsey, M. A. Fisher and Wartak: Phys. Rev. A **33** (1986) 1117.

[33] U. Weiss, H. Grabert, P. Hänggi and P. Riseborough: Phys. Rev. B **35** (1987) 9535.

[34] R. Görlich and U. Weiss: Phys. Rev. B **38** (1988) 5254.

[35] J. Kondo: Prog. Thor. Phys. **32** (1964) 37.

[36] *Fermi Surface Effects*, Vol. 77 of Springer Series in Solid State Sciences, eds. J. Kondo and A. Yoshimori (Springer, Berlin, 1988).

[37] P. Nozières and C. T. de Dominicis: Phys. Rev. **178** (1969) 1097.

[38] A. M. Tsvelick and P. B. Wiegmann: Adv. Phys. **32** (1983) 453.

[39] J. Kondo: Physica **84B** (1976) 40.

[40] J. Kondo: Physica **125B** (1984) 279.

[41] K. Yamada: Prog. Theor. Phys. **72** (1984) 195.

[42] F. Guinea, V. Hakim and A. Muramatsu: Phys. Rev. B **32** (1985) 4410.

[43] G. Yuval and P. W. Anderson: Phys. Rev. B **1** (1970) 1522.

[44] M. Sassetti, and U. Weiss, Phys Rev. **A 41**, 5383 (1990).

[45] S. Chakravarty and J. Rudnick: Phys. Rev. Lett. **75** (1995) 501.

[46] T. A. Costi and C. Kieffer: Phys. Rev. Lett. **76** (1996) 1683.

[47] A. J. Bray and M. A. Moore: Phys. Rev. Lett. **49** (1982) 1546.

[48] S. Chakravarty: Phys. Rev. Lett. **50** (1982) 1811.

[49] A. Schmid: Phys. Rev. Lett. **51** (1983) 1506.

[50] M. P. A. Fisher and W. Zwerger: Phys. Rev. B **32** (1985) 6190.

[51] U. Eckern and F. Pelzer: Europhys. Lett. **3** (1987) 131.

[52] W. Zwerger: Phys. Rev. B **35** (1987) 4737.

[53] U. Weiss and M. Woolensak: Phys. Rev. B **37** (1988) 2729.

[54] U. Weiss and H. Grabert: Phys. Lett. **108A** (1985) 63.

[55] Y.-C. Chen, J. L. Lebowitz and C. Liverani: Phys. Rev. B **40** (1989) 4664.

[56] U. Weiss, M. Sassetti, T. Negele and M. Wollensak: Z. Phys. B **84** (1991) 471.

[57] M. Sassetti, M Milch and U. Weiss: Phys. Rev. **46** (1992) 4615.

[58] A. J. Leggett: Prog. Theor. Phys. Suppl. **69** (1980) 80.

[59] A. J. Leggett: in *Chance and Matter*, edited by J. Souletie, J. Vannimenus and R. Stora, p.395 (Elsevier Science Publishers, 1987).

[60] K. Hida and U. Eckern: Phys. Rev. B **30** (1984) 4096.

[61] L. Gunther and B. Barbara (eds.): *Quantum Tunneling of Magnetization* - QTM '94 (Kluwer Academic Publishers, 1995).

[62] I. M. Lifshitz and Y. Kagan: Sov. Phys. JETP **35** (1972) 206.

[63] T. Nakamura, Y. Kanno and S. Takagi: Phys. Rev. B **51** (1995) 8446.

[64] A. J. Leggett and A. Garg: Phys. Rev. Lett. **54** (1985) 857.

[65] A. Brone and G. Paterno: *Physics and Apprications of the Josephson Effect*, chap.6 (Wiley, New York, 1982).

[66] G. Schön and Z. D. Zaikin: Phys. Rep. **198** (1990) 237.

[67] R. F. Voss and R. A. Webb: Phys. Rev. Lett. **47** (1981) 265.

[68] S. Washburn, R. A. Webb, R. F. Voss and S. M. Faris: Phys. Rev. Lett. **54** (1985) 2712.

[69] J. M. Martinis, M. H. Dovoret and J. Clarke: Phys. Rev. Lett. **55** (1985) 1543.

[70] J. M. Martinis, M. H. Devoret and J. Clarke: Phys. Rev. B **35** (1987) 4682.

[71] W. den Boer and R. de Bruyn ouboter: Physica **98B** (1980) 185.

[72] S. Han, J. Lapointe and J. E. Lukens: Phys. Rev. Lett. **66** (1991) 810.

[73] D. B. Schwartz, B. Sen, C. N. Archie and J. E. Lukens: Phys. Rev. Lett. **55** (1985) 1547.

[74] R. Rouse, S. Han and J. E. Lukens: Phys. Rev. Lett. **75** (1995) 1614.

[75] S. Han, R. Rouse and J. E. Lukens: Phys. Rev. Lett. **76** (1996) 3404.

[76] N. F. Perdersen: in *Low Temperature Physics*, edited by C. J. Gorter (North Holland, Amsterdam, 1986), Vol. 5.

[77] V. G. Storchak and N. V. Prokof'ef: Rev. Mod. Phys. **70** (1998) 929.

[78] Yu. Kagan and N. V. Prokof'ef: Sov. Phys. JETP **63** (1986).

[79] Yu. Kagan and N. V. Prokof'ef: Sov. Phys. JETP **66** (1987) 211.

[80] F. Guinea: Phys. Rev. Lett. **53** (1984) 1268.

[81] F. Sols and F. Guinea: Phys. Rev. B **36** (1987) 7775.

[82] M. Sassetti, E. G. d'Agliano and N. Napoli: Physica B **154** (1989) 359.

[83] R. J. Kadono, J. Imazato, K. Nishiyama, K. Kagamine, T. Yamazaki, D. Richter and J. -M. Welter: Phys. Rev. B **39** (1989) 23.

[84] G. M. Luke, J. H. Brewer, S. R. Kreitzman, D. R. Noakes, M. Celio, R. Kadono and E. J. Ansalso: Phys. Rev. B **43** (1991) 3284.

[85] P. Hedegård and A. O. Caldeira: Phys. Rev. B **35** (1987) 106.

[86] P. Hedegård and A. O. Caldeira: Phys. Rev. B **35** (1987) 533.

[87] P. Hedegård: Phys. Scr. **35** (1987) 609.

[88] G. T. Zimanyi, K. Vladar and A. Zawadowski: Phys. Rev. B **36** (1987) 3186.

[89] A. Rosch and Thilo Kopp: Phys. Rev. Lett. **75** (1995) 1988.

[90] G. D. Mahan: *Many-Particle Physics* chap. 6 (Plenum Press, New York, 1990).

[91] J. Yamashita and T. Kurosawa: J. Chem. Solids **5** (1958) 34.

[92] T. Holstein: Ann. Phys. (N. Y.) **8** (1959) 325.

[93] T. Holstein: Ann. Phys. (N. Y.) **8** (1959) 343.

[94] C. P. Flynn and A. M. Stoneham: Phys. Rev. B **1** (1970) 3966.

[95] Y. Kagan and M. I. Klinger: J. Phys. C **7** (1974) 2791.

[96] H. Teichler and A. Seeger: Phys. Lett. **82** A (1981) 91.

[97] T. A. Fulton and R. C. Dynes: Solid State Commun. **12** (1973) 57.

[98] P. S. Lomdahl, O. H. Soerensen and P. L. Christiansen: Phys. Rev. B **48** (1982) 5737.

[99] A. Matsuda and T. Kawakami: Phys. Rev. Lett. **51** (1983) 694.

[100] A. Fujimaki, K. Nakajima and Y.Sawada: Phys. Rev. Lett. **59** (1987) 2895.

[101] Z. Hermon, A. Stern and E. Ben-Jacob: Phys. Rev. B **49** (1994) 9757.

[102] Z. Hermon, A. Shnirman and E. Ben-Jacob: Phys. Rev. Lett. **74** (1995) 4915.

[103] D. W. McLaughlin and A. C. Scott: Phys. Rev. A **18** (1978) 1652.

[104] A. Davidson, B. Dueholm, B. Kryger and N. F. Pedersen: Phys. Rev. Lett. **55** (1985) 2059.

[105] N. F. Pedersen and D. Welner: Phys. Rev B **29** (1984) 2551.

[106] V. Ambegaokar and A. Baratoff: Phys. Rev. Lett. **10** (1963) 486.

[107] A. Davidson, B. Dueholm and N. F. Pedersen: J. Appl. Phys. **60** (1986) 1447.

[108] L. N. Bulaevskii, V. V. Kuzii and A. A. Sobyanin: Solid State Comm. **25** (1978) 1053.

[109] B. I. Spivak and S. A. Kivelson: Phys. Rev. B **43** (1991) 3740.

[110] V. B. Geshkenbein, A. I. Larkin, and A. Barone: Phys. Rev. B **36** (1987) 235.

[111] M. Sigrist and T. M. Rice: J. Phys. Soc. Jpn. **61** (1992) 4283.

[112] W. Braunisch, N. Knauf, V. Kataev, S.Neuhausen, A. Grütz, A. Kock, B. Roden, D. Khomskii and D. Wohlleben: Phys. Rev. Lett. **68** (1996) 1908.

[113] D. A. Wollman, D. J. Van Harlingen, W. C. Lee, D. M. Ginsberg and A. J. Leggett: Phys. Rev. Lett. **71** (1993) 2134.

[114] D. A. Brawner and H. R. Ott: Rhys. Rev B **50** (1994) 6530.

[115] C. C. Tsuei, J. R. Kirtley, C. C. Chi, L. S. Yu-Jahnes, A. Gupta, T. Shaw, J. Z. Sun and M. B. Ketchen: Phys. Rev. Lett. **73** (1994) 593.

[116] J. R. Kirtley, C. C. Tsuei, M. Rupp, J. Z. Sun, L. S. Yu-Jahnes, A. Gupta, M. B. Ketchen, K. A. Moler and M. Bhushan: Phys. Rev. Lett. **76** (1996) 1336.

[117] D. -X. Chen and A. Hernando: Phys. Rev. B **50** (1994) 10107.

[118] J. H. Xu, J. H. Miller, Jr. and C. S. Ting: Phys. Rev. B **51** (1995) 11958.

[119] A. B. Kuklov, V. S. Boyko and J. Malinsky: Phys. Rev. B **51** (1995) 11965.

[120] C. S. Owen and D. J. Scalapino: Phys. Rev. **164** (1967) 538.

[121] There exists an error for the calculation of f_c in ref. [119].

[122] M. Imada, A. Fujimori and Y. Tokura: Rev. Mod. Phys. **70** (1998) 1039.

[123] R. Kubo: J. Phys. Soc. Jpn. **12** (1957) 570.

[124] D. J. Scalapino, S. R. White and S. Zhang: Phys. Rev. B **47** (1993) 7995.

[125] W. Kohn: Phys. Rev. **133** (1964) A171.

[126] B. S. Shastry and B. Sutherland: Phys. Rev. Lett. **65** (1990) 243.

[127] R. Egger, H. Grabert and U. Weiss: Phys. Rev. E **55** (1997) 3809.

[128] For example, ref. [51] and ref. [53] fail in deriving the T^2-suppression term.

[129] J. E. Mayer and M. G. Mayer: *Statistical Mechanics* (John Wiley & Sons, New York, 1940)

[130] L. D. Landau and E. M. Lifshitz: *Statistical Physics*, Part 1, 3rd. ed. (Pergamon Press, Oxford, 1980)

[131] P. Debye and G. Hückel: Physik. Z. **24** (1923) 305.

[132] J. Mayer: J. Chem. Phys. **18** (1950) 1426.

[133] A. Ishihara: Phys. Rev. **178** (1969) 412.

[134] A. Ishihara and M. Wadachi: Phys. Rev. **183** (1969) 312.

[135] W. L. Slattery, G. D. Doolen and H. E. DeWitt: Phys. Rev. A **21** (1980) 2087.

[136] W. L. Slattery, G. D. Doolen and H. E. DeWitt: Phys. Rev. A **26** (1982) 2255.

[137] A. Lenard: J. Math. Phys. **2** (1961) 682.